School of Doctoral Studies in Biological Sciences

University of South Bohemia in České Budějovice

Faculty of Science

The regulatory role of cyanobacterial High light inducible proteins

Ph.D. Thesis

Mahendra Kumar Shukla

Supervisor: **Doc. Ing. Roman Sobotka, Ph.D.**

Institute of Microbiology, Academy of Sciences of the Czech Republic

České Budějovice 2018

This thesis should be cited as:

▪ Annotation

The aim of the thesis was to elucidate the role of High light inducible proteins (Hlips) in the protection/regulation of the biogenesis of photosynthesis machinery. During the project two Hlip proteins (HliC and HliD) were isolated from the cyanobacterium *Synechocystis* PCC 6803; either as a pure oligomer (HliC protein) or as a small complex with a putative Photosystem II assembly factor Ycf39 (HliD protein). Pigments bound to purified Hlips were analyzed by state-of-art spectroscopic techniques to elucidate the mechanism of thermal energy dissipation. In addition, this work explained the mechanism of how the HliC protein regulates the interaction between chlorophyll synthase enzyme and the Ycf39 protein. This conceptually new mechanism is based on the replacement of HliD dimers in chlorophyll synthase complexes by stress-induced HliD-HliC heterodimers, which changes the affinity of Ycf39 towards chlorophyll synthase.

▪ Declaration [in Czech]

Prohlašuji, že svoji disertační práci jsem vypracoval samostatně pouze s použitím pramenů a literatury uvedených v seznamu citované literatury.

Prohlašuji, že v souladu s § 47b zákona č. 111/1998 Sb. v platném znění souhlasím se zveřejněním své disertační práce, a to v úpravě vzniklé vypuštěním vyznačených částí archivovaných Přírodovědeckou fakultou elektronickou cestou ve veřejně přístupné části databáze STAG provozované Jihočeskou univerzitou v Českých Budějovicích na jejích internetových stránkách, a to se zachováním mého autorského práva k odevzdanému textu této kvalifikační práce. Souhlasím dále s tím, aby touž elektronickou cestou byly v souladu s uvedeným ustanovením zákona č. 111/1998 Sb. zveřejněny posudky školitele a oponentů práce i záznam o průběhu a výsledku obhajoby kvalifikační práce. Rovněž souhlasím s porovnáním textu mé kvalifikační práce s databází kvalifikačních prací Theses.cz provozovanou Národním registrem vysokoškolských kvalifikačních prací a systémem na odhalování plagiátů.

České Budějovice, 2nd March 2018   Mahendra Kumar Shukla

This thesis originated from a partnership of Faculty of Science, University of South Bohemia, and Centre Algatech, Institute of Microbiology, Academy of Sciences of the Czech Republic.

- **Acknowledgements**

First of all, I would like to thank my supervisor Dr. Roman Sobotka. Thank you for accepting me as a PhD student in your group. I am grateful to you for providing me wonderful research environment and excellent topic to work on. I am really thankful for your excellent guidance, endless support and patience during these five years. From giving your valuable suggestion for solving a research problem to providing me transportation to the institute, you were always there when I need you. I have always valued your constructive criticism. I admire your capability of solving multiple problem, you have been constant inspiration for me.

I am also grateful to Prof. Josef Komenda for being excellent laboratory head and providing outstanding scientific platform in the lab. I am thankful to him for the great conference trip to Romania. I really admire him as great scientist. I am also obliged to Dr. Martin Tichý for his overall help. I am grateful to Prof. Neil Hunter for providing me fantabulous research environment during my stay in Sheffield University. I thanks Jana

List of publications and author's contributions

The thesis is based on the following papers and manuscripts (listed chronologically):

I.   Staleva, H., Komenda J., **Shukla, M.K.**, Šlouf, V., Kana, R., Polívka, T., Sobotka, R. **Mechanism of photoprotection in the cyanobacterial ancestor of plant antenna proteins.** Nature Chemical Biology, 2015, 11:287-291.
MKS isolated the pigmented Ycf39-HliD complex, and performed a detail characterization of its protein and pigment compositions by biochemical methods.

II.   LIansola-Portoles, M.J., Sobotka, R., Kish, E., **Shukla, M.K.**, Pascal, A.A., Polívka, T., Robert, B. **Twisting a β-carotene, an adaptive trick from nature for dissipating energy during photoprotection.** Journal of Biological Chemistry, 2016, 292:1396-1403.
MKS purified the Ycf39-HliD complex in a quantity and purity required for Resonance Raman spectroscopy.

III.   **Shukla, M.K.,** Llansola-Portoles, M.J., Tichý, M., Pascal, A.A., Robert, B., Sobotka, R. **Binding of pigments to the cyanobacterial high-light-inducible protein HliC**. Photosynthesis Research, 2017, doi.org/10.1007/s11120-017-0475-7.
MKS constructed mutant strains and developed a protocol for the purification of His-HliC protein. He performed the biochemical characterization of His-HliC including pigment HPLC and 2D gel electrophoresis.

IV.   **Shukla, M.K.**, Jackson, P.J., Moravcová, L., Zdvihalová, B., Brindley, A.A., Hunter, C.N., Sobotka, R. **Cyanobacterial LHC-like proteins control formation of the chlorophyll-synthase-Ycf39 complex.** (*Unsubmitted manuscript*).
MKS performed all experiments except the protein quantification by mass spectrometry and participated in writing the manuscript.

V. Hontani, Y., Kloz, M., Polívka, T., **Shukla, M.K.**, Sobotka, R., Kennis, J.T.M. **Molecular origin of photoprotection in oxygenic photosynthesis probed by femtosecond Raman spectroscopy.** (*Submitted manuscript – J. Phys Chem Lett.*).

MKS obtained the His-HliC protein in a purity and quality required for the femtosecond Raman technique.

I hereby confirm that Mahendra Kumar Shukla contributed to the mentioned publications as described above.

Doc. Ing. Roman Sobotka, Ph.D.

Table of contents

List of abbreviations

Chl	Chlorophyll
ROS	Reactive oxygen species
HliA	High light inducible protein A
HliB	High light inducible protein B
HliC	High light inducible protein C
HliD	High light inducible protein D
PSI	Photosystem I
PSII	Photosystem II
RCII	Reaction center complex II
ALA	5-aminolaevulinic acid
GluRS	Glutamyl-tRNA synthetase
GluTR	Glutamyl-tRNA reductase
GSAT	Glutamate-1-semialdehyde aminomutase
ALAD	ALA dehydratase
MgCH	Mg-chelatase
Pchlide	Protochlorophyllide
Chlide	Chlorophyllide
Chl-synthase, ChlG	Chlorophyll synthase
LPOR	Light-dependent NADPH : Pchlidee oxidoreductase
DPOR	Dark-operative protochlorophyllide oxidoreductase
SRP	Signal recognition particle
NPQ	Non-photochemical quenching
β-car	β-carotene

1 INTRODUCTION

1.1 Preface

Oxygenic photosynthesis is one of the most vital events for the sustainability of life on Earth providing a natural machinery for the conversion of solar energy into organic compounds and generating almost all the organic matter on the planet (Nelson and Ben-Shem, 2004). In general, oxygenic phototrophs use water as an unlimited source of electrons. They are able to utilize the energy of photons to break the water molecules into oxygen, protons and electrons and use the released electrons to regenerate reducing power [NAD(P)H] in the cell. Electron transport is coupled with the transfer of protons into the thylakoid lumen and, consequently, with the generation of proton motive force required for the synthesis of ATP. Subsequently, NADPH and ATP molecules are utilised in the fixation of CO_2 into organic compounds.

The utilization of water as electron donor was one of the major breakthrough in life evolution. Releasing of oxygen as a waste of photosynthesis leads to the formation of oxygenic atmosphere, an event most likely triggering the evolution of complex multicellular forms of life (Hohmann-Marriott and Blankenship, 2011). There is, however, a price paid by all oxygenic phototrophs for dealing with oxygen molecules. The combination of Chl molecules (Chl), light, and oxygen is a toxic cocktail, particularly if the light energy absorbed by Chls is not immediately utilized for photosynthesis. If excited for 'too long' ($>10^{-9}$ s) Chls tend to switch to a triplet excited state that can react with oxygen, forming damaging reactive oxygen species (ROS).

Under high irradiance, phototrophs absorb more light energy than they need or at least can safely dissipate, which makes their electron transport components too reduced, blocking further utilization of photon energy and leaving Chl pigments in excited state. Produced ROS can damage (oxidize) cellular structures including proteins, lipids, and nucleic acids and thus, pose threat to cell viability (Nishiyama *et al.*, 2011; Sharma *et al.*, 2012). To avoid this, photosynthetic organisms developed photo-protective mechanisms which can balance the absorption of light and also ensures its maximum utilization and safe distributions. To minimize the damage caused by ROS is particularly challenging under the combination of several stress factors, which is, however, a typical situation in nature. It is not just light intensity but also temperature, the availability of different nutrients or salinity and drought, which fluctuate and thus, photosynthetic organisms

have to employ a mixture of sophisticated molecular mechanisms to adapt themselves to harsh environments.

During my PhD project, I have studied a family of small cyanobacterial proteins known as High-light inducible proteins (Hlips) that play an essential role under stress conditions. Interestingly, Hlips possess the same conserved Chl *a*/*b* binding motif as light-harvesting antenna proteins of green algae and plants (LHCs; Fig. 1). They, thus belong to so called LHC superfamily of proteins, a large and diverse group, which include also eukaryotic proteins that certainly do not contribute to light-harvesting but rather play a similar photoprotective role like the Hlips in cyanobacteria (Heddad *et al.*, 2012). Although numerous functions have been ascribed for Hlips as well as for eukaryotic LHC-like proteins, how these proteins function, remains unexplained.
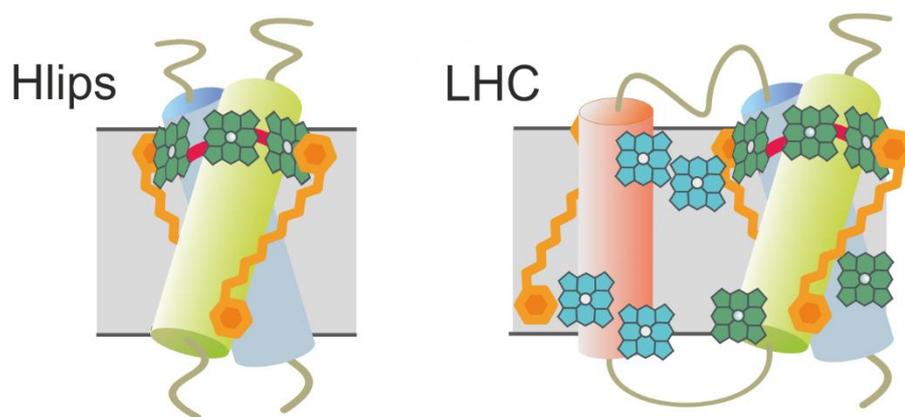
Figure 1. Structural model of cyanobacterial Hlips and plant LHCs. Single-helix Hlips (left) need to form a dimer to bind Chl *a* (green colour) and carotenoid (orange colour) (Staleva *et al.*, 2015; **Result I**; Shukla *et al.*, 2017; **Result III**). In contrast to Hlips, LHC proteins (right) have three membrane-spanning helixes and helixes 1 and 3 show clear homology to Hlips (Dolganov *et al.*, 1995). Chl *b* is marked by blue colour; red strips indicate the position of the conserved Chl-binding motif.

The experimental work described in this thesis was performed using the cyanobacterium *Synechocystis* PCC 6803 (hereafter *Synechocystis*). It is a well-established model for the studies on biogenesis and acclimation of photosynthetic apparatus, pigment biosynthesis, photoinhibition, photoprotection and other aspects of the physiology of photosynthetic cell. The *Synechocystis* is a unicellular organism with spherical shaped cell (~1.5 μm in diameter; Fig. 2) and, as an ancestor of eukaryotic plastid, many components of the

photosynthetic apparatus of this cyanobacterium are similar to chloroplast (Deusch *et al.*, 2008; Falcón *et al.*, 2010). Nonetheless, in contrast to algae and plants, inactivation, modification and controlled gene expression became routine in *Synechocystis* due to natural transformation and efficient homologous recombination. Fast growth and the possibility to scale up the culture volume make this organism excellent for the biochemical and biophysical studies which demands on the purification of proteins and protein complexes.
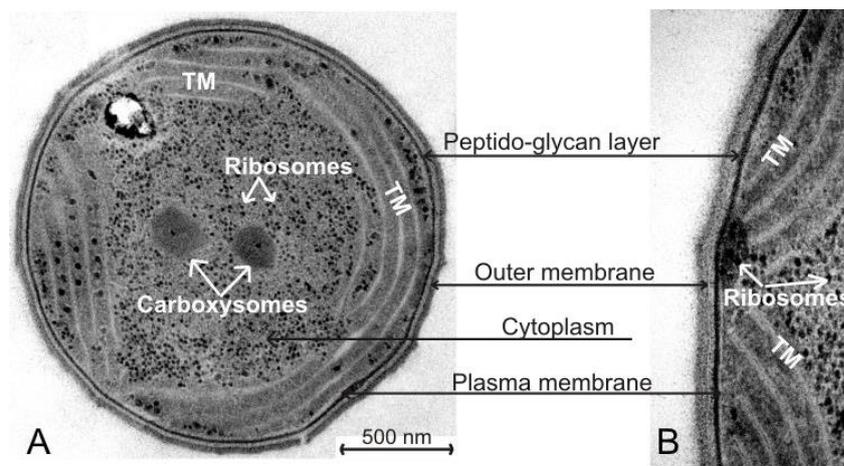
Figure 2. Transmission electron microscopy of the *Synechocystis* cell. A) Organization of thylakoid membranes (TM), ribosomes and carboxysomes. B) A detail of cytoplasmatic membrane, periplasmatic space, and thylakoid membrane. Courtesy of Lenka Bučinská.

In the first part of this text, I will describe the photosynthetic apparatus in cyanobacteria, the current knowledge about the biosynthesis of Chl and about the insertion of Chl molecules into apoproteins; particularly the core subunits of PSII. Later, the function of Hlips will be discussed in detail.

1.2 Photosynthetic apparatus in plants and cyanobacteria

Oxygenic photosynthesis was evolved in prokaryotic cyanobacteria about three billion years ago (Holland, 2006) and roughly one billion years ago, an endosymbiotic event between a eukaryotic cell and a cyanobacterium created the first ancestor of algae and plants. Although the original engulfed cyanobacterium was drastically reduced and modified during the process that resulted in modern chloroplasts, the photosynthetic

apparatus remained remarkably preserved in cyanobacteria and plants despite the amount of time that has passed since the primary endosymbiosis.

In all oxygenic phototrophs, light-dependent photosynthetic reactions occur in thylakoid membranes. In cyanobacteria, these thylakoid membranes are dispersed in the cytoplasm, whereas in chloroplast they are arranged into grana and stroma. Photosystem I (PSI) and photosystem II (PSII) are complicated pigment-protein structures that belong to the most abundant proteins complexes embedded in thylakoid membranes and are responsible for the photochemical reactions powering photosynthesis. PSII utilizes light to oxidize water and the consequently obtained electrons are passed via plastoquinone molecules to cytochrome b_6f - a heme-binding protein complex, which consumes energy of electrons to pump protons into the thylakoid lumen. The low-energy electrons are then transferred to the lumenal protein plastocyanin. At this point, the PSI must provide very strong redox potential in order to transfer electrons from plastocyanin to stromal ferredoxin. The redox potential of this electron carrier is sufficient to reduce NADP to NADPH. The proton gradient generated by the photosynthetic electron transport chain powers ATP synthase, an enzyme that converts ADP to ATP (Fig. 3).

PSII is one of the most studied membrane protein complexes and details about its structure have been resolved during last decades (Umena *et al.*, 2011). At the heart of PSII reaction center, two Chl-binding proteins called D1 and D2 form a heterodimer. Subjoined by a couple of small subunits, this subcomplex is already capable of primary photochemical reaction but not of water oxidation. Serving as inner light-harvesting antennae of PSII two larger Chl-proteins CP43 and CP47 are attached to the D1-D2 core (Fig. 3) and an inorganic Mn_4CaO_5 cluster is associated on the lumenal side providing a scaffold for the photooxidation of water. The Mn_4CaO_5 cluster is protected and stabilized by several extrinsic lumenal proteins (De Las Rivas *et al.*, 2004). The PSII is generally organized as a dimeric structure, though monomeric PSII complexes also exist in cyanobacterial cells (Komenda *et al.*, 2004). In total, the monomer of PSII is composed of 17 transmembrane proteins and 3 peripheral proteins, which together hold 35 Chls, 12 β-carotene, 2 pheophytins, 1 heme and 1 non-heme iron as cofactors (Umena *et al.*, 2011; Suga *et al.*, 2015). Proper positioning of these proteins and cofactors are essential for the light driven electron transport through PSII (Ferreira *et al.*, 2004; Guskov *et al.*, 2009; Umena *et al.*, 2011).

The PSI reaction center is assembled from a PsaA/PsaB hetero-dimer along with 10 additional proteins. Also, there are around 100 Chls and 12-16 β-carotenes associated with monomeric PSI (Fig. 3), bound mostly on the PsaA/B subunits (Jordan *et al.*, 2001). The stromal subunits PsaC, PsaD, and PsaE create a binding site for ferredoxin and coordinate Fe-S clusters that serve for electron transport. In cyanobacteria, the PSI is organized mostly as a trimer (Fig. 3), while in algae and plants PSI is exclusively in the monomeric form, surrounded by a ring of light-harvesting antenna proteins, a feature that is not present in cyanobacteria (Li *et al.*, 2014).

In order to drive photosynthetic processes, the first and utmost requirement is the absorption of light and charge separation in the reaction center of photosystems. In oxygenic phototrophs, these tasks are carried out by light-harvesting antenna systems. Two types of antenna can be recognized: a) an integral membrane antenna system, which is a structural part of photosystem complexes and utilizes Chl molecules as the main light-harvesting pigment (PSI core proteins and CP43 and CP47 subunits of PSII); b) peripheral antenna systems, which are associated with photosystems (mostly with PSII) but they are not integral parts (Blankenship, 2013). While the integral antenna system in plants, algae, and cyanobacteria are almost identical, there are striking differences in the structure of peripheral light-harvesting complexes used by various oxygenic phototrophs. Plants and green algae possess transmembrane, Chl-based antenna system (LHC, see Fig 1) containing Chl *a* and *b* and carotenoids as light-harvesting pigments (Minagawa, 2011). In contrast, cyanobacteria (and red algae) do not use Chl-based antenna system as peripheral antennae; instead, they contain phycobilisome complexes with covalently bound linear tetrapyrrole (phycobilin) as chromophore (Fig. 3).

A fascinating feature of eukaryotic LHC proteins is their ability to switch from a light-harvesting conformation to a quenching conformation in which the light energy absorbed by Chl molecules is safely dissipated as a heat. Multiple molecular mechanisms have been proposed to explain the principle of this energy dissipation in LHCs (Holt *et al.*, 2005; Ruban *et al.*, 2007), yet none are supported by convincing evidence. This issue concerns Hlips because they are also able to dissipate absorbed light energy and it is possible that this old cyanobacterial mechanism for thermal energy dissipation is utilized by modern LHC proteins (Staleva *et al.*, 2015; **Result I**).

1.3 Biogenesis and repair of PSII

The biogenesis of PSII is a complex and highly regulated process requiring a number of assisting proteins (auxiliary factors). The current knowledge about this process is typically based on the analysis of only a few model organisms - *Synechocystis*, green algae *Chlamydomonas reinhardtii* and plants *Arabidopsis thaliana* and *Nicotiana tabacum* (Suzuki *et al.*, 2003; Komenda *et al.*, 2012; Jarvi *et al.*, 2015) and it is still rather fragmented. However, it appears that the molecular mechanisms responsible for the building of PSII complexes are highly conserved in oxygenic phototrophs (Nickelsen and Rengstl, 2013). According to the accepted model, PSII complexes are assembled from individual subunits in a strictly stepwise manner. As a very early step of the PSII biogenesis, four assembly modules are pre-assembled separately (Komenda *et al.*, 2012), each consisting of one large Chl-binding proteins (D1, D2, CP43, and CP47) and several low-mass polypeptides, pigments and other cofactors. The D1 and D2 modules associate, creating reaction center complex (RCII complex). Following this, the CP47 module is attached to the RCII assembly intermediate and the resulting RC47 complex (Komenda *et al.*, 2012) is subsequently subjoined by CP43 module (Boehm *et al.*, 2011). Light-dependent attachment of oxygen-evolving Mn_4CaO_5 complex and the dimerization of PSII are final steps of PSII assembly (Komenda *et al.*, 2008; Nixon *et al.*, 2010).

Beside of de novo PSII assembly described above, oxygenic phototrophs developed a sophisticated mechanism, which allows repairing the damaged PSII complexes. Core proteins of the PSII reaction center (especially D1 protein) are frequent targets of stress-induced ROS and can be damaged within minutes, which can result in complete inhibition of PSII activity (Aro *et al.*, 1993). A particularly large pool of damaged PSII complexes is generated by a combination of abiotic stresses such as high light intensity coupled with low temperature (Yamashita *et al.*, 2008, Shukla *et al.*, **Result IV**). To replace the damaged D1 or both D1 and D2 core proteins with its newly synthesized intact copies (Nixon *et al.*, 2004), the dimeric PSII must be first monomerized and the oxygen evolving complex must de-attach completely. Since the D1 protein is shielded by CP43 antenna, this protein has to also dissociate. In the resulting RC47 complex the D1 copy is recognized by a FtsH protease, degraded and replaced by new D1 protein (Nixon *et al.*, 2010; Boehm *et al.*, 2012; Komenda *et al.*, 2012). How do the FtsH proteases differentiate between damaged and undamaged proteins remains unclear, however, the disassembly of PSII and the consequent accessibility of the protease to PSII

core proteins is probably the crucial determinant in the triggering of D1/D2 degradation (Krynická *et al.*, 2015).
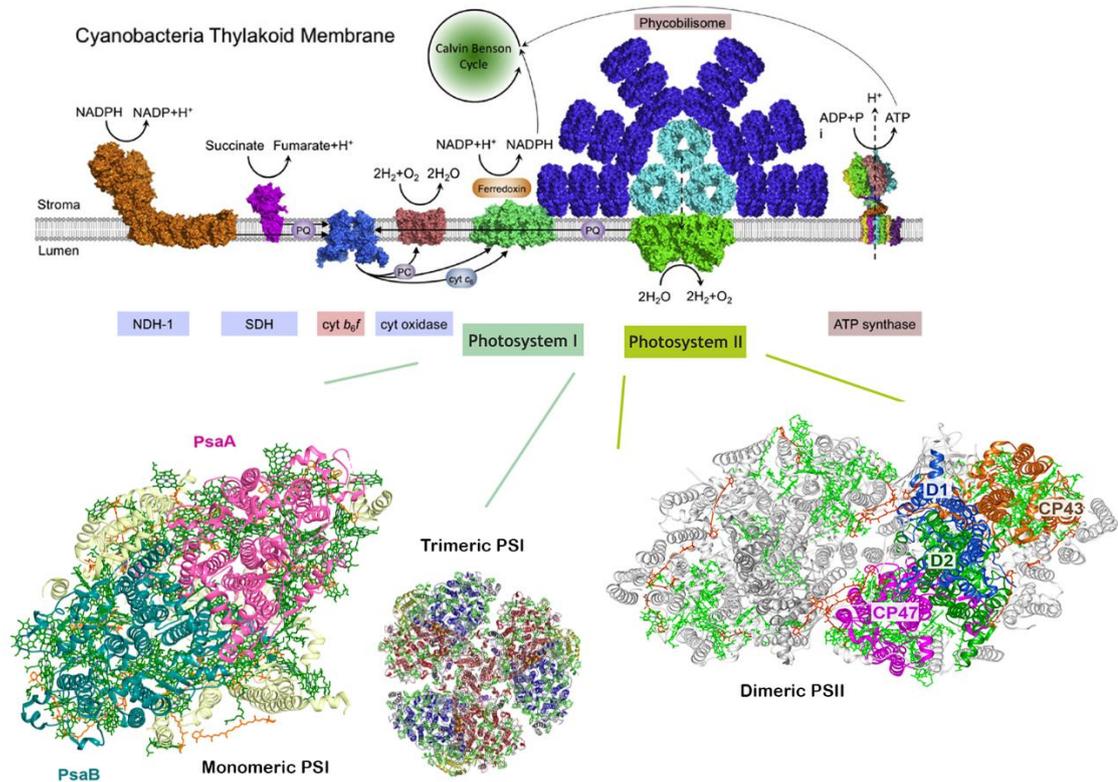

Figure 3. Cyanobacterial thylakoid membranes harbour the elements of both photosynthetic and respiratory electron transfer chain. This schematic model shows photosynthetic complexes with extrinsic phycobilisomes as well as respiratory membrane complexes from a side view (top; modified from (Liu, 2016). Crystal structures of trimeric PSI (Jordan *et al.*, 2001) and dimeric PSII (Umena *et al.*, 2011) are shown from the stromal side (below). A detailed view of a (monomeric) PSI unit is also shown (left). Individual Chl-binding subunits (PsaA/B, D1, D2, CP47 and CP43) of both photosystems are highlighted by different colours. In cyanobacteria, almost all Chl molecules (~95%) are bound to these five proteins (Xu *et al.*, 2004).

Both de novo PSII assembly and PSII repair cycle are essentially connected to Chl metabolism as the maintaining of a minute pool of Chl molecules available for the PSII biogenesis seems to be critical for the viability (Kopečná *et al.*, 2013; Hollingshead *et al.*, 2016). How this is managed in the cell is not known and it is further complicated by the fact that Chl molecules are much longer-living (days) than PSII core subunits (hours; Vavilin and Vermaas, 2007; Yao *et al.*, 2012). Chl molecules are then apparently re-used

many times and Hlips are expected to participate in this regulation. This regulation facilitates PSII biogenesis/repair (the details will be discussed later).

1.4   Chlorophyll-biosynthetic pathway

Chl is synthesized via a common tetrapyrrole pathway, which later gets branched into Chl and heme/bilin pathways (Fig. 4). The initial precursor for all tetrapyrroles is 5-aminolaevulinic acid (ALA), which is produced from glutamate in three enzymatic steps. The first reaction is ligation of glutamate to $tRNA_{glu}$. The consequently formed glutamyl-tRNA is then reduced by the glutamyl-tRNA reductase into glutamate-1-semialdehyde. As the final step, this intermediate is modified by glutamate-1-semialdehyde aminomutase, which results in ALA molecule (Fig 4). By several additional enzymatic reactions, ALA is converted into protoporphyrin IX, the last common precursor of Chl and heme biosynthesis. Insertion of Fe^{+2} into protoporphyrin IX, a step catalyzed by ferrochelatase, results in heme while the incorporation of Mg^{+2} by magnesium chelatase leads towards the formation of Mg-protoporphyrin IX - the first intermediate of the Chl branch. Down to the pathway, Mg-protoporphyrin IX is methylated by Mg-protoporphyrin IX methyl transferase. In the subsequent step, Mg-protoporphyrin IX monomethyl ester cyclase catalyses formation of the isocyclic 'fifth' ring. The resulting intermediate protochlorophyllide (Pchlide) is then reduced at the ring D to form the last Chl precursor chlorophyllide (Chlide). The Chl molecule is completed by attachment of a phytol tail to Chlide by teamwork of the Chl-synthase and geranylgeranyl-reductase enzymes (Sobotka, 2014; Wang and Grimm, 2015).

The demands for Chl, heme and other tetrapyrrole derivatives like phycobilins are highly influenced by environmental conditions and hence this pathway needs a high degree of metabolic regulations. Although the tetrapyrrole biosynthesis is well studied in term of enzymes involved, the regulation of the pathway is unclear. As this metabolic pathway involves a number of phototoxic intermediates, the regulation has to be very tight not only to prevent larger pools of intermediates but also to produce enough of each end-product under different environmental conditions. Most of the studies dealing with the regulation of Chl biosynthesis are focused on the step of ALA formation and the branching point towards heme and Chl. Formation of ALA was indeed recognised as a crucial regulatory point and enzymes involved in the synthesis of ALA are under tight

control including an expected feedback inhibition by heme (Czarnecki and Grimm, 2012).

Another key regulatory step is the branching point leading to heme and Chl end-products (Fig. 4; Masuda and Fujita, 2008). In plants, the Chl branch is prevalent in the presence of light; however after transition to dark, precursors are directed into the heme branch (Papenbrock *et al.*, 1999). How these regulation works is not known and differences certainly exist between plants, red/green algae, and cyanobacteria. In organisms that possess phycobilisomes (cyanobacteria and red algae), the main light harvesting pigments phycobilins are produced via heme oxidation. The synthesis and the distribution of heme should reflect the high concentration of phycobilins in these organisms as well as the different needs for phycobilisomes according to growing conditions.

In contrast to higher plants, cyanobacteria and algae also posses two different enzymes which convert Pchlide to Chlide and are designated as light-dependent NADPH:Pchlide oxidoreductase (LPOR) and dark-operative Pchlide oxidoreductase (DPOR; Fig. 4). Despite of catalyzing the same reaction, these enzymes show significant differences on structural as well as on functional level. The LPOR requires energy of photons for the catalysis, it is present in virtually all oxygenic phototrophs and belongs to a family of short-chain alcohol dehydrogenase (He *et al.*, 1998). In contrast, the DPOR that shows significant similarities with nitrogenase enzyme (Nomata *et al.*, 2005; Rees *et al.*, 2005), is not present in higher plants. Similar to nitrogenase, the DPOR is sensitive to oxygen (Yamazaki *et al.*, 2006). Although the LPOR is responsible for almost all de novo Chls synthesis in *Synechocystis* and cannot be replaced by DPOR (Kopečná *et al.*, 2013), cyanobacteria and algae, but not higher plants, have a capacity to synthesize Chl in dark.

Despite the described differences in the regulation of Chl biosynthesis between oxygenic phototrophs, a mechanism providing the interplay between synthesis of Chl-binding proteins and the rate of Chl formation could be universal. For all phototrophs, the Chl molecule is not the end-product of the pathway, it is a toxic intermediate of the biogenesis of Chl-binding protein complexes. In fact, fully assembled and active photosystem complexes are the final and safe place for Chl molecules and the regulation must somehow reflect this point. Importantly, recent results demonstrated a tight interconnection between the last enzyme of the Chl biosynthesis (Chl-synthase, also called ChlG; Fig. 4) and translocons producing Chl-binding proteins (Chidgey *et al.*,

2014). Regarding the regulation, the interface between Chl biosynthesis and proteosynthesis is a critical point and, indeed, it is the place where Hlips operate (Komenda and Sobotka, 2016 ; Shukla *et al.*, **Result IV**).

1.5   Synthesis of chlorophyll-binding proteins

The core proteins of PSI (PsaA, PsaB) and PSII (D1, D2, CP43 and CP47) are the main Chl-binding proteins present in cyanobacteria (Fig. 3). They are synthesized on membrane bound ribosomes and the insertion of elongating nascent chain into thylakoid membrane occurs co-translationally (Chua *et al.*, 1976; Kim *et al.*, 1994; Tyystjarvi *et al.*, 2001). To be integrated and folded into the correct conformation, Chl-proteins require the assistance of a translocon system but our knowledge about this process in cyanobacteria is rather scarce. However, many aspects of translocon-assisted insertion of proteins into membranes have been studied in model bacteria (Dalbey *et al.*, 2011). Briefly, the first hydrophobic segment of nascent chain released from cytosolic ribosome is recognized by a conserved signal recognition particle (SRP). The ribosome-SRP complex is then targeted to the membrane bound FtsY receptor and then transferred to the translocon apparatus. It usually includes SecYEG translocon and YidC insertase, which is essential for the insertion and correct folding of various membrane proteins (Dalbey *et al.*, 2011). The role of YidC is not clear yet, but it has been suggested to support the partitioning of trans-membrane segments into the lipid bilayer and to facilitate the folding of nascent membrane proteins (Nagamori *et al.*, 2004).

The main difference between insertion of non-Chl and Chl-binding membrane proteins is the crucial role of Chl for the completion of translation and also for the correct incorporation into the membrane. For correct Chl-protein folding the co-translational insertion of Chl appears to be a prerequisite (Eichacker *et al.*, 1996; Muller and Eichacker, 1999). Moreover, de novo Chl is the strict requirements for the synthesis of trimeric PSI (Kopečná *et al.*, 2012) and the antenna proteins of PSII (CP43 and CP47), though the CP47 protein is more sensitive to de novo Chl than the CP43. On the contrary, the synthesis of D1 and D2 subunits is maintained in strains with drastically reduced de novo Chl biosynthesis. Therefore, it is possible that the short-living D1/D2 subunits are synthesized utilizing the same pool of Chl molecules, this pool is however not sufficient or available for the synthesis of other Chl-proteins (Knoppová *et al.*, 2014 ; Fig.5).
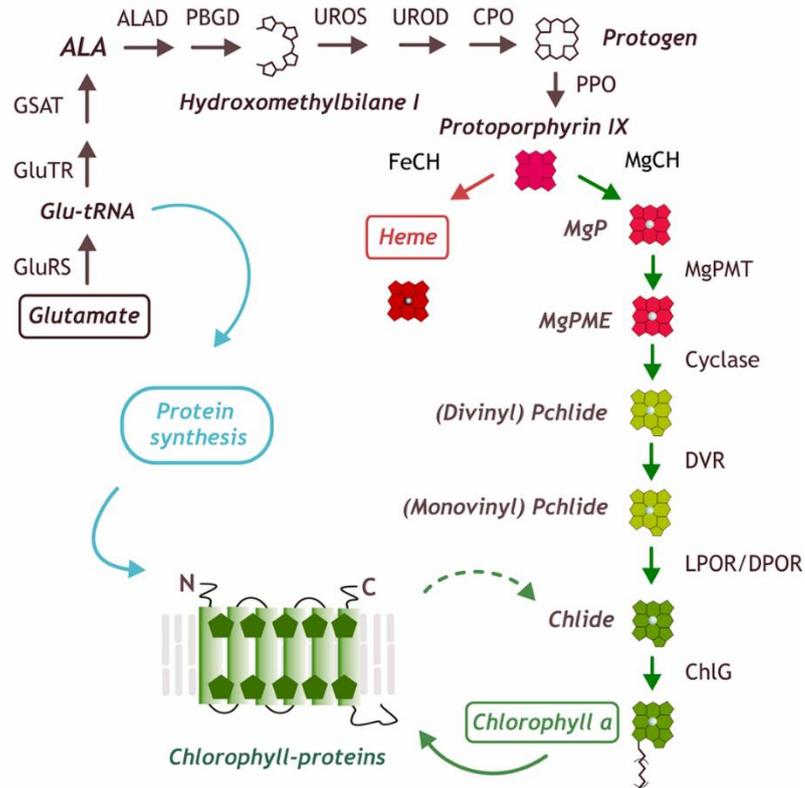
Figure 4. **A scheme of the tetrapyrrole biosynthetic pathway in cyanobacteria including Chl-reutilization cycle and the interconnection with Chl-protein synthesis**. Abbreviations of enzymes: GluRS, glutamyl-tRNA synthetase; GluTR, glutamyl-tRNA reductase; GSAT, glutamate-1-semialdehyde aminomutase; ALAD, ALA dehydratase; PBGD, porphobilinogen deaminase; UROS uroporphyrinogen III synthase; UROD, uroporphyrinogen III decarboxylase; CPO, coproporphyrinogen III oxidase; PPO, protoporphyrinogen oxidase; FeCH, ferrochelatase; MgCH, Mg-chelatase; MgPMT, Mg-protoporphyrin IX methyltransferase; Cyclase, Mg-protoporphyrin IX monomethyl ester oxidative cyclase; DVR, divinyl-(proto)chlorophyllide reductase; LPOR light-dependent protochlorophyllide oxidoreductase; DPOR, light-independent protochlorophyllide oxidoreductase; ChlG, Chl-synthase. Abbreviations of intermediates: Glu-tRNA, glutamyl-tRNA(Glu); MgP, Mg-protoporphyrin IX; MgPME, Mg-protoporphyrin IX monomethyl ester; Pchlide, protochlorophyllide. Modified from (Sobotka, 2014).

How the machinery for the synthesis of Chl protein is organized, remains unclear. Based mostly on indirect evidence, the presence of a large biosynthetic center in cyanobacteria is hypothesized, which would allow fast channeling of Chl precursors and thereby reduce the chance to losing control over these toxic compounds (Sobotka, 2014). Moreover, the tight integration of this complex to photosystem assembly machinery would ensure a control over insertion of Chl molecules into apoproteins. Although, the connection between Chl and PSII protein synthesis are reported in previous articles (Dobáková *et al.*, 2009; Schottkowski *et al.*, 2009) , their mechanism of interaction was not clear until

the report of Chidgey *et al.*, (2014). The authors co-purified Chl-synthase enzyme with YidC insertase that plays an important role in the synthesis of membrane proteins. This work has provided a first convincing evidence of linkage between proteosynthesis and Chl biosynthesis (Chidgey *et al.*, 2014). Purified Chl-synthase was also associated with Hlips (HliC and HliD) and with a putative alcohol dehydrogenase Ycf39, which is known to associate (together with HliC/D) also with the newly synthesized D1 protein (Knoppová *et al.*, 2014). These results led to a model describing the synthesis of D1 protein (Fig. 5) and this scheme might be valid for other Chl-proteins as well. The model suggests that the Chl-proteins are synthesized by ribosomes docked on the SecY-YidC translocons and Chl molecules are inserted into the newly synthesized Chl-proteins directly from Chl-synthase, which is physically bound to YidC insertase. This process is assisted by assembly factors such are Ycf48 (Fig. 5) or Pam68, both proteins facilitating Chl insertion (Yu *et al.*, submitted; Bučinská *et al.*, 2018) and by Hlips (Knoppová *et al.*, 2014).
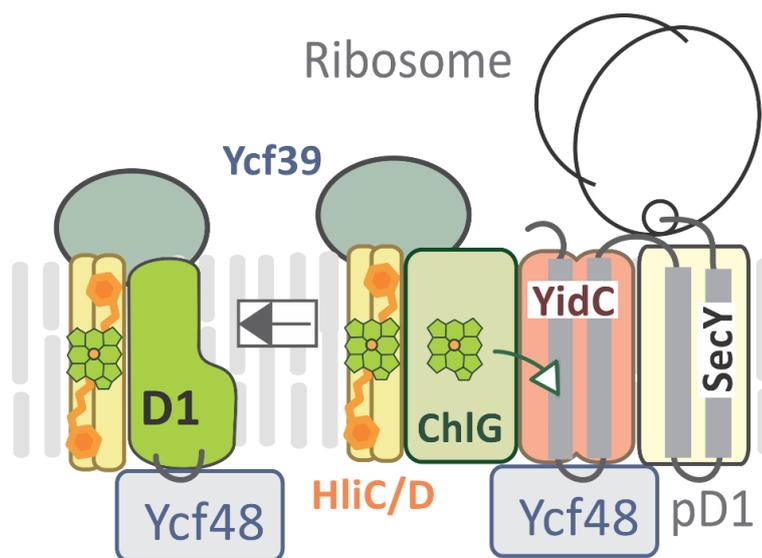
Figure 5. A working model of the D1 protein synthesis in *Synechocystis*. Translated D1 protein is inserted into the membrane via SecY translocon. Chl-synthase loads Chl into the nascent proteins and the finalized, fully pigmented D1 module is released into the lipid bilayer, where it is protected by Hlips. This process is assisted by the lumenal Ycf48 protein (Yu *et al.*, submitted) and the stromal Ycf39 protein; the later one docks two Hlips (HliC/D) on the newly-synthesized D1 (Knoppová *et al.*, 2014).

1.6 Hlips – an ubiquitous cyanobacterial protein family

As already noted Hlips are one helix proteins which show an obvious similarity with the first and third helix of plant and algae LHC including the conserved Chl a/b (Cab) binding

motif - a signature of the whole LHC superfamily (Jansson, 1999). A first gene coding for a Hlip (*hliA*) has been identified in the cyanobacterium *Synechococcus* PCC 7942 before fully sequenced cyanobacterial genomes become available (Dolganov *et al.*, 1995). The expression of the reported *hliA* gene was strongly induced by high light conditions (Dolganov *et al.*, 1995), a feature that gave the name to the whole Hlip family. The sequencing of cyanobacterial genomes has later revealed that virtually all cyanobacteria, ranging from marine to freshwater species, possess genes coding for Hlips; however, their numbers are variable. For example, the marine cyanobacterium *Prochlorococcus* MED4 contains more than 20 *hli* genes (Bhaya *et al.*, 2002) and even the primitive thylakoid-less cyanobacterium *Gloeobacter violaceus* contains at least five genes encoding Hlip homologs. Since, *Synechocystis* has been used as a bench mark model for illustrating the function of Hlips (including this thesis), it is important to discuss here the current knowledge of Hlips in this strain.

The *Synechocystis* genome encodes four small Hlips, which are designated as HliA-D (Fig. 6). Another Hlip (domain), which is most similar to HliC, is fused with the C-terminus of ferrochelatase enzyme and this fusion is a typical feature of ferrochelatases from all groups of oxygenic phototrophs (Sobotka *et al.*, 2011). The expression of all four genes coding for Hlips (*hliA-D*) is elevated under high light conditions, however, their expression is induced by low temperature as well as by various nutrient deficiencies such as low iron, carbon, nitrogen or phosphorus (Kopf *et al.*, 2014). In this sense the designation 'High light induced' is a bit misleading.

Although *hli* genes are generally stress-responsive, the expression follows a characteristic up-and-down pattern. For instance, after a shift to high light the expression of all *hli* genes is massively increased in 30 min, reaching a maximum in 1-2 hours, but then the expression ceases (Dolganov *et al.*, 1995; Xu *et al.*, 2004). A fast accumulation is manifested also on the protein level. After a stress treatment, the Hlips are detectable in a few minutes (Komenda J., personal communication), and high levels of Hlips are present in the cell much longer during stress (12 h) even the expression is lowered (He *et al.*, 2001). On the other hand, it appears that the individual *Synechocystis hli* genes are expressed differently. Particularly, the expression pattern of *hliA* and *hliB* is fairly similar but the expression of *hliC* and *hliD* genes react differently on different nutrient deficiencies and also HliC and HliD proteins show different stability during and after applying a stress (He *et al.*, 2001; Kopf *et al.*, 2014). This is an important observation

because quite similar amino-acid sequences of *Synechocystis* Hlips (Fig. 6) could imply that these are redundant copies with the same function but the obtained expression data argue against such view.

Synechocystis mutants lacking Hlips were created more than 15 years ago (He *et al.*, 2001) but single mutants (lacking a single Hlip) exhibited subtle or no obvious phenotypes under various light regimes (He *et al.*, 2001; Xu *et al.*, 2004). On the other hand, strains lacking all four Hlips proteins (or five including the ferrochelatase Hlip domain) were clearly sensitive to high light or treatment with stress-inducing chemicals such a methyl viologen (He *et al.*, 2001; Storm *et al.*, 2008). It has been concluded that the lack of one or two Hlips is tolerated in *Synechocystis* under high irradiance. Most of the later studies on Hlips have been performed using *Synechocystis* mutants lacking all four/five Hlips, often combined with PSI/PSII-less genetic backgrounds (Xu *et al.*, 2004; Vavilin *et al.*, 2007). This approach identified a connection between Hlips and Chl metabolism and indicated a complex regulatory function of Hlips but along with a little progress in understanding the molecular mechanisms behind their stress-protective role.
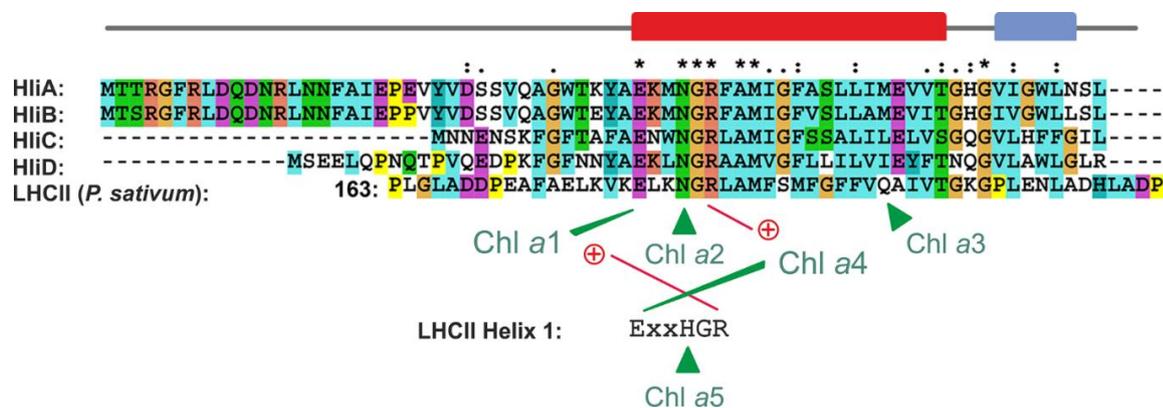

Figure 6. Amino acid sequence alignment of *Synechocystis* Hlips and the third trans-membrane helix of the pea LHCII protein. Chl-binding sites within the conserved Chl-binding motif are highlighted; Chls are named according to nomenclature from Standfuss *et al.*, (2005). LHC Chl a_1 and a_4 are ligated by charge-compensated ion-pairs between a Glu side-chain carboxylate of one LHCII helix and an Arg guanidinium group of another (Kuhlbrandt *et al.*, 1994; Hoober *et al.*, 2007) – note that these residues are conserved in Hlips. On the other hand, Chl a_3 is ligated by a Gln residue that is not conserved in Hlips. Boxes above the alignment indicate trans-membrane (red) and amphipathic (blue) α-helices (adapted from Shukla *et al.*, 2017; **Result III**).

Identification of Hlip-interacting proteins, isolation of pure Hlips and recently described phenotypes of single mutants lacking HliC and HliD (see later) draw first contours of how Hlips work. Given their small size and strong hydrophobicity, the exploring Hlip

interactome is a challenging and is still continuing task. The first dedicated attempt to isolate Hlips has been performed by using *Synechocystis* strains expressing each Hlip fused with His-tag (He *et al.*, 2001). The fractionation of purified Hlips revealed that HliA and HliB proteins tend to migrate as a higher mass fraction (~ 100 kDa) while HliC and HliD form a lower mass heterodimer of ~ 50 kDa fraction (He *et al.*, 2001).

 Promnares and co-authors have demonstrated that the HliB protein is present in monomeric as well as dimeric PSII and also in the PSII core complexes lacking the CP43 subunit (Promnares *et al.*, 2006). In the same study, single particle analysis revealed the localization of the HliB at the periphery of PSII complex in the vicinity of the CP47 subunit (Promnares *et al.*, 2006). Interaction with PSII subunits was further confirmed by Yao *et al* (2007); three Hlips (HliA/B/C) were found to interact with CP47. As these three Hlips can be co-purified with the CP47 assembly module, Hlips probably bind to newly synthesized CP47 and the CP47 module including Hlips is then integrated into PSII (Bučinská *et al.*, 2018). In contrast, the HliD protein was never associated with CP47 or with fully assembled PSII.

Applying the 3xFlag epitope for the isolation of protein complexes from *Synechocystis* have let to important discoveries. The putative dehydrogenase Ycf39 mentioned earlier was isolated using this approach in a complex with the PSII assembly intermediate RCII containing the D1/D2 core, the Ycf48 protein and also HliC and HliD proteins (Fig. 5). This complex was named RCII* (Knoppová *et al.*, 2014). It was shown that the Ycf39 is tightly attached to a HliC/D hetero-oligomer and the presence of this small subcomplex is somehow implicated in the regulation of the delivery of Chl molecules to PSII D1/D2 core subunits (Knoppová *et al.*, 2014). In a parallel study, Flag-tagged Chl-synthase was purified with HliD and HliC and a larger assembly complex containing YidC and Ycf39 was also described (Chidgey *et al.*, 2014). Importantly, both studies have shown that HliC/D proteins are yellow-green colored when separated on the native-gel electrophoresis and a detail analysis of the pigment-Hlip interaction was a part of my PhD project.

1.7   Binding of pigments to Hlips in a dissipative configuration

In mid of nineties Kuhlbrandt *et al.*, (1994) determined the structure on plant LHCII at 3.4 Å resolution, showing for the first time how Chl-*a/b* and carotenoid molecules are bound to these most abundant membrane proteins on Earth. The structure revealed a

highly conserved ExxH/NxR motif that co-ordinates four Chl-*a* molecules (see Fig. 1 and Fig. 6). The positively charged guanidinium group of the arginine side chain from one helix is placed in juxtaposition to the negatively charged glutamic acid side chain of the other helix and co-ordinates two Chls. Asn and His residues positioned between Glu-Arg pairs ligate another two Chl molecules (Fig. 6).

The ability of this motif to ligate Chl molecules has been verified experimentally. Eggink and Hoober (2000), created a 17-amino-acid long synthetic peptide containing the ExxHxxR motif which was able to bind two Chl molecules. According to molecular modeling the peptide is not structured and can form an intra-molecular loop, by the electrostatic pairing of Glu and Arg, from which is exposed the side chain of His (Eggink and Hoober, 2000). In LHC the motif is, however, a part of the transmembrane helix and the conserved Glu and Arg residues are spatially too far apart to form such a pair on a single helix. It means that two helices must interact via Glu-Arg salt bridges to create a functional four Chl-binding motif (Fig. 1; Fig. 6).

Given the presence of ExxH/NxR in Hlips, their potential to bind Chl molecules was speculated from their discovery (Xu *et al.*, 2004). As mentioned above, the fact that HliC/D proteins are associated with pigments were spotted first on the native electrophoresis (Knoppová *et al.*, 2014) but the first detailed study was conducted by Staleva *et al.*,(2015; **Result I**). The authors isolated Hlips via a Flag-tagged version of Ycf39 using a buffer system that let to dissociation of the RCII* complex. It allowed obtaining a pure Ycf39-HliC/D complex. Since, the Ycf39 does not bind pigments, all the pigments of this complex were associated specifically with Hlips. It showed that HliC/D contain Chl and β-carotene in the 3:1 ratio and, expecting dimer as a minimal possible configuration for pigment binding, it is expected 6 Chls and 2 β-carotenes per dimer (Staleva *et al.*, 2015; **Result I**). Interestingly, two different populations of β-carotene associated with Ycf39-Hlips complex were identified by Raman spectroscopy; one population clearly exhibiting red-shifted absorption spectra (520 nm; (Llansola-Portoles *et al.*, 2017; **Result II**). This is indeed intriguing given the prediction that Hlips are organized as dimers exhibiting 2D symmetry (see Fig. 7).

The drawback of immuno-affinity chromatography used for the preparation of Ycf39-Hlips complex is its high cost and relatively low yield. We later developed a cost-effective His-tag approach for the isolation of HliC protein in a purity and quantity required for state-of-art spectroscopic techniques such as Raman spectroscopy (Shukla

et al., 2017; **Result III**). In this work the His-HliC eluted from a nickel column was analysed also using 2D clear-native/SDS electrophoresis which demonstrated very stable dimer of HliC, partially preserved even after denaturing SDS electrophoresis. Analysis of pigments bound to the HliC revealed Chls and carotenoid ratio 2:1, which differs from the 3:1 ratio obtained for the HliD protein (Staleva *et al.*, 2015).

Probably the most fascinating discovery regarding Hlips is their ability to dissipate the absorbed light energy as heat, a process known as thermal dissipation or non-photochemical quenching (NPQ; (Staleva *et al.*, 2015; **Result I**; Hontani *et al*., **Result V**). NPQ is generally connected with photoprotection as a way how to safely dissipate excess of energy absorbed by photosynthetic pigments. In plants and algae, the NPQ is regulated by a sophisticated mechanism, which is not completely understood. Nonetheless, it is widely accepted that carotenoids bound to LHC proteins, and probably also to structurally similar minor PSII antennae, work as dissipaters (Holt *et al.*, 2005; Ruban *et al.*, 2007). LHCs have an inbuilt ability to switch from harvesting mode to dissipative mode most likely by subtle changes in protein/pigment conformation (Krüger *et al.*, 2014). How these changes are achieved is not known and even the molecular mechanism of energy dissipation is a matter of intensive research. There are incompatible models based on: a) reductive quenching of Chl-*a* excited state via electron transfer to the carotenoid (Holt *et al.*, 2005); b) singlet-singlet energy transfer from Chl *a* to carotenoids (Ruban *et al.*, 2007) or (c) on excitonic interaction between Chl *a* and carotenoids (Bode *et al.*, 2009).

The possible contribution of Hlips to NPQ in *Synechocystis* was hypothesized by (Havaux and Kloppstech, 2001) one and half decades ago but there was no evidence, until recently. Purified Hlips are strongly quenching Chl fluorescence, which can be detected even in native gel or in gel-filtration column after excitation by blue light (Staleva *et al.*, 2015; **Result I**; Niedzwiedzki *et al.*, 2016). Analysis of the Ycf39-Hlips complex by femtosecond absorption spectroscopy demonstrated the direct energy transfer from Q_y state of Chl *a* to S_1 state of carotenoids bound to HliD proteins. Interestingly, the S1 spectrum of the isolated β-carotene, excited at 530 nm, was matching with the one which was populated via Q_y-S_1 pathway. This suggests that only red shifted β-carotene population in Hlips is responsible for the quenching process. As further demonstrated by resonance Raman spectroscopy the red-shifted β-carotene has

highly twisted β-ring, which seems to provide a permanent energy channel (Llansola-Portoles *et al.*, 2017; **Result II**).
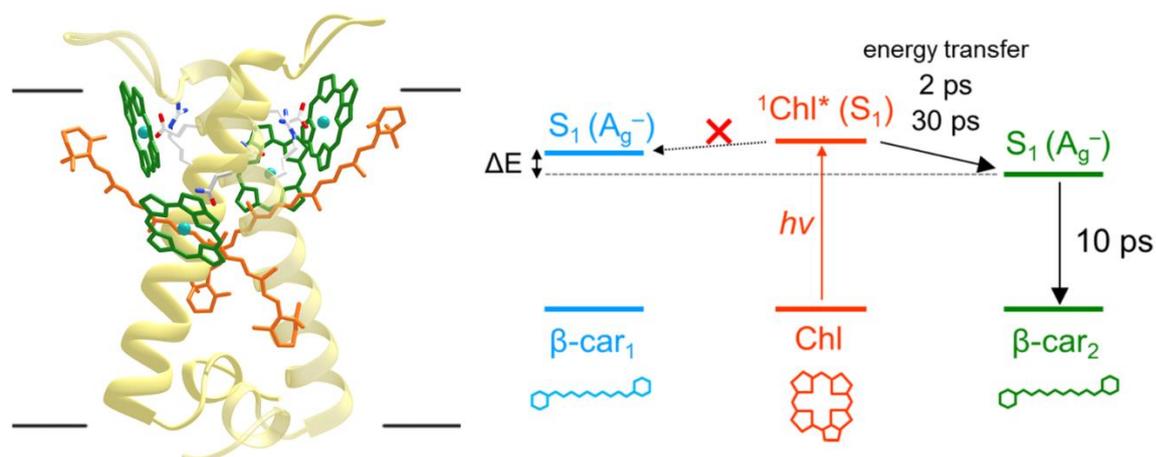

Figure 7. A structural model of the putative HliC dimer and the energy flow upon excitation of Chl. Left: Side view on the HliC protein along the membrane plane; for clarity, only porphyrin rings of Chl molecules are shown (Shukla *et al.*, 2017 ; **Result III**). Right: After excitation of Chl, excited-state energy transfer occurs specifically to the lower energy (red-shifted) β-carotene (β-car2) in 2 and 30 ps. The decay of the S1 state β-car2 proceeds in 10 ps. The higher-energy β-car1 is not populated because of unfavourable energetic (Hontani *et al*., **Result V**).

The purified HliC protein (Shukla *et al.*, 2017; **Result III**) shows an identical quenching mechanism but the quality and the concentration of sample allowed to analyze energy transfer by femtosecond stimulated Raman spectroscopy. Again, this work revealed that of the two β-carotenes bound to HliC, only one (red-shifted) is active in quenching the Chl excited state (Fig. 7). The S1 energy level of the active β-carotene is located substantially below that of the non-quenching β-carotene, which might be a key property in creating dissipative energy transfer pathways in closely confined Chl – carotenoid geometries. It is possible that the principle of quenching based on the lowering of carotenoid S1 energy is conserved in the whole LHC family (Hontani *et al*., **Result V**).

1.8   Are Hlips regulatory or photoprotective proteins?

Various functions have been ascribed for these small, pigment-binding proteins to explain their stress-protective role. This includes the regulation of Chl biosynthesis, transient binding of pigment molecules, Chl turnover, scavenging of ROS or energy

dissipation during biogenesis of PSII complexes as reviewed in (Komenda and Sobotka, 2016).

As described above, Hlips accumulate very quickly (in minutes) in the cell once the environment becomes challenging. These proteins thus apparently act in first line as a fast anti-stress response before later stress-protective mechanisms are activated. Hlips (at least HliC and HliD) have capacity to bind Chls and carotenoids in a dissipative conformation and, very importantly, they can dissipate energy from the whole RCII* complex including Chls bound to D1/D2 proteins (Knoppová *et al.*, 2014). Moreover, HliA and HliB proteins bind to CP47 assembly modules of PSII (Bučinská *et al.*, 2018) and, again, they can serve as an energy dissipater for the whole module. These are arguments for the important role of Hlips in photoprotection and in scavenging of ROS. If induced by a stress, Hlips quickly associate with PSII assembly/repair intermediates to prevent photooxidative damage. Moreover, they could trap the escaped free Chl molecules and thus also can act as temporary Chls reservoir (Vavilin *et al.*, 2007; Nixon *et al.*, 2010). However, many other results argue for an important (crucial) regulatory role of Hlips and the ability to perform NPQ might be rather a useful feature how to deal with Chl molecules/proteins than a primary function.

The regulatory role of Hlips has been first reported in the regulation of tetrapyrrole pathway. Xu and co-workers employed a *Synechocystis* strain (PSI-less/Δ*chL*), which can be almost completely devoid of Chl in dark and then the process of re-greening can be monitored after shift to light. The deletion of *hliA* or *hliB* genes against this genetic background has a little impact on either the total level of Chl or its precursors whereas the deletion of *hliC* or *hliD* genes causes remarkably changed dynamics of Chl re-accumulation (Xu *et al.*, 2002; Yao *et al.*, 2007). Interestingly, the HliC protein seems to be also the crucial *Synechocystis* Hlip for Chl recycling as the elimination of this protein in the PSI-less strain reduces the Chl half-life to ~40 %, whereas it drops to only ~ 70 % after deletion of both *hliA* and *hliB* genes. (Vavilin *et al.*, 2007).

A part of my work has therefore been focused on the regulatory role of HliC. We found that under optimal growth conditions the Chl-synthase is organized as a mixture of monomers and dimers associated with HliD proteins (Shukla *et al.*, **Result IV**). This pattern however quickly changes under stress conditions. The accumulated HliC protein hampers the formation of oligomeric Chl-synthase-HliD assemblies and re-organizes it into the smaller monomeric Chl-synthase-Hlip complexes (see Fig. 8 for a scheme).

Moreover, HliC/D heterodimers also disrupt the Ycf39 dimers, perhaps by a similar principle. (Shukla *et al.*, **Result IV**). I speculate that both Chl synthase and Ycf39 interact with the N-terminal part of HliD but not with very short N-terminus of HliC. The HliC/D heterodimers thus, are capable to stably attach to one copy of Chl synthase and Ycf39.
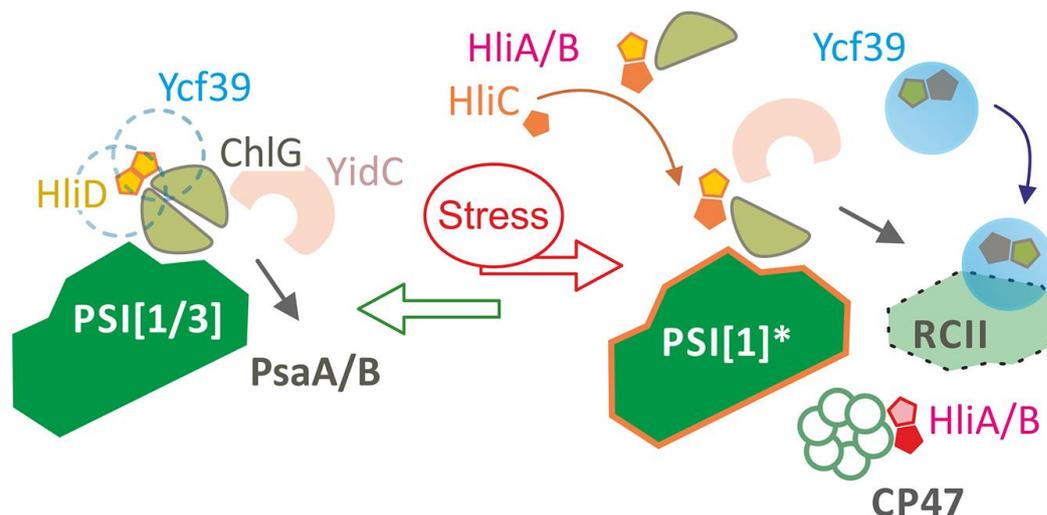

Figure 8. A working model of the regulation and photoprotection of photosystem biogenesis by Hlips. Under low stress, the produced Chl molecules are distributed mostly into the synthesized PsaA/B subunits of PSI (Kopečná *et al.*, 2012). ChlG-HliD complexes are organized as oligomers docked to trimeric or to monomeric PSI and can be also associate with Ycf39, most likely with its dimeric form. The HliC protein quickly accumulates if the growth conditions become challenging and the formed HliC/D heterodimers replace HliD homodimers in ChlG complexes. HliC, however, does not physically interact with ChlG, which causes melting of ChlG oligomers and releasing of the Ycf39 protein (Shukla *et al*., **Result IV**). On the other hand, the resulting monomeric ChlG-HliC/D complexes can be attached to a low abundant form of PSI (PSI[1]*; REF), which might participate in Chl re-utilization. The HliC/D pairs also associate with Ycf39 and are docked to the newly synthesized RCII assembly intermediates (Knoppová *et al.*, 2014). We hypothesize that during intensive PSII repair this mechanism ensures a sufficient production of the Hlip-protected D1/D2 assembly modules by utilizing Chl molecules from degraded proteins. Similarly, the HliA/B proteins accumulate during stress conditions and bind to newly synthesized CP47 assembly module (Bučinská *et al.*, 2018). However, if they thus photoprotect the CP47, it remains to be elucidated.

The biological role of Ycf39 and the reason this protein associates with Chl-synthase is not clear yet. However, connections between Ycf39, Hlips, PSII core proteins and Chl-synthase suggest that the Ycf39 plays an important role in the delivery of Chls to the newly synthesized D1/D2 subunits. Knoppová *et al.*, (2014) reported a positive role of Ycf39 on the synthesis of RCII complexes specifically after inhibition of the tetrapyrrole pathway by gabaculine. This is indeed in agreement with a putative role of the Ycf39-Hlip complex in Chl turnover/delivery. Under stress conditions, the turnover of D1

protein is fast and it is known that the synthesis of D1/D2 proteins can almost fully rely on the 'recycled' Chl molecules (Hollingshead *et al.*, 2016). The main role of Ycf39-Hlips might be to maintain a (quenched) pool of Chls around the synthesized D1 and D2 core proteins, particularly under stress conditions when the *de novo* Chl biosynthesis is very limited align with an intensive repair of PSII (Shukla *et al*., **Result IV**; Fig. 8). When the PSII repair is not so intensive, the cell need to synthesize other (large) Chl-binding proteins. In this condition, the association of the Ycf39-Hlips complex with RCII might be needless (e.g. impeding fast PSII assembly) and the pool of Ycf39 is stored on the Chl-synthase complexes.

The previous data indicate an interaction between Hlips (HliA/B) and PSI, however, the finding is still on scrutiny (Komenda and Sobotka, 2016). Interestingly, a high level of PSI trimers and monomers were co-isolated with Chl synthase, a finding that cannot be explained by a contamination of the pulldown (Shukla *et al*., **Result IV**). Under stress conditions the Chl synthase-Hlip complex interacts also with an low-abundant monomeric PSI designated as PSI[1]* (Chidgey *et al.*, 2014). Notably, the interaction between PSI[1]* and Chl synthase seems to be abolished if the *hliC* gene is deleted (Fig. 8; Shukla et al., **Result IV**). It is in line with other data that Hlips as well PSI complexes could act as temporary reservoirs of Chl molecules available under harsh conditions for the PSII repair.

The remaining *Synechocystis* Hlips, HliA and HliB, are clearly connected with the biogenesis of the CP47 assembly module (Ref, see Fig. 8). It is however not known yet, whether these two Hlips are able to associate with pigments, and if so, are they able to quench Chl molecules incorporated into the CP47 protein. Intriguingly, the HliC protein can bind to HliB, most likely by replacing the HliA (Komenda J, unpublished data). As discussed earlier, the HliA/B proteins are stress-induced but the expression pattern differs from the HliC (He *et al.*, 2001; Kopf *et al.*, 2014). Therefore, I'm tempting to speculate that the HliC might also modulate proteins interacting with the N-terminal regions of a HliA/B heteromer.

2 SUMMARY

Although it was speculated that the cyanobacterial High light inducible proteins (Hlips) bind pigments, the first convincing evidence was demonstrated in the work of Staleva *et al.,* (2015, **Result I**). Using Flag-tagged version of the putative alcohol dehydrogenase Ycf39, we isolated this protein in a small complex with Hli protein HliD from the cyanobacterium *Synechocystis* PCC 6803. This complex was associated with chlorophylls (Chls) and β-carotene pigments in 3:1 ratio. As the Ycf39 itself does not bind pigments, all pigments were associated with HliD. Analysis of this complex by femtosecond transient absorption spectroscopy revealed the direct transfer of energy from Q_y state of Chl to S_1 state of β-carotene. Hlips are most likely the ancestors of the light harvesting antennae (LHC) of algae and plants and the described quenching mechanism might therefore operate in the whole LHC family.

In the publication of LIansola-Portoles *et al.*, (2017; **Result II**), we analysed Ycf39-HliD complex by resonance Raman spectroscopy. The results demonstrated that the HliD protein binds two different β-carotene populations, one with a highly twisted β-ring. This flat conformation suggests an increase in the conjugation length and consequently lowers the S_1 energy state. We suggest that this twisted conformation of β-carotene with low S_1 energy opens a permanent energy dissipation channel for the absorbed light energy.

A cost effective protocol for the isolation of another Hli protein HliC from the cyanobacterium *Synechocystis* 6803 was described in Shukla *et al.*, (2018; **Result III**). The isolated HliC forms a stable dimer, partially preserved even after denaturing SDS electrophoresis and binds Chls and carotenoids in 2:1 ratio. Analysis of the pure HliC complex by transient Raman spectroscopy revealed that at least one Chl molecule in the HliC proteins has distorted macrocycle. We observed two populations of β-carotene, one with distorted macrocycle similarly to previously described HliD protein.

The regulatory role of the stress induced HliC protein was explored in Shukla, *et al.*, **(Result IV)**. Under optimum growth conditions, the chlorophyll synthase enzyme (Chl-synthase) forms a pigmented protein complex with HliD protein and they can contain one or two copies of Chl synthase per a putative HliD dimer. The Ycf39 protein, an assembly factor of Photosystem II mentioned earlier, can also bind to Chl-synthase-HliD complex. However, under the stress conditions, the Chl-synthase associates with a heterodimer of HliC-HliD proteins rather than with HliD only. And as the HliC cannot

physically interact with Chl-synthase, the HliC-HliD pair disrupts the dimeric organization of Chl-synthase complex and all bound Ycf39 is released from the Chl-synthase-HliD complex. Instead, the Ycf39 forms a small complex with HliC-HliD heterodimers, which is required for the repair of Photosystem II. We speculate that the Ycf39-HliC/D complex facilitates the delivery of (quenched) Chl molecules to the newly synthesized Photosystem II core proteins.

In the last manuscript (Hontani et al., **Result V**) we collaborated with the group of Prof. John Kennis (VU Amsterdam) on the analysis of purified HliC protein by femtosecond stimulated Raman spectroscopy. Upon Chl excitation a 2-ps rise of the C=C stretch band of the S_1 state of β-carotene was observed demonstrating energy transfer quenching and fast excess-energy dissipation. This work confirmed two distinct β-carotene conformers in Hlips and verified that only the β-carotene whose S_1 energy level is significantly lowered is involved in quenching. It implies that the low carotenoid S_1 energy that results from specific pigment-protein or pigment-pigment interactions is the key property for creating a dissipative energy channel.

3   RESULTS

3.1   Result I

Mechanism of photoprotection in the cyanobacterial ancestor of plant antenna proteins

Staleva, H., Komenda J., **Shukla, M.K.**, Šlouf, V., Kana, R., Polívka, T., Sobotka, R. Nature Chemical Biology, 2015, 11:287-291.

Mechanism of photoprotection in the cyanobacterial ancestor of plant antenna proteins

Hristina Staleva[1], Josef Komenda[1,2], Mahendra K Shukla[1,2], Václav Šlouf[1], Radek Kaňa[1,2], Tomáš Polívka[1,3] & Roman Sobotka[1,2]*

Plants collect light for photosynthesis using light-harvesting complexes (LHCs)—an array of chlorophyll proteins that are able to reversibly switch from harvesting to energy-dissipation mode to prevent damage of the photosynthetic apparatus. LHC antennae as well as other members of the LHC superfamily evolved from cyanobacterial ancestors called high light–inducible proteins (Hlips). Here, we characterized a purified Hlip family member HliD isolated from the cyanobacterium *Synechocystis* sp. PCC 6803. We found that the HliD binds chlorophyll-*a* (Chl-*a*) and β-carotene and exhibits an energy-dissipative conformation. Using femtosecond spectroscopy, we demonstrated that the energy dissipation is achieved via direct energy transfer from a Chl-*a* Q_y state to the β-carotene S_1 state. We did not detect any cation of β-carotene that would accompany Chl-*a* quenching. These results provide proof of principle that this quenching mechanism operates in the LHC superfamily and also shed light on the photoprotective role of Hlips and the evolution of LHC antennae.

All photosynthetic organisms have to cope with unpredictable changes in light intensity as overexcitation of photosystems results in generation of reactive oxygen species. To prevent this, the LHCs of plants and algae have an inbuilt ability to switch from light harvesting to a quenching state in which energy is dissipated. Although researchers have proposed multiple molecular mechanisms that directly involve a carotenoid molecule to explain the principle of energy dissipation in LHCs, the mechanics behind this process remain unconfirmed. Scientists have suggested reductive quenching of the Chl-*a* excited state via electron transfer to carotenoid[1], energy transfer quenching through energy transfer from Chl-*a* to carotenoid[2] and quenching due to excitonic interaction between Chl-*a* and carotenoid[3] in plants. Researchers observed the reductive quenching *in vivo*, but for the individual LHCs, they observed a low yield of carotenoid radical formation only in minor LHCs and have not yet reported reductive quenching in major LHCII antenna[4,5]. Researchers have proposed that the quenching attributed to excitonic interaction operates both *in vivo* and in isolated LHCs[3], whereas they proposed that energy transfer quenching works mainly in isolated complexes[2,6] even though others have challenged the experimental evidence for this mechanism[7]. Thus, the quenching mechanism operating at the level of individual LHCs remains an open question.

Cyanobacteria harvest light predominantly using phycobilisomes, but they also have a family of Hlips that are considered ancestors of the whole LHC superfamily[8–10]. Hlips are small (~7 kDa), single-helix proteins that exhibit similarity to the first and third helix of plant LHC antenna and have a characteristic Chl-*a*–binding motif conserved in the whole LHC superfamily[8,10]. Genes encoding Hlips are common in cyanobacterial genomes and are strongly expressed under various stress conditions[11], but their exact role in the cell is mostly unknown. Hlips most likely have a photoprotective function[12] during various processes that deal with Chl-*a* molecules, including synthesizing Chl-binding proteins[13], recycling Chl-*a*[14] and assembling photosystem II[15]. We have shown recently in the cyanobacterium *Synechocystis* sp. PCC 6083 that two

Hli proteins named HliD and HliC assist in synthesizing photosystem II's functional core. Particularly, we identified these Hlips as components of a larger protein complex designated RC*, which consists of the photosystem II assembly intermediate RCa and the Ycf39 protein belonging to short-chain dehydrogenase/reductase superfamily[16]. Notably, a subcomplex consisting of Ycf39 and Hlips as well as Hlips alone partially dissociated from RC* during native electrophoresis and migrated as pigmented bands[16]. Here, we purified the Ycf39–HliD subcomplex and demonstrated that HliD binds Chl-*a* with β-carotene and dissipates absorbed energy via direct energy transfer from the Chl-*a* Q_y state to the β-carotene S_1 state. These results provide proof of principle that the carotenoid-induced Chl-*a* quenching achieved via energy transfer can operate in LHC superfamily. Because we proved this quenching in a Hlip, the ancestor of the whole LHC superfamily, we hypothesize that the mechanism of LHC-based nonphotochemical quenching may be an ancient cyanobacterial invention redesigned later by algae and plants for the control of light harvesting.

RESULTS

HliD protein binds Chl-*a* and β-carotene pigments

To determine the composition of pigments attached to Hlips, we employed 3×Flag-tagged Ycf39 (f.Ycf39) and isolated an almost pure yellowish f.Ycf39–Hlip complex (**Fig. 1a** and **Supplementary Results**, **Supplementary Fig. 1a**). Although analysis of the eluate by MS revealed the presence of HliC (**Supplementary Table 1**), HliD was the only Hli protein detectable in the preparation by the two-dimensional gel (**Supplementary Fig. 1b**), and deletion of the *hliC* gene caused no apparent difference in size or pigmentation of the purified complex (**Supplementary Fig. 1c**). Because we have previously found no pigmentation of the isolated Hlip-free f.Ycf39 protein[16], we concluded that the HliD alone bound all pigments in the purified complex, which we termed the f.Ycf39–HliD complex.

Native electrophoresis demonstrated that f.Ycf39–HliD quenched chlorophyll fluorescence in a way that is comparable to the quenching in the trimeric photosystem I (**Supplementary Fig. 2**), and the

[1]Faculty of Science, University of South Bohemia, České Budějovice, Czech Republic. [2]Institute of Microbiology, Academy of Sciences of the Czech Republic, Třeboň, Czech Republic. [3]Biology Centre, Institute of Plant Molecular Biology, Academy of Sciences of the Czech Republic, České Budějovice, Czech Republic. *e-mail: sobotka@alga.cz
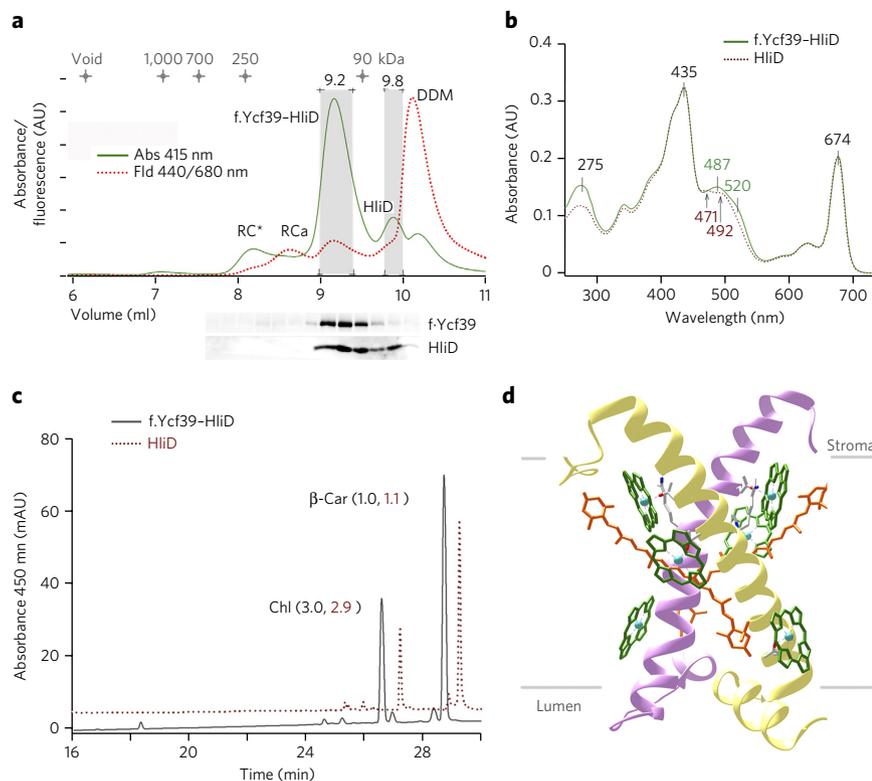
Figure 1 | Biochemical characterization of the f.Ycf39–HliD complex. (**a**) Gel filtration of the f.Ycf39–HliD pull-down assay. Pigments eluted from the column were detected by absorbance and by Chl-*a* fluorescence (Online Methods); collected fractions were subjected to immunoblot analysis. AU, arbitrary units; RC*, photosystem II reaction center associated with Ycf39–HliD. RCa, photosystem II reaction center; DDM, dodecyl-β-maltoside. (**b**) Absorption spectra of f.Ycf39–HliD and HliD as recorded by a diode-array detector. (**c**) HPLC analysis of pigments co-eluted with f.Ycf39–HliD and HliD and extracted from pooled fractions (indicated by gray columns in **a**). The calculated molar stoichiometry of Chl-*a* (Chl) and β-carotene (β-Car) is shown in parentheses. (**d**) A structural model of the putative HliD dimer with bound Chl-*a* and carotenoid pigments shown as a side view along the membrane plane. Model was prepared using the crystal structure of pea LHCII[18] and thus contains xanthophyll lutein instead of the β-carotene that should be present in the HliD structure. For clarity, only porphyrin rings of Chl-*a* molecules are shown.

Chlorophyll-to-carotenoid energy transfer in HliD

To measure the Chl-*a* lifetime, we investigated the f.Ycf39–HliD complex by femtosecond transient absorption spectroscopy. We excited the complex at 620 nm to allow recording of absorption kinetics in the Q_y region (**Fig. 2**). The Chl-*a* signal exhibited multiexponential decay, and the magnitude of the initial bleaching decreased to less than 50% during the first 100 ps (**Fig. 2a**), confirming the efficient quenching of excited Chl-*a* observed in the native gel (**Supplementary Fig. 2**). To obtain information about excited-state dynamics, we fitted the whole spectro-temporal data set recorded in the 450–720-nm spectral window globally. To visualize the dynamics, we used a sequential model for the fitting, in which the initially excited state decays into other states with increasing lifetimes. The resulting spectra of individual states are depicted in **Figure 2b**. The first spectrum was clearly caused by Chl-*a* as it consisted of a sharp bleaching signal peaking at 675 nm because of the Q_y absorption band of Chl-*a* and the weak, featureless excited-state absorption extending from 450 nm to 650 nm. This Chl-*a* spectrum decayed in 2.1 ps to another state whose most interesting feature was the presence of a new band peaking at 580 nm, accompanied by a negative signal in the 450–520-nm region. Clearly, this signal was not associated with Chl-*a*; instead, such signals are typically observed when a carotenoid molecule is in its first excited state, S_1. The population of the carotenoid S_1 state is identified by its characteristic S_1-S_n excited-state absorption, which peaks in the 520–600-nm region[19]. Thus, the straightforward interpretation of the red spectrum in **Figure 2b** is that the 580-nm band is the S_1-S_n transition of β-carotene in the f.Ycf39–HliD complex. This assignment was further supported by the bleaching signal below 520 nm that matched the absorption profile of β-carotene in the complex. Appearance of the β-carotene signal monitored at the S_1-S_n maximum at 580 nm is shown in **Figure 2c**. The same kinetics were likewise obtained after direct excitation into the Q_y band at 670 nm (**Supplementary Fig. 4**). **Figure 2a** depicts decay of the Chl-*a* bleaching signal at 675 nm.

Associating the red spectrum in **Figure 2b** with the β-carotene S_1 state implies that we should obtain essentially the same S_1 spectrum if the carotenoid is excited directly. We thus measured transient absorption spectra after direct excitation of β-carotene at 490 and 530 nm (**Fig. 3a**). Whereas the S_1 spectrum of β-carotene excited at 490 nm differed from the spectrum obtained after Chl-*a* excitation, exciting β-carotene at 530 nm provided a reasonable match. Also, the bleaching regions of the spectra taken after 530- and 620-nm excitations were similar. Although the S_1 spectrum of β-carotene excited at 530 nm correlated with that obtained after Chl-*a* excitation (**Fig. 3a**), the lifetimes of the S_1 states were clearly different (**Fig. 3b**). The S_1 state of β-carotene populated via the Q_y-S_1 channel predominantly with a 12-ps time constant, but direct excitation of β-carotene led to <10-ps S_1 lifetimes (**Fig. 3b**). To provide deeper insight into the excited-state dynamics of β-carotene, we carried out full analysis of the data recorded after direct excitation
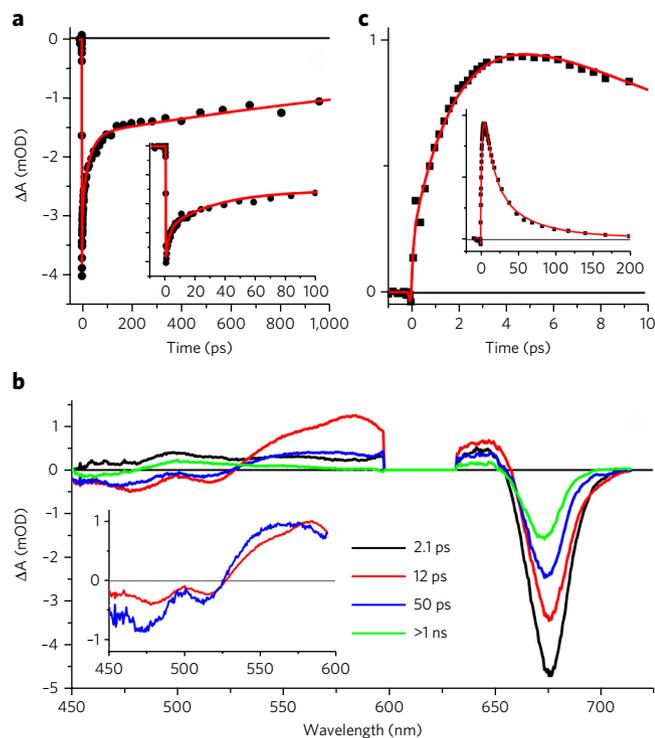
strong chlorophyll quenching was evident also during purification of the complex by gel filtration (**Fig. 1a**). The quantum yield of f.Ycf39–HliD fluorescence was ~0.01 (**Supplementary Fig. 3**). We eluted the f.Ycf39–HliD complex from the column with a relative molecular weight of ~100 kDa (f.Ycf39 = 39 kDa), and it exhibited chlorophyll (435 nm and 674 nm) and carotenoid absorbance (487 nm and 520 nm; **Fig. 1b**). Moreover, we observed the less abundant pigmented complex that eluted later, which also quenched chlorophyll fluorescence but had a slightly blue-shifted carotenoid absorbance (**Fig. 1a,b**). We believe that this peak represented an HliD oligomer dissociated from f.Ycf39–HliD (**Fig. 1b**); we also saw this 'free' HliD on the two-dimensional gel (**Supplementary Fig. 1**). The analysis of pigments co-eluted with f.Ycf39–HliD and HliD peaks showed that both complexes contained Chl-*a* and β-carotene with the ratio 3:1 (**Fig. 1c**). On the basis of the sequence similarity between LHCII antennae and HliD protein, we expect that at least two copies of HliD are essential for pigment binding in a 3:1 stoichiometry. In LHCII, two of four Chl-*a* bound to the conserved ExxH/NxR motif are coordinated by glutamate-arginine ion pairs[17,18], and to achieve such a configuration, the HliD protein has to form an oligomer. Therefore, we proposed a hypothetical model for HliD: a dimer containing six Chl-*a* and two β-carotene molecules (**Fig. 1d**).

28

Figure 2 | Transient absorption spectroscopy of the f.Ycf39–HliD complex. (**a**–**c**) The sample was excited into the Chl-*a* vibrational band at 620 nm. (**a**) Decay of the Chl-*a* signal monitored at the maximum of ground state bleaching at 675 nm. Inset: the dynamics within the first 100 ps. (**b**) EAD spectra obtained from global fitting of the data. The initially excited state (black EADS) decays in 2.1 ps to form the red EADS that has features of the β-carotene spectrum. Inset: normalized EAD spectra corresponding to two decay component of the S_1 state. (**c**) Kinetics showing the rise of the carotenoid signal at 580 nm after excitation of Chl-*a*. Inset: the dynamics at a longer timescale, demonstrating the decay of the β-carotene excited state.

of β-carotene in the f.Ycf39–HliD complex at 530 nm (**Fig. 3c**) or at 490 nm (**Supplementary Fig. 5**). For both excitations, the first evolution-associated difference spectrum (EADS) corresponding to the excited S_2 state of β-carotene decayed within 130 fs. The S_1 lifetimes of β-carotene in the f.Ycf39–HliD complex are readily determined from the time constants associated with the red EADS, which have the typical shape associated with the S_1 spectrum. The S_1 lifetimes obtained after direct excitation of β-carotene, 8.7 ps (excitation at 490 nm) and 5.9 ps (excitation at 530 nm), were markedly shorter than the S_1 lifetimes of β-carotene populated via Chl-*a* (12 ps; **Fig. 3b**). The fitting results shown in **Figure 2b** revealed the presence of slower channels characterized by the time constants of 12 ps and 50 ps, which both occurred with substantial amplitude in the Chl-*a* bleaching region.

The presence of the 12-ps time constant in the Chl-*a* bleaching region may be due to the fact that fitting the multiexponential decay of Chl-*a* can easily pick a time constant associated with the carotenoid decay (12 ps). To clarify this, we fitted the carotenoid and Chl-*a* regions separately (**Supplementary Fig. 6**). Indeed, although the carotenoid region must be fitted with both 12- and 50-ps time constants, which monitor decays of two spectrally distinct S_1 states, in the Chl-*a* bleaching region these two components merged into one 30-ps time constant that precisely reproduced the slower phase of Chl-*a* decay. Thus, the slower channel is most likely associated with 30-ps energy transfer from Chl-*a*, populating the spectrally distinct carotenoid S_1 state, whose lifetime is 50 ps.
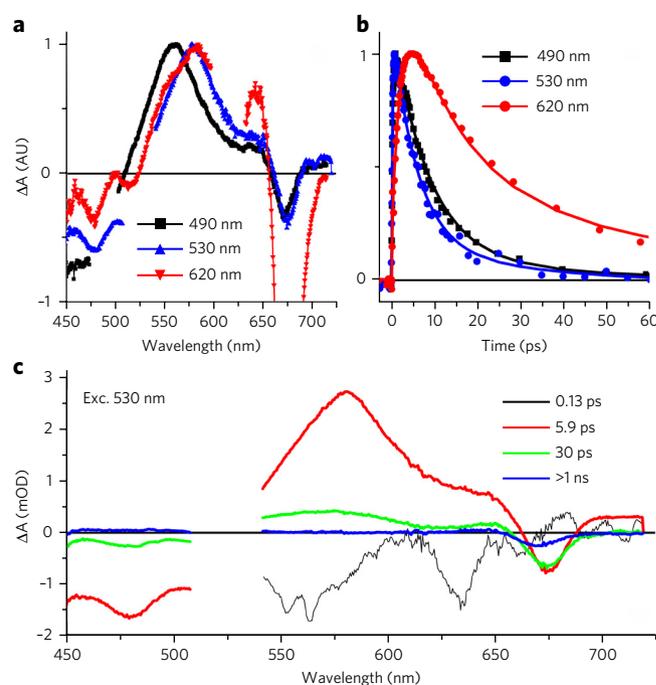

Figure 3 | Transient absorption data recorded after direct excitation of β-carotene. (**a**) Transient absorption spectra recorded at 3 ps either after direct excitation of β-carotene (490 and 530 nm) or after excitation of Chl-*a* (620 nm). The spectrum of β-carotene excited at 530 nm matches the spectrum of the β-carotene S_1 state populated from Chl-*a* excited at 620 nm. Spectra are normalized to the maximum of β-carotene excited-state absorption. (**b**) Kinetics monitoring the decay of β-carotene S_1 state after different excitation wavelengths. Decay of the β-carotene S_1 state populated via Chl-*a* (excitation at 620 nm) is substantially slower than that of the S_1 state populated by direct excitation of β-carotene at either 490 or 530 nm. (**c**) EAD spectra extracted from globally fitting the data recorded after direct excitation of β-carotene in the f.Ycf39–HliD complex at 530 nm (exc. 530 nm). The black EADS corresponds to the initially excited state (carotenoid S_2 state), and the red EADS has typical features of the S_1 state with the minor contribution of Chl-*a* bleaching caused by carotenoid-Chl energy transfer.

To test whether electron transfer between excited Chl-*a* and carotenoid, a process that has also been associated with quenching in photosynthetic systems[1], occurs in the HliD protein we recorded transient absorption spectra in the near-infrared region. The signal of a carotenoid cation would be expected to be in the 900–1,000-nm spectral range if such a mechanism were active in the HliD protein[20]. Because the spectra in the near-infrared region did not exhibit any hint of a carotenoid cation (**Supplementary Fig. 7**), we concluded that no electron transfer between carotenoid and Chl-*a* occurred in the f.Ycf39–HliD complex.

DISCUSSION

Population of the S_1 state of β-carotene after Chl-*a* excitation at 620 nm provided clear evidence for quenching of the Chl-*a* Q_y state via energy transfer to the S_1 state of β-carotene. A quenching mechanism based on direct energy transfer from a Chl-*a* Q_y state to a carotenoid S_1 state has previously been proposed to operate in LHCII from higher plants[2] and in the IsiA protein from cyanobacteria[21]. However, because of the suggested slow (>100 ps) Chl-*a*–to-carotenoid energy transfer, the carotenoid S_1 state could not be sufficiently populated. Consequently, signatures of the carotenoid S_1 state have not been apparent, and the validity of the model has been challenged[7]. Here, the appearance of the β-carotene
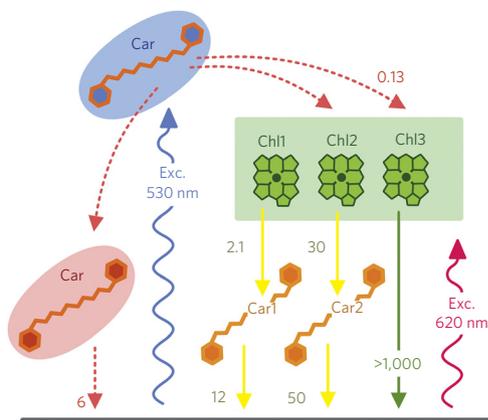
Figure 4 | Scheme of energy transfer pathways in HliD. Solid lines denote processes induced by the excitation of Chl-*a* at 620 nm (exc. 620 nm); dashed lines represent processes observed after excitation of the carotenoid S_2 state at 530 nm (exc. 530 nm; blue oval). Global fitting reveals two quenching channels (yellow arrows). Energy acceptors in these two quenching processes are two spectrally distinct carotenoid S_1 states (Car1 and Car2). A different S_1 state (red oval) is populated via internal conversion from the S_2 state (blue oval). Color coding of carotenoid states does not necessarily imply these states belong to different carotenoid pools. Time constants (in picoseconds) are associated with each pathway in diagram. Car, carotenoid.

signal after Chl-*a* excitation was evident. The kinetic trace recorded at 580 nm in the maximum of the S_1-S_n band of β-carotene (**Fig. 2c**) showed that the 2.1-ps rise, which monitors the arrival of excitations to the S_1 state of β-carotene after excitation of Chl-*a* in the f.Ycf39–HliD complex, accounted for about 80% of the signal. We excluded the possibility of reductive quenching by electron transfer from carotenoid to Chl-*a*[1] (**Supplementary Fig. 7**), and the slow, 2.1-ps rise of the S_1 signal after Chl-*a* excitation also ruled out any mechanism involving excitonic coupling between carotenoid and Chl-*a*[3].

Matching the S_1 spectrum of β-carotene excited at 530 nm to the carotenoid spectrum observed after Q_y excitation of Chl-*a* (**Fig. 3a**) led us to the conclusion that a red-shifted β-carotene in the f.Ycf39–HliD complex was responsible for the quenching associated with the 2.1-ps component. Different populations of β-carotene are consistent with the observed shift in β-carotene absorbance between the f.Ycf39–HliD complex and the dissociated HliD (**Fig. 1b**). In our structural model of HliD, two β-carotene molecules bind symmetrically to a dimer (**Fig. 1d**); however, the interaction with Ycf39 protein might influence the binding pocket of one β-carotene and consequently facilitate energy transfer via this carotenoid. It should be noted that the association with Ycf39 is not required for such quenching because the overall ability to quench Chl-*a* fluorescence was comparable for the Ycf39–HliD complex and 'free' HliD (**Fig. 2a** and **Supplementary Fig. 1a**).

Although there was a spectral similarity between the S_1 states populated directly from the carotenoid S_2 state and those populated via the Q_y pathway, the difference in lifetimes suggested that the situation is more complex. As direct excitation of β-carotene did not generate an S_1 state whose lifetime would be comparable to that of a quencher (12 ps), we suggest that excitations arriving from the Q_y state likely end in a minimum at the S_1 potential surface that is not accessible from the S_2 state. The key difference between the direct excitation of β-carotene and the Q_y quenching pathway lies in the fact that the former process generates the S_1 state via S_2-S_1 relaxation. The latter process occurs via energy transfer from Q_y to S_1; thus, β-carotene is initially in its ground state, implying that it is formally an S_0-S_1 transition. Because the S_1 potential surface of

carotenoids is believed to be rather complicated, with multiple minima, it is not unrealistic that approaching the S_1 state 'from above' (S_2) or 'from below' (S_0) may result in different minima at the S_1 potential surface. Indeed, researchers have observed longer S_1 lifetimes of β-carotene in solution after populating the S_1 state directly from the ground state via two-photon excitation[22].

The global fitting of data recorded after direct excitation of carotenoid also revealed two interesting features. First, the fast 130-fs decay characterizing depopulation of the S_2 state was associated with appearance of Chl-*a* bleaching at 674 nm, indicating that some fraction of the S_2 population was transferred to Chl-*a*. Comparing the magnitudes of Chl-*a* bleaching and S_1-S_n excited state absorption (**Fig. 3c**) suggested that this energy transfer channel is only minor. The f.Ycf39–HliD complex is tuned to be an efficient quencher, and weak carotenoid-to-Chl-*a* energy transfer is likely an inevitable consequence of pigment arrangement within the f.Ycf39–HliD complex. Second, global fitting revealed the presence of a long decay component of 50 ps (excitation at 490 nm) and 30 ps (excitation at 530 nm). These components characterize the dominant Chl-*a* decay channel after carotenoid excitation, proving that Chl-*a*, populated via the minor energy transfer channel from β-carotene, is also efficiently quenched. Notably, the shape of the EADS associated with these components is reminiscent of the carotenoid S^* state in the 450–600-nm region[23]. This indicates that the Chl-*a* molecules in the f.Ycf39–HliD complex that are populated via energy transfer from β-carotene are quenched through a slower channel correlating to either a population of the S^* state or an S_1 state of some β-carotene, which was spectrally distinct from the main quencher. A scheme of energy transfer pathways is shown in **Figure 4**.

The inability to correlate the lifetimes of β-carotene S_1 state populated via S_2-S_1 internal conversion and via the Q_y-S_1 pathway indicated that the carotenoid S_1 potential surface is likely more complex than previously thought. Yet the data presented here unequivocally identified the energy transfer from the Q_y state of Chl-*a* to the S_1 state of a carotenoid as the mechanism of nonphotochemical quenching in the f.Ycf39–HliD complex. Pigments in the complex were clearly bound to HliD (**Fig. 1a,b**), which belongs to proteins assumed to be ancestors of the whole LHC superfamily[10]. Although LHC antenna proteins are the best-characterized members of the LHC superfamily, this large and diverse group also includes single-helix, double-helix and triple-helix proteins that certainly do not contribute to light harvesting but rather play a similar photoprotective role in eukaryotes like the Hlips in cyanobacteria[24].

As we clarified here, the function of Hlips relies on efficient dissipation of the Chl-*a* excited state energy via the carotenoid S_1 state. Given the highly conserved Chl-*a*–binding motif, it is feasible that the arrangement of Chl-*a* molecules and surrounding carotenoids shares a similar pattern in the whole LHC superfamily, though the carotenoid species (quencher) may vary in different proteins[18,25,26]. Researchers have already revealed such variation on a common theme by solving crystal structures of plant major and minor LHC antennae[26]. We therefore propose a hypothesis that the quenching mechanism described for HliD may be principally unchanged in LHC-like proteins as well as in LHC antennae[2]. The situation for intact thylakoid membranes is likely more complicated, and this type of quenching may work along with other quenching mechanisms[1,3]. However, if our hypothesis is correct, the evolution of LHC antennae had to include structural changes that allowed high flexibility between energy dissipation and harvesting[27]. The subfamily of LHC proteins specialized for light harvesting is thought to emerge at the basis of the green and red algal lineage, and apart from the plant-like antennae, it also involves fucoxanthin Chl-*a/c*–binding proteins[9,28]. Notably, the quenching in both LHC and fucoxanthin Chl-*a/c*–binding protein antennae is strongly enhanced by low pH[29,30], but we observed a rather negative effect for low pH on f.Ycf39–HliD quenching (**Supplementary Fig. 8**).

30

It is therefore possible that the eukaryotic invention of pH-activated quenching in an ancient, photoprotective LHC-like protein was a critical step for the evolution of LHC antennae. A gradual transition from fixed to flexible quenching is supported by the recent discovery of LHC stress-related (LHCSR) proteins in green algae and mosses[31]. LHCSRs exhibit constitutive, yet pH-sensitive, quenching and might represent a transition state between photoprotective LHC-like proteins and the LHC-based light-harvesting systems.

METHODS
Methods and any associated references are available in the online version of the paper.

References
1. Holt, N.E. *et al.* Carotenoid cation formation and the regulation of photosynthetic light harvesting. *Science* **307**, 433–436 (2005).
2. Ruban, A.V. *et al.* Identification of a mechanism of photoprotective energy dissipation in higher plants. *Nature* **450**, 575–578 (2007).
3. Bode, S. *et al.* On the regulation of photosynthesis by excitonic interactions between carotenoids and chlorophylls. *Proc. Natl. Acad. Sci. USA* **106**, 12311–12316 (2009).
4. Avenson, T.J. *et al.* Zeaxanthin radical cation formation in minor light-harvesting complexes of higher plant antenna. *J. Biol. Chem.* **283**, 3550–3558 (2008).
5. Fuciman, M. *et al.* Role of xanthophylls in light harvesting in green plants: a spectroscopic investigation of mutant LHCII and Lhcb pigment-protein complexes. *J. Phys. Chem. B* **116**, 3834–3849 (2012).
6. Berera, R., van Stokkum, I.H.M., Kennis, J.T.M., van Grondelle, R. & Dekker, J.P. The light-harvesting function of carotenoids in the cyanobacterial stress-inducible IsiA complex. *Chem. Phys.* **373**, 65–70 (2010).
7. Müller, M.G. *et al.* Singlet energy dissipation in the photosystem II light-harvesting complex does not involve energy transfer to carotenoids. *ChemPhysChem* **11**, 1289–1296 (2010).
8. Dolganov, N.A.M., Bhaya, D. & Grossman, A.R. Cyanobacterial protein with similarity to the chlorophyll a/b binding proteins of higher plants: evolution and regulation. *Proc. Natl. Acad. Sci. USA* **92**, 636–640 (1995).
9. Neilson, J.A.D. & Durnford, D.G. Structural and functional diversification of the light-harvesting complexes in photosynthetic eukaryotes. *Photosynth. Res.* **106**, 57–71 (2010).
10. Engelken, J., Brinkmann, H. & Adamska, I. Taxonomic distribution and origins of the extended LHC (light-harvesting complex) antenna protein superfamily. *BMC Evol. Biol.* **10**, 233 (2010).
11. Bhaya, D., Dufresne, A., Vaulot, D. & Grossman, A. Analysis of the *hli* gene family in marine and freshwater cyanobacteria. *FEMS Microbiol. Lett.* **215**, 209–219 (2002).
12. He, Q., Dolganov, N., Bjorkman, O. & Grossman, A.R. The high light-inducible polypeptides in *Synechocystis* PCC6803. Expression and function in high light. *J. Biol. Chem.* **276**, 306–314 (2001).
13. Chidgey, J.W. *et al.* A cyanobacterial chlorophyll synthase-HliD complex associates with the Ycf39 protein and the YidC/Alb3 insertase. *Plant Cell* **26**, 1267–1279 (2014).
14. Vavilin, D., Yao, D. & Vermaas, W.F.J. Small cab-like proteins retard degradation of photosystem II-associated chlorophyll in *Synechocystis* sp PCC 6803—Kinetic analysis of pigment labeling with N-15 and C-13. *J. Biol. Chem.* **282**, 37660–37668 (2007).
15. Yao, D. *et al.* Localization of the small CAB-like proteins in photosystem II. *J. Biol. Chem.* **282**, 267–276 (2007).
16. Knoppová, J. *et al.* Discovery of a chlorophyll binding protein complex involved in the early steps of photosystem II assembly in *Synechocystis*. *Plant Cell* **26**, 1200–1212 (2014).
17. Liu, Z. *et al.* Crystal structure of spinach major light-harvesting complex at 2.72 Å resolution. *Nature* **428**, 287–292 (2004).
18. Standfuss, J., Terwisscha van Scheltinga, A.C., Lamborghini, M. & Kühlbrandt, W. Mechanisms of photoprotection and nonphotochemical quenching in pea light-harvesting complex at 2.5 Å resolution. *EMBO J.* **24**, 919–928 (2005).
19. Polívka, T. & Sundström, V. Ultrafast dynamics of carotenoid excited states—from solution to natural and artificial systems. *Chem. Rev.* **104**, 2021–2071 (2004).
20. Jeevarajan, J.A., Wei, C.C., Jeevarajan, A.S. & Kispert, L.D. Optical absorption spectra of dications of carotenoids. *J. Phys. Chem.* **100**, 5637–5641 (1996).
21. Berera, R. *et al.* A mechanism of energy dissipation in cyanobacteria. *Biophys. J.* **96**, 2261–2267 (2009).
22. Kosumi, D. *et al.* Ultrafast relaxation kinetics of the dark S-1 state in all-*trans*-β-carotene explored by one- and two-photon pump-probe spectroscopy. *Chem. Phys.* **373**, 33–37 (2010).
23. Gradinaru, C.C. *et al.* An unusual pathway of excitation energy deactivation in carotenoids: singlet-to-triplet conversion on an ultrafast timescale in a photosynthetic antenna. *Proc. Natl. Acad. Sci. USA* **98**, 2364–2369 (2001).
24. Tanaka, R. *et al.* LIL3, a light-harvesting-like protein, plays an essential role in chlorophyll and tocopherol biosynthesis. *Proc. Natl. Acad. Sci. USA* **107**, 16721–16725 (2010).
25. Adamska, I., Roobol-Boza, M., Lindahl, M. & Andersson, B. Isolation of pigment-binding early light-inducible proteins from pea. *Eur. J. Biochem.* **260**, 453–460 (1999).
26. Pan, X. *et al.* Structural insights into energy regulation of light-harvesting complex CP29 from spinach. *Nat. Struct. Mol. Biol.* **18**, 309–315 (2011).
27. Krüger, T.P., Wientjes, E., Croce, R. & van Grondelle, R. Conformational switching explains the intrinsic multifunctionality of plant light-harvesting complexes. *Proc. Natl. Acad. Sci. USA* **108**, 13516–13521 (2011).
28. Koziol, A.G. *et al.* Tracing the evolution of the light-harvesting antennae in chlorophyll a/b-containing organisms. *Plant Physiol.* **143**, 1802–1816 (2007).
29. Ruban, A.V., Young, A. & Horton, P. Modulation of chlorophyll fluorescence quenching in isolated light-harvesting complex of photosystem II. *Biochim. Biophys. Acta* **1186**, 123–127 (1994).
30. Kaňa, R., Kotabová, E., Sobotka, R. & Prášil, O. Non-photochemical quenching in cryptophyte alga *Rhodomonas salina* is located in chlorophyll a/c antennae. *PLoS ONE* **7**, e29700 (2012).
31. Bonente, G. *et al.* Analysis of LhcSR3, a protein essential for feedback de-excitation in the green alga *Chlamydomonas reinhardtii*. *PLoS Biol.* **9**, e1000577 (2011).

Author contributions
M.K.S. purified the f.Ycf39–HliD complex under the supervision of R.S.; J.K., R.K. and R.S. performed biochemical analyses. H.S. and V.Š. performed ultrafast spectroscopic experiments and analyzed data under the supervision of T.P.; R.S., T.P. and J.K. designed the study and wrote the paper. The whole study was supervised by R.S. All authors discussed the results and commented on the manuscript.

Competing financial interests
The authors declare no competing financial interests.

Additional information
Supplementary information is available in the online version of the paper. Reprints and permissions information is available online at http://www.nature.com/reprints/index.html. Correspondence and requests for materials should be addressed to R.S.

ONLINE METHODS

Construction of *Synechocystis* strains. Construction of the *Synechocystis* f.*ycf39*/Δ*ycf39*/Δ*psbB* strain was described in a previous study[16]. An identical strain lacking HliC protein was obtained by the transformation of f.*ycf39*/Δ*ycf39*/Δ*psbB* strain by genomic DNA isolated from the *Synechocystis* Δ*hliC* mutant[32].

Purification of the f.Ycf39–HliD complex. For purification of the f.Ycf39–HliD complex, 20 L of the *Synechocystis* f.*ycf39*/Δ*ycf39*/Δ*psbB* cells or the f.*ycf39*/Δ*ycf39*/Δ*psbB*/Δ*hliC* cells were grown in 10-L flasks under 40 μmol of photons m^{-2} s^{-1} light at 28 °C in BG11 medium supplemented with 5 mM glucose. The cell culture was agitated with a magnetic stirrer and bubbled with air. Purification of the f.Ycf39–HliD complex was performed essentially as described[16] except the MES buffer containing divalent cations was replaced by a phosphate buffer (25 mM potassium phosphate, pH 7.5, 50 mM NaCl$_2$, 10% glycerol).

Two-dimensional clear-native/SDS-electrophoresis and immunoblot. For native electrophoresis, the f.Ycf39 eluate was concentrated fivefold on a 100-kDa cutoff micro-concentrator (Millipore) and separated on 4–12% clear-native gel[33]. Individual components of protein complexes were resolved by incubating the gel strip from the first dimension in 2% SDS and 1% dithiothreitol for 30 min at room temperature, and proteins were separated in the second dimension by SDS electrophoresis in a denaturing 12–20% polyacrylamide gel containing 7 M urea[34]. For immunoblotting, proteins were separated by SDS electrophoresis, transferred onto a PVDF membrane (Sigma-Aldrich, Germany) and incubated with specific primary antibodies as well as with secondary antibody conjugated with horseradish peroxidase (Sigma-Aldrich, Germany, catalog number A6154). Primary antibody against Ycf39 was raised in rabbits against synthetic peptides 4–14, and the antibody against the HliD was purchased from Agrisera (Sweden, catalog number AS10 1610).

Gel filtration and pigment analysis. The f.Ycf39–HliD eluate was immediately injected onto an Agilent-1200 HPLC machine and separated on Bio-sep 3000 column (Phenomenex) using 25 mM MES buffer, 10 mM MgCl$_2$, 10 mM CaCl$_2$, pH 6.5, containing 0.1% dodecyl-β-maltoside at a flow rate of 0.2 ml min^{-1} at 10 °C. Eluted proteins and complexes were detected by a diode-array detector and a fluorescence detector set to 440/680 nm (excitation/emission wavelengths). The column was calibrated using photosynthetic complexes with known size: trimeric photosystem I (~1 MDa), dimeric photosystem II (~700 kDa), monomeric photosystem II lacking oxygen-evolving complex (~250 kDa) and the purified His-tagged CP43 subcomplex (~90 kDa)[35]. To identify the pigments associated with f.Ycf39–HliD and HliD, fractions representing the 9.2-ml and 9.8-ml peaks were pooled and concentrated ~20 times on 30-kDa cutoff micro-concentrators (Millipore). This solution was extracted with 90% methanol and the extract analyzed by Agilent-1200 HPLC. Separation was carried out on a reverse phase column (Kinetex C8, 2.6 μm particle size, 3.9 × 150 mm; Phenomenex) with 35% methanol and 15% acetonitrile in 0.25M pyridine (solvent A) and 20% methanol, 20% acetone in acetonitrile as solvent B. Pigments were eluted with a linear gradient of solvent B (30–95% in 25 min) followed by 95% of solvent B at a flow rate of 0.8 ml min^{-1} at 40 °C. Pigment stoichiometries were estimated using extinction coefficients for Chl-*a* and β-carotene[36].

Fluorescence quantum yield. The fluorescence quantum yield was calculated according to the equation[37]

$$Q = Q_R \times \frac{I}{I_R} \times \frac{OD_R}{OD} \times \frac{n^2}{n_R^2}$$

where Q is the fluorescence quantum yield, I is the integrated fluorescence intensity, OD is the optical density and n the refractive index of the sample. The subscript R indicates a reference fluorophore with known quantum yield.

Femtosecond spectroscopy. The femtosecond spectrometer used for collecting transient absorption spectra is based on a laser system Integra-i (Quantronix). It consists of Er-fiber oscillator and Ti:Sapphire amplifier producing ~130-fs pulses at a repetition rate of 1 kHz. The central wavelength of the output pulses is 795 nm with 1.7 mJ per pulse. The amplified pulses were divided into two paths. The first one was directed to the optical parametric amplifier TOPAS (Light Conversion, Lithuania) to generate tunable excitation pulses. The second one was used to produce white light–continuum probe pulses by focusing a fraction of the amplifier output to a 3-mm sapphire plate. The white-light pulses, which were directed and focused only by reflective optics to prevent dispersion, were further divided into the probe beam that overlapped with the excitation beam at the sample and a reference beam that passed through the sample outside the excitation spot. The probe and the reference beams were brought to the slit of a spectrograph, where it was dispersed onto a dual CCD detector with 2,048 elements allowing measurements of transient spectra in a spectral window of ~240 nm. During all measurements, we kept the number of photons per pulse per cm^2 under 2×10^{14} to achieve reasonable signal-to-noise ratio while avoiding sample degradation and/or annihilation processes. In all measurements, the mutual polarization of the pump and probe beams was set to the magic angle (54.7°) by placing a polarization rotator in the pump beam. All measurements were carried out in a 2-mm quartz cuvette with a micro-stirrer to continuously mix the sample during measurements.

Global fitting. The spectro-temporal data sets obtained from the measurements were analyzed globally by fitting package DAFit (Pascher Instruments). The data were fitted to a sum of exponentials, including numerical deconvolution of the response function, and a fourth degree polynomial describing the chirp. The fitting procedure used general linear regression for the amplitudes of the exponentials and the Nelder-Mead simplex method for the rate constants, the FWHM and the chirp polynomial. To visualize the excited state dynamics, we assumed that the excited states evolved according to a sequential, irreversible scheme A → B, B → C, C → D. The arrows represent increasingly slower monoexponential processes, and the time constants of these processes correspond to lifetimes of the species A, B, C, D, etc. The spectral profiles of the species are called EAD spectra, and although in complex systems they do not directly correspond to the individual excited state species, they provide information about the time evolution of the whole system[38].

32. Xu, H., Vavilin, D., Funk, C. & Vermaas, W.F.J. Multiple deletions of small cab-like proteins in the cyanobacterium *Synechocystis* sp PCC 6803—Consequences for pigment biosynthesis and accumulation. *J. Biol. Chem.* **279**, 27971–27979 (2004).

33. Wittig, I., Karas, M. & Schägger, H. High resolution clear native electrophoresis for in-gel functional assays and fluorescence studies of membrane protein complexes. *Mol. Cell. Proteomics* **6**, 1215–1225 (2007).

34. Dobáková, M., Sobotka, R., Tichý, M. & Komenda, J. Psb28 protein is involved in the biogenesis of the photosystem II inner antenna CP47 (PsbB) in the cyanobacterium *Synechocystis* sp PCC 6803. *Plant Physiol.* **149**, 1076–1086 (2009).

35. Boehm, M. *et al.* Investigating the early stages of Photosystem II assembly in *Synechocystis* sp PCC 6803. Isolation of CP47 and CP43 complexes. *J. Biol. Chem.* **286**, 14812–14819 (2011).

36. Eijckelhoff, C. & Dekker, J.P. A routine method to determine the chlorophyll alpha, pheophytin-α and β-carotene contents of isolated Photosystem II reaction center complexes. *Photosynth. Res.* **52**, 69–73 (1997).

37. Lakowicz, J.R. *Principles of Fluorescence Spectroscopy* 1st edn. (Kluwer Academic, 1999).

38. van Stokkum, I.H., Larsen, D.S. & van Grondelle, R. Global and target analysis of time-resolved spectra. *Biochim. Biophys. Acta* **1657**, 82–104 (2004).

Supplementary Information

Mechanism of photoprotection in the cyanobacterial ancestor of plant antenna proteins

Hristina Staleva[a], Josef Komenda[a,b], Mahendra K. Shukla[a,b], Václav Šlouf[a], Radek Kaňa[a,b], Tomáš Polívka[a,c] and Roman Sobotka[a,b]

[a]Faculty of Science, University of South Bohemia, Branišovská 31, 37005 České Budějovice, Czech Republic

[b]Institute of Microbiology, Academy of Sciences of the Czech Republic, Opatovický mlýn, 379 81, Třeboň, Czech Republic

[c]Biology Centre, Institute of Plant Molecular Biology, Academy of Sciences of the Czech Republic, Branišovská 31, 37005, České Budějovice, Czech Republic

Correspondence and requests for materials should be addressed to R.S. (sobotka@alga.cz)

Supplementary Results

Supplementary Table 1. Identification of Hli proteins in the f.Ycf39-HliD pull-down eluate. Proteins were identified by nanoLC-MS/MS and database searching essentially as described previously[1].

| Protein	Gene Name	Mass (Da)	Coverage (%)	Peptides
High light inducible protein HliD	*ssr1789*	6468	44	K.FGFNNYAEK.L M.SEELQPNQTPVQEDPK.F
High light inducible protein HliC	*ssl1633*	5146	27	K.FGFTAFAENWNGR.L
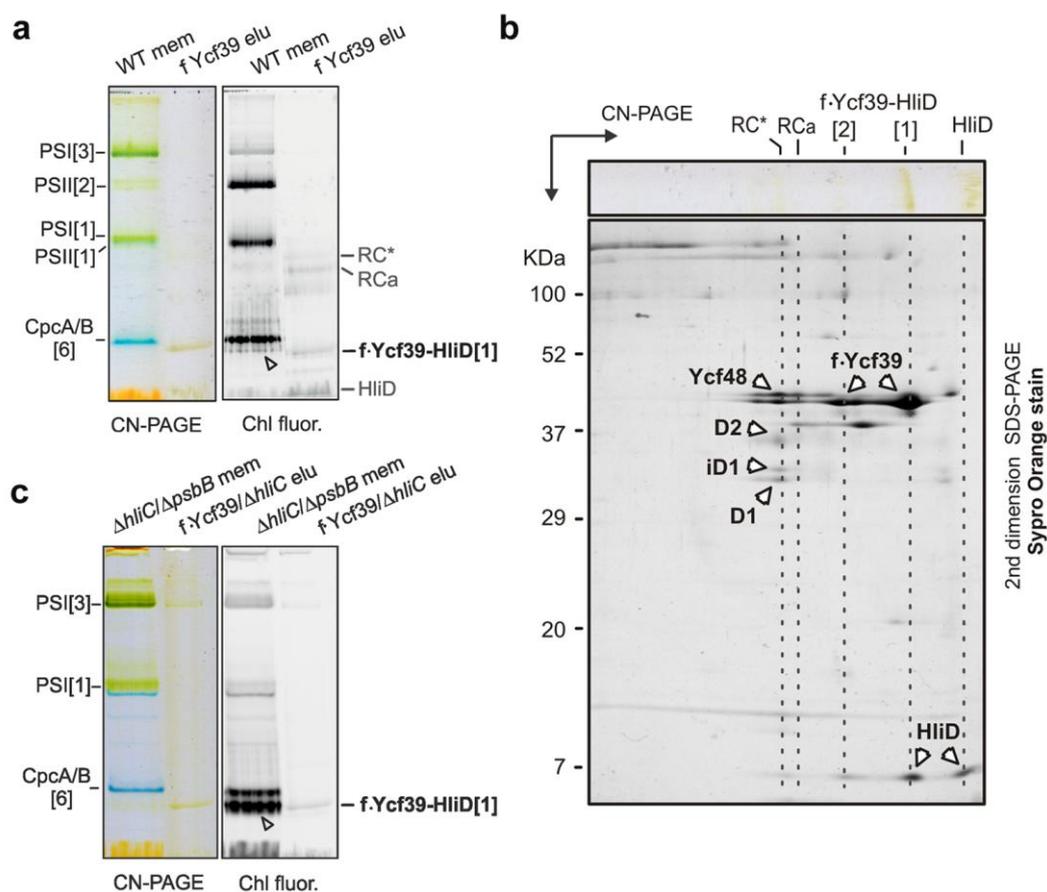
Supplementary Figure 1. Two-dimensional electrophoresis of the f·Ycf39 eluate and identification of individual protein spots. **a,** Separation of the eluted f·Ycf39 complexes by Clear-Native electrophoresis (CN-PAGE). Solubilised membranes (3 μg of Chl-*a*) from the *Synechocystis* wild-type strain show mobility of photosynthetic complexes: PSI[1] and PSI[3], monomer and trimer of PSI, respectively; PSII[1] and PSII[2], monomer and dimer of PSII; CpcA/B[6], 107 kDa heterohexamer of CpcA and CpcB phycobiliproteins. The major orange band was assigned as monomeric f·Ycf39-HliD complex and the position of the dissociated HliD is also indicated. RC* - reaction centre assembly intermediate of PSII (RCa) associated with the f·Ycf39-HliD complex. The intensity of Chl-*a* fluorescence detected "in gel" after excitation by blue light is also shown (Chl fluor); white arrow indicates fluorescence of the CP43 protein. **b**, A gel strip from CN-PAGE with separated f·Ycf39 eluate was further separated in a second dimension by SDS-PAGE. The gel was stained by Sypro Orange and the identity of designated spots on the stained gel was assigned according to Knoppová *et al.*,[2]. RCa - reaction centre assembly intermediate of PSII containing D1, D2

and Ycf48 as the main components. **c**, Separation of the eluted f·Ycf39 complex purified from the Δ*hliC* genetic background. The CN-PAGE was performed essentially as described for (**a**).
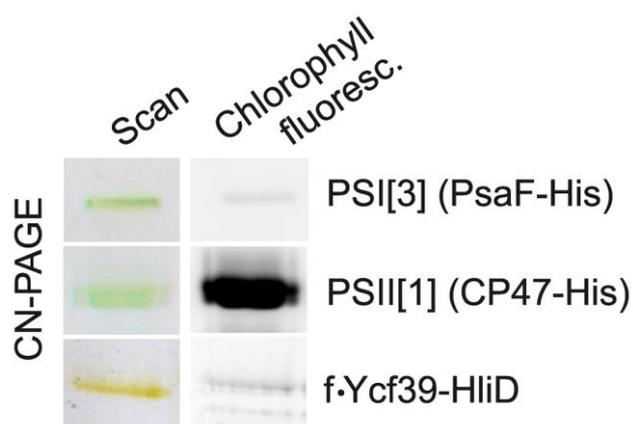

Supplementary Figure 2. Comparison of Chl-*a* fluorescence of the f.Ycf39-HliD complex and photosystem I and II. The purified f.Ycf39-HliD complex was separated by Clear-Native gel and Chl-*a* fluorescence detected "in gel" after excitation by blue light. The fluorescence intensity is compared with the trimeric photosystem I (PSI[3]) and the monomeric photosystem II (PSII[1]) purified from *Synechocystis* via His-tagged subunits as indicated. The similar amount of Chl-*a* (~0.5 μg) was loaded for each complex.
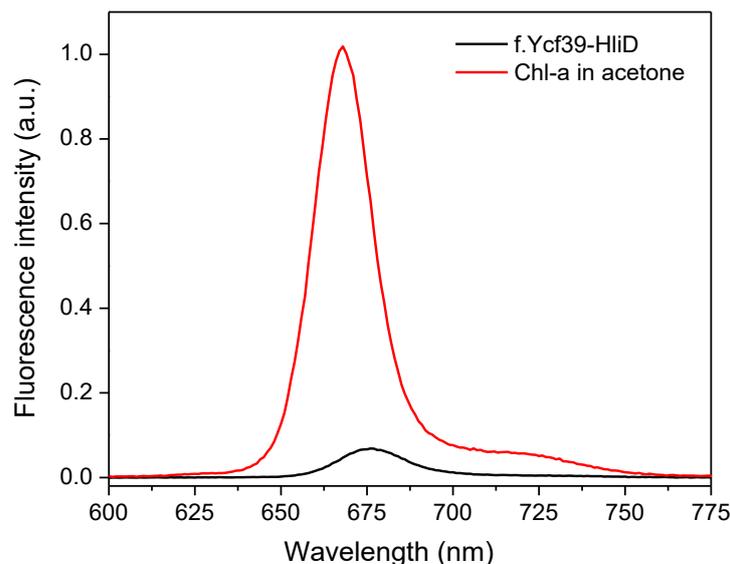
Supplementary Figure 3. Fluorescence quantum yield of the f.Ycf39-HliD complex. The fluorescence of the f.Ycf39-HliD complex (black) is compared to the fluorescence of a free Chl-*a* in acetone (red). The optical density was set identical at 667 nm for the Chl-*a* in acetone and in the f.Ycf39-HliD complex. Excitation wavelength was 435 nm. Integrating the fluorescence spectra shown above and using the value of $Q_R = 0.30$ for Chl-*a*[3] gives fluorescence quantum yield $Q = 0.014$ for the f.Ycf39-HliD complex. To test validity of our calculations, the data shown in figure were complemented with measurements in which two standard dyes, Rhodamine 800 and cresyl violet, were used as a reference. Using the same approach, we have obtained values of $Q = 0.011 – 0.013$.
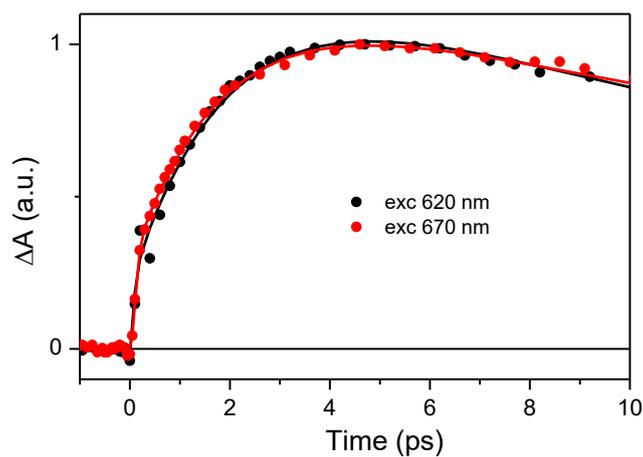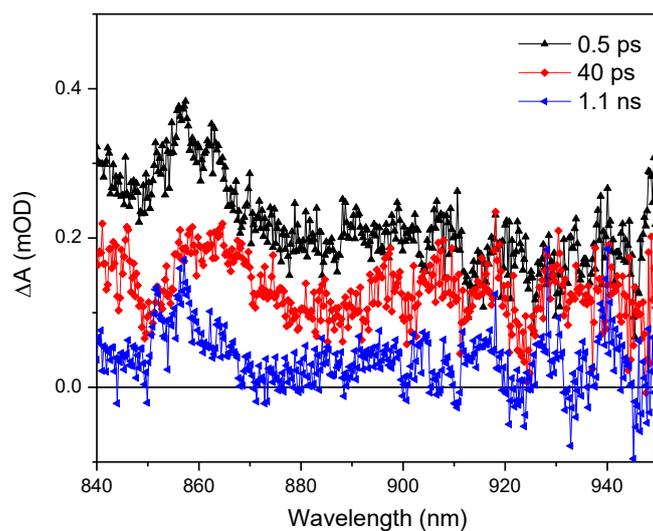
Supplementary Figure 4. Kinetics of absorption changes at 580 nm measured after excitation at two different wavelengths 620 nm (black) and 670 nm (red). The onset of the β-carotene signal exhibits identical dynamics after both excitation wavelengths, indicating that the quenching process occurs also after excitation of the Q_y band at 670 nm.
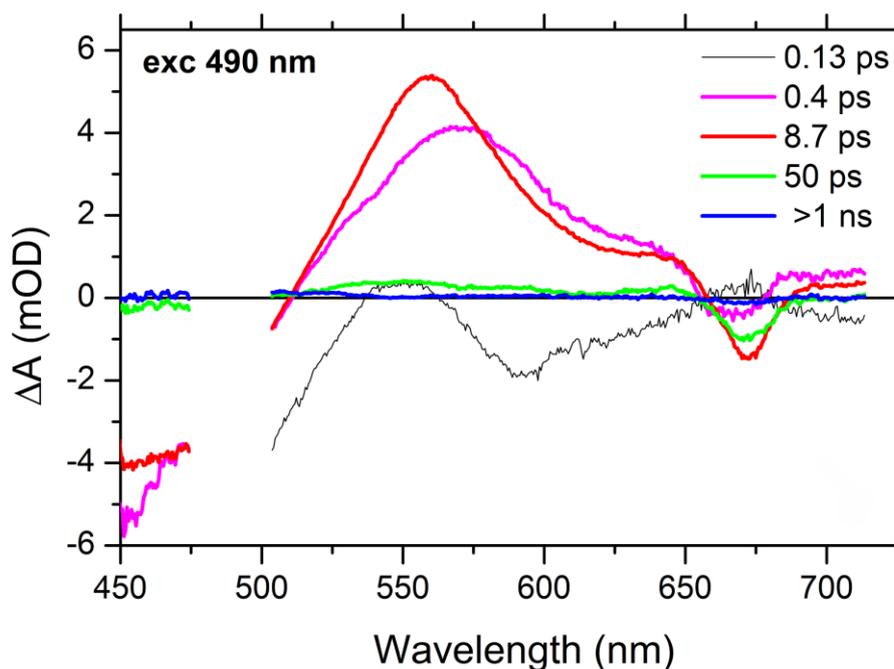
Supplementary Figure 5. **Evolution-associated difference spectra (EADS) extracted from global fitting the data recorded after direct excitation of β-carotene in the f.Ycf39-HliD complex at 490 nm**. The black EADS corresponds to the initially excited state (carotenoid S_2 state), while the red EADS has typical features of the S_1 state with minor contribution of Chl-*a* bleaching due to carotenoid-Chl energy transfer. The EADS shown in magenta is typical for non-relaxed, hot S_1 state[4].
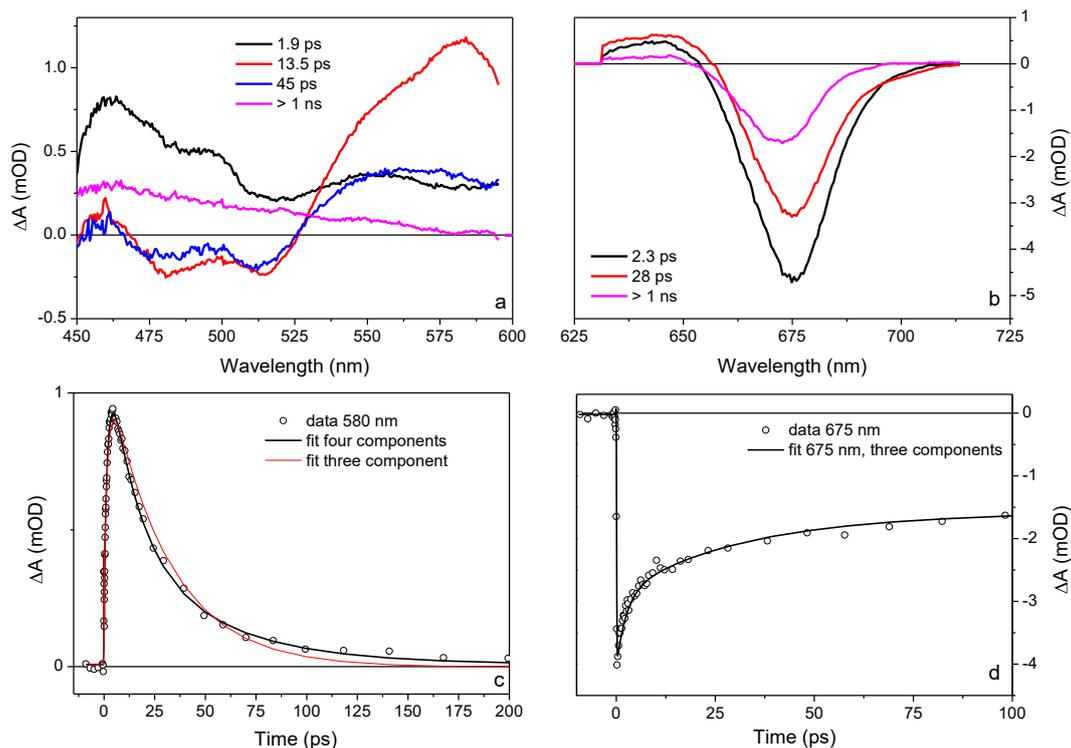
Supplementary Figure 6. Global fitting of data obtained after excitation of Chl-*a* at 620 nm. To identify decay components associated solely with β-carotene and Chl-*a*, spectral regions dominated by the β-carotene signal (450-600 nm) and the Chl-*a* signal (630-730 nm) were fitted separately. **a**, EADS obtained from the fitting in the β-carotene spectral region. Both spectral profiles and lifetimes of EADS are essentially the same as those extracted from fitting the whole dataset (Fig. 3a). **b**, EADS obtained from fitting the Chl-*a* bleaching region. Restriction of fitting solely to Chl-*a* spectral region allows to fit the data with three components only, revealing the lifetimes of three Chl-*a* population of 2.3 ps, 28 ps and > 1 ns. **c**, Kinetic measured at the maximum of β-carotene S_1-S_n transition. The black line is fit with four components shown in panel (a), the red line is the fit obtained with only three components. It is clear that three components are not enough to fit the decay in the β-carotene spectral region. **d**, Kinetic measured at the maximum of Chl-*a* bleaching together with a three-component fit (black line). In contrast to the β-carotene region, decay of Chl-*a* is readily fitted with three components.

Supplementary Figure 7. Transient absorption spectra in the near-IR spectral region. To test whether β-carotene radical is formed after Chl-*a* excitation, we measured transient absorption spectra after 620 nm excitation also in the spectral region where the β-carotene radical signal could be expected[5]. The transient absorption spectra exhibit no features attributable to β-carotene cation radical. The signal is extremely weak and is solely due to a weak ESA signal of Chl-*a*.
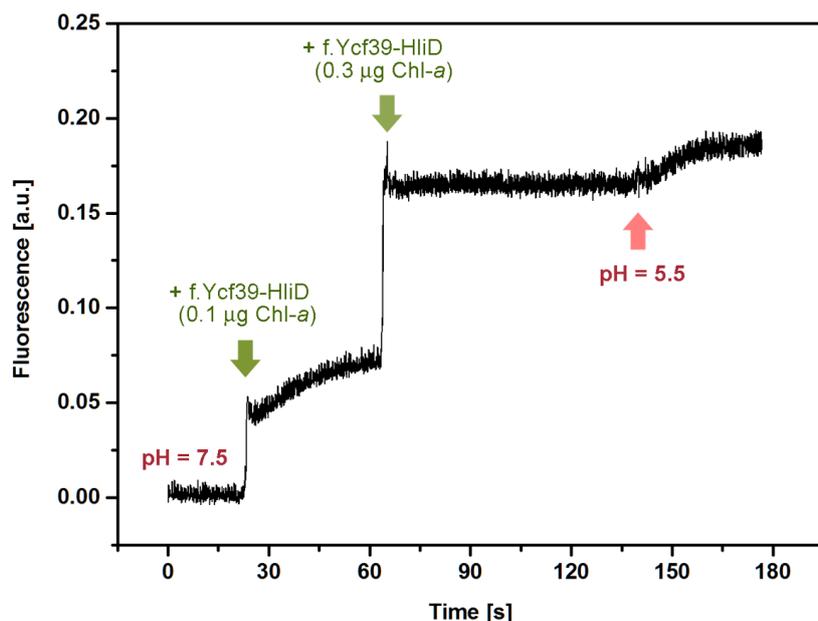
Supplementary Figure 8. Effect of pH on the quenching of f.Ycf39-HliD complex measured as described previously[6]. A small volume of the purified f.Ycf39-HliD (40 μL, ~0.4 μg of Chl-*a*) was mixed in two steps with 0.5 mL of HEPES-Na-Citrate buffer, pH 7.5 (see green arrows) in a constantly stirring cuvette. After indicated time the solution was acidified by 5% HCl to pH 5.5 (red arrow). During the whole assay Chl-*a* fluorescence was recorded by FL 100 fluorimeter (Photon System Instrument, Brno, Czech Republic) with blue light excitation (150 μmol m^{-2} s^{-1}).

References

1   Janouškovec, J. *et al.* Split photosystem protein, linear-mapping topology, and growth of structural complexity in the plastid genome of *Chromera velia*. *Mol. Biol. Evol.* **30**, 2447-2462, (2013).

2   Knoppová, J. *et al.* Discovery of a chlorophyll binding protein complex involved in the early steps of photosystem II assembly in *Synechocystis*. *Plant Cell* **26**, 1200-1212, (2014).

3   Weber, G. & Teale, F. W. J. Determination of the absolute quantum yield of fluorescent solutions. *Trans. Faraday Soc.* **53**, 646-655 (1957).

4   Billsten, H. H., Zigmantas, D., Sundström, V. & Polívka, T. Dynamics of vibrational relaxation in the S$_1$ state of carotenoids having 11 conjugated C=C bonds. *Chem. Phys. Lett.* **355**, 465-470 (2002).

5   Jeevarajan, J. A., Wei, C. C., Jeevarajan, A. S. & Kispert, L. D. Optical absorption spectra of dications of carotenoids. *J. Phys. Chem.* **100**, 5637-5641, (1996).

6   Ruban, A. V., Young, A. & Horton, P. Modulation of chlorophyll fluorescence quenching in isolated light-harvesting complex of Photosystem-II. *Biochim. Biophys. Acta* **1186**, 123-127, (1994).

3.2 Result II

Twisting a β-carotene, an adaptive trick from nature for dissipating energy during photoprotection

LIansola-Portoles, M.J., Sobotka, R., Kish, E., **Shukla, M.K.**, Pascal, A.A., Polívka, T., Robert, B. Journal of Biological Chemistry, 2016, 292:1396-1403.

Twisting a β-Carotene, an Adaptive Trick from Nature for Dissipating Energy during Photoprotection*

[ORCID] **Manuel J. Llansola-Portoles**[‡1,2], **Roman Sobotka**[§1], **Elizabeth Kish**[‡1], **Mahendra Kumar Shukla**[§], **Andrew A. Pascal**[‡], **Tomáš Polívka**[¶], and **Bruno Robert**[‡]

From the ‡Institute for Integrative Biology of the Cell (I2BC), CEA, CNRS, Univ Paris-Sud, Université Paris-Saclay, F-91198, Gif-sur-Yvette cedex, France, the §Centre Algatech, Institute of Microbiology, Academy of Sciences of the Czech Republic, Třeboň, 379 81, Czech Republic, and the ¶Institute of Physics and Biophysics, Faculty of Science, University of South Bohemia, České Budějovice 370 01, Czech Republic

Edited by James N. Siedow

Cyanobacteria possess a family of one-helix high light-inducible proteins (Hlips) that are homologous to light-harvesting antenna of plants and algae. An Hlip protein, high light-inducible protein D (HliD) purified as a small complex with the Ycf39 protein is evaluated using resonance Raman spectroscopy. We show that the HliD binds two different β-carotenes, each present in two non-equivalent binding pockets with different conformations, having their (0,0) absorption maxima at 489 and 522 nm, respectively. Both populations of β-carotene molecules were in all-*trans* configuration and the absorption position of the farthest blue-shifted β-carotene was attributed entirely to the polarizability of the environment in its binding pocket. In contrast, the absorption maximum of the red-shifted β-carotene was attributed to two different factors: the polarizability of the environment in its binding pocket and, more importantly, to the conformation of its β-rings. This second β-carotene has highly twisted β-rings adopting a flat conformation, which implies that the effective conjugation length N is extended up to 10.5 modifying the energetic levels. This increase in N will also result in a lower S_1 energy state, which may provide a permanent energy dissipation channel. Analysis of the carbonyl stretching region for chlorophyll a excitations indicates that the HliD binds six chlorophyll a molecules in five non-equivalent binding sites, with at least one chlorophyll a presenting a slight distortion to its macrocycle. The binding modes and conformations of HliD-bound pigments are discussed with respect to the known structures of LHCII and CP29.

In nature, photosynthetic organisms obtain their energy by collecting solar photons, using complex arrays of pigments known as antennas. Subsequently, the energy harvested by the antennas is transferred to reaction centers to be transduced into electrochemical potential. Finally after a cascade of molecular steps, this energy is stored as potential chemical energy that is easy to store and transport (1). To accomplish this process, these organisms have developed a large number of different protein antenna assemblies, a notable subgroup of which are the light-harvesting complexes (LHCs)[3] of green plants and algae. LHCs constitute a large family of proteins, which can exist as monomers, dimers, or trimers in the membrane, and have related amino acid sequences. It is hypothesized that in the evolution of photosynthesis there was, and continues to be, a selective advantage for the organism to make optimum use of low light conditions to drive the relatively slow downstream metabolic reactions of legacy biochemistry (2). Plants, algae, and cyanobacteria are oxygenic photosynthetic organisms that are exposed to random fluctuations in light intensity. In the case of low light requiring large antennas, during high light exposure, most of the energy absorbed is in excess of that required to drive downstream metabolism. If excess light energy is not dealt with properly, it may cause oxidative damage to the organism, mostly as the consequence of singlet oxygen generation. Hence it is vital for oxygenic photosynthetic organisms to develop mechanisms to deal with the abrupt overexposure to excess light and protect themselves from light-induced oxidative stress by dissipating excess absorbed energy as heat. Probably the most important of these mechanisms at a molecular level is the so-called nonphotochemical quenching. When photosynthetic activity is high, it induces a progressive acidification of the lumen because of the creation of the proton gradient, which in turn induces the presence of energy traps in the photosynthetic membrane (3, 4).

Nonphotochemical quenching is a complex regulatory mechanism, which is composed of diverse phases. The best-characterized phase in induced in seconds to minutes, and is called high-energy quenching (qE). During qE, energy traps may appear (or disappear) in seconds, thus originating from the re-organization of the photosynthetic membrane, and not from *de novo* synthesis of new proteins. The molecular mechanisms behind the qE process have been extensively discussed in the last decade, and although it is more and more generally admitted that the energy traps are localized in LHC proteins, several different hypotheses have been formulated about their chemical origin. Most of these hypotheses involve the LHC-bound

---

[1] These authors contributed equally to this work.
[2] To whom correspondence should be addressed. Tel.: 33-0-1-69-08-63-03; E-mail: manuel.llansola@cea.fr.

[3] The abbreviations used are: LHC, light-harvesting complex; qE, high-energy quenching; Chl *a*, chlorophyll *a*; Hlips, high light-inducible proteins; HliD, high light-inducible protein D.

carotenoid molecules, although it was also proposed that they arise from interacting chlorophyll molecules (5). Among the molecular mechanisms involving a carotenoid molecule, it was proposed that the quenching is induced by the reductive quenching of the chlorophyll *a* (Chl *a*) excited state via electron transfer to the carotenoid (6), by energy transfer quenching through singlet-singlet energy transfer from Chl *a* to the carotenoid (7), or by excitonic interaction between Chl *a* and the carotenoid (8).

Hlips are single-helix proteins (~7 kDa) ubiquitous in cyanobacteria that show significant sequence similarity to the first and third helices of eukaryotic LHCs. These small proteins possess a Chl *a* binding motif common to (and conserved among) all LHC proteins; and thus Hlips should be considered as members of the extended LHC superfamily (9–11). The genes that encode Hlips are strongly expressed under various stress conditions (12, 13), nevertheless, the exact role of Hlips in cells remains unclear. They are likely to play photoprotective and regulatory functions during synthesis and degradation of chlorophyll-binding proteins and during assembly and repair of Photosystem II (14). The cyanobacterium *Synechocystis* PCC 6083 contains four different Hlips (HliA-HliD) and all four of these small membrane proteins bind to early intermediates of the Photosystem II assembly (15, 16). Moreover, the HliD and HliC also form stable complexes with chlorophyll synthase, the terminal enzyme of Chl *a* biosynthesis (17, 18), and with the Ycf39 protein (15, 17). Ycf39 is a putative alcohol dehydrogenase with a conserved NADPH binding pocket but the exact role of this protein is not known yet. However, it has been already determined that the absence of this protein has a negative effect on the chlorophyll biosynthesis in *Synechocystis* (16).

The Ycf39-HliD complex was recently purified from *Synechocystis* and, because the Ycf39 itself does not bind pigments (15), the analysis of the Ycf39-HliD complex allowed for identification of certain spectroscopic properties of the HliD protein. The results revealed that HliD binds Chl *a* and β-carotene in a conformation that dissipates energy via singlet-singlet energy transfer from the Chl *a* Q_y state to the β-carotene S_1 state (19). Nevertheless, once the participation and the role of at least one of the two β-carotenes on the mechanism of energy dissipation were proven, the effect of the pigment configuration on the structure of the complex became crucial for the comprehension of the energy dissipation process. HliD binds Chl *a* and β-carotene with a stoichiometry of 3:1 (19). Fig. 1 proposes a model for HliD being a dimer binding six Chl *a* and two β-carotene molecules. In addition, it was shown in Staleva *et al.* (19) that at least one of the β-carotenes exhibits an extraordinary red-shifted absorption up to 550 nm, which may suggest that nature tailored a particular configuration and/or conformation of this β-carotene. Resonance Raman spectroscopy has been proven to be of great value to extract information on colored cofactors from biological materials as complex as the photosynthetic membrane, as it exhibits very high specificity through the resonance effect. Indeed, the Raman signal may be enhanced by up to 6 orders of magnitude when the frequency of the exciting light matches the energy of an electronic transition of the irradiated molecule. In a complex system containing many chromophores, the contribution of each chromophore to the
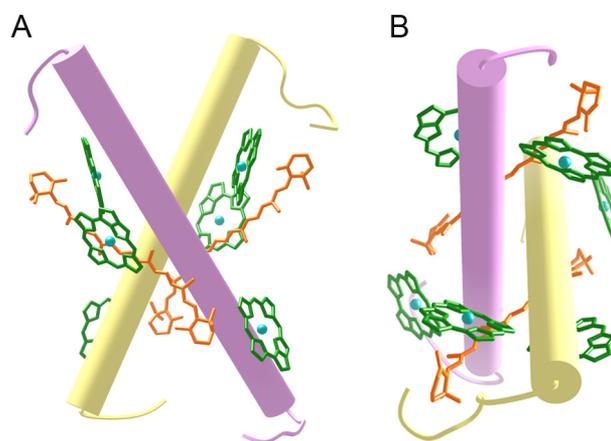

FIGURE 1. **A model of the Chl *a* and β-carotene positions in the putative HliD dimer shown as a side view along the membrane plane (*A*) and a top view from the stromal side (*B*).** The model was prepared using the crystal structure of pea LHCII (33). For clarity, only porphyrin rings of Chl molecules are shown.

Raman spectrum will depend on the excitation light. In systems containing more than one carotenoid the individual contribution of each molecule may be probed by controlling the precise frequency of the exciting beam. For example, this technique has been utilized for studies of the major LHC protein from higher plants, LHCII, which contains two luteins, one neoxanthin and up to one xanthophyll cycle carotenoid per monomer (20–22). Resonance Raman spectroscopy is also useful for analysis of the conformation, chemical, and intermolecular interactions of chlorophyll (23, 24).

In this work, we performed resonance Raman spectroscopy of the purified Ycf39-HliD complex at 77 K and room temperature with the aim of better understanding the role of pigment conformation in the molecular mechanisms that govern the fast fluorescence quenching. We identify and characterize the approximate number of Chl *a* and β-carotenes, and then analyze their configuration, conformation, and local environment in the HliD protein. The results are discussed with respect to the proposed structural model for this protein (19), and to the potential mechanisms underlying the dissipation process.

Results

Absorption Spectra of the Ycf39-HliD Complex—As there is no protocol yet how to isolate "pure" Hlips in quantities required for Raman spectroscopy we isolated the Ycf39-HliD complex via FLAG-tagged Ycf39 as described before (19). The absorption spectrum of the purified Ycf39-HliD complex measured at room temperature is shown in Fig. 2. It has a shape characteristic of an LHC absorption spectrum, consisting of Chl *a* Soret transitions with maxima at 436 and 420 nm and a Q_y band peaking at 675 nm. Absorbance shows two different peaks that can only arise from the bound β-carotene molecules. To minimize the error, we used second derivative analysis to determine the peak positions (Fig. 2, *inset*). One peak is observed at 492 nm, slightly red-shifted from β-carotene in *n*-hexane (478.2 nm), whereas the second peak is observed at 522 nm, with absorption extending up to 550 nm. These two absorption maxima have previously been attributed to two populations of
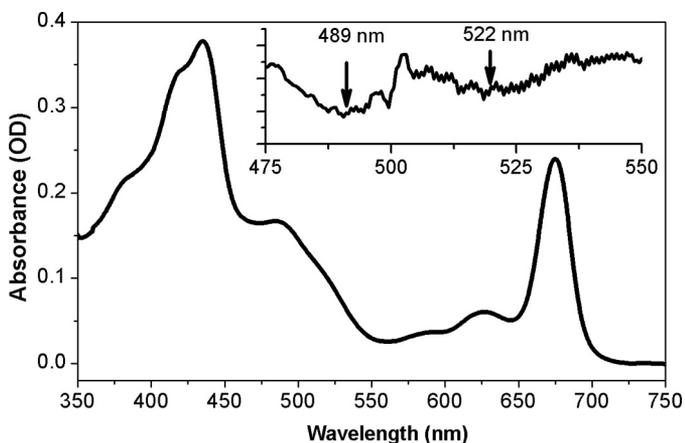
48

FIGURE 2. **Absorption spectra of the Ycf39-HliD complex at room temperature.** *Inset,* second derivative of absorption spectra at room temperature to identify the peak positions of the two β-carotenes.

FIGURE 3. **Resonance Raman spectra at 77 K excited at 413.1 nm for Ycf39-HliD, LHCII, and CP29.**

TABLE 1

Frequencies of Chl *a* keto carbonyl stretching modes in CP29, LHCII, and HliD (in cm^{-1}), measured by resonance Raman spectroscopy

CP29	LHCII	HliD
	1655	
1659	1659	
1665–1675	1670–1675	1666–1675
1685	1685	1682
	1700	1700

β-carotene, called β-car$_1$ and β-car$_2$, respectively (19). We therefore attempted to determine whether these two β-carotene populations have different conformation and/or configuration in the protein, which may be responsible for these differences in absorption properties.

Resonance Raman of Chl a Molecules Bound to HliD—Resonance Raman spectra of Chl *a* molecules contain bands that arise from the vibrational modes coupled with the electronic transition used to produce the resonance effect, usually with the highest energy Soret band to avoid interference with the Chl *a* fluorescence (25). These modes often arise from vibrations delocalized on the Chl *a* macrocycle, some in the low frequency range (around 300 cm^{-1}), which involve the central magnesium atom, and others in the mid-frequency range (800–1500 cm^{-1}) sensitive to the Chl *a* macrocycle conformation (26). However, none of these modes in the low to mid frequencies undergo shifts large enough so that they can be used for conclusive analysis of pigment protein complexes containing as many chlorophylls as LHCs. The position of bands in the high-frequency region (1500–1615 cm^{-1}) is sensitive to the conformation of (bacterio)chlorophyll. The band around 1550 cm^{-1}, attributed to complex vibrational modes of the chlorin ring (27), along with the methine bridge stretching mode around 1600 cm^{-1}, are sensitive to the macrocycle core size and have been widely used to assess the number of axial ligands bound to the central magnesium of these molecules (26, 28). This methine bridge mode is observed at about 1600 cm^{-1} when the central magnesium is six-coordinated, and is up-shifted to 1610–1615 cm^{-1} for five-coordinated magnesium. Additionally, stretching modes of conjugated C = O groups (keto-carbonyl for Chl *a*) are observed above 1630 cm^{-1} (29). The keto stretching modes of Chl *a* contribute at about 1700 cm^{-1} when free from interaction in non-polar environments (30). This frequency downshifts up to 40 cm^{-1} when this group is involved in intermolecular interactions (H-bonds), the extent of the downshift being proportional to the strength of the interaction. Smaller downshifts occur (5–10 cm^{-1}) when the C = O is present in a polar environment.

Fig. 3 shows the resonance Raman spectra at 77 K of Ycf39-HliD, LHCII (31), and CP29 (31) excited at 413.1 nm (Table 1
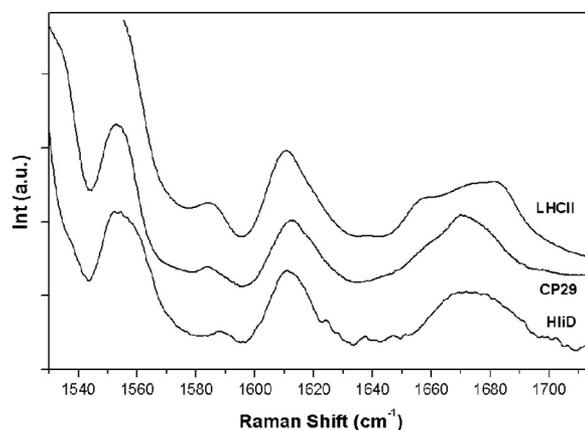
shows the frequencies of Chl *a* keto carbonyl stretching modes). In LHCII and CP29, modes sensitive to Chl conformation are localized around 1612 and 1550 cm^{-1}, indicating that the central magnesium atoms of most if not all Chl *a* molecules are five-coordinated in each case. These results were confirmed after comparing with the already resolved structure of LHCII (32, 33). In Ycf39-HliD, this shows a main component peaking at 1552 cm^{-1} and a clear additional component at 1558 cm^{-1}. This suggests that there is at least one Chl *a* with a distorted macrocycle attached to HliD. General distortions of the macrocycle, such as reduction of its core size generally affect the whole set of distortion-sensitive bands. In this case, we observed an additional component at 1558 cm^{-1} without any significant change in the band at 1612 cm^{-1}. It is thus likely that the distortion experienced by this Chl *a* concerns only a partial subset of the macrocycle angles between the pyrrole rings. In the keto carbonyl stretching mode region, the Ycf39-HliD complex presented a wide congested cluster of peaks at 1666–1675, 1682.0, and possibly one at 1695 cm^{-1}. Considering the intensity of the two latter bands, it is likely that at least four carbonyl modes contribute to the 1666–1675 cm^{-1} region, leading to a stoichiometry of at least six Chl *a* molecules, in fair agreement with the results of pigment analysis. For comparison, the spectra of CP29 and LHCII containing eight Chl *a* each are displayed in Fig. 3. It is of note that the population at 1659 cm^{-1} in LHCII and CP29, likely corresponding to two Chls *a* in each case and hypothesized to constitute a common structural motif for these proteins (31), is not present in the Ycf39-HliD spectrum.

Resonance Raman of β-Carotene Bound to HliD—Resonance Raman spectra of carotenoid molecules display four main groups of intense bands, which provide information on conformation and configuration for these molecules. One of the
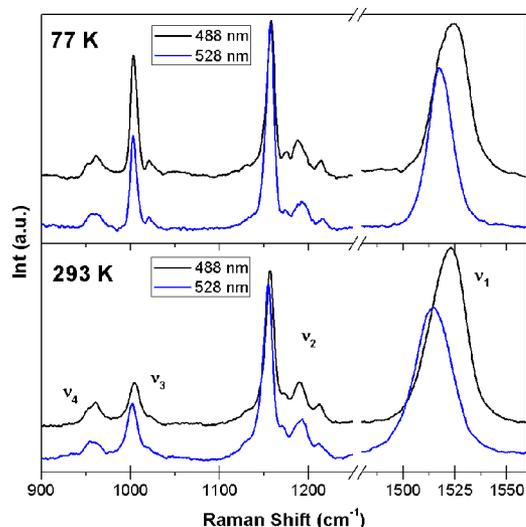
49

FIGURE 4. **Resonance Raman spectra at 77 K (*upper panel*) and 293 K (*lower panel*) of the Ycf39-HliD complex (excited at 488.0 and 528.7 nm).**

FIGURE 5. **Resonance Raman spectra at 77 K of Ycf39-HliD.** *a*, the 1500–1545 cm^{-1} region excited at 488.0, 514.5, and 528.7 nm. *Vertical red dashed lines* represent the center of the peaks corresponding to the two different β-carotenoids. *b*, 990–10155 cm^{-1} region excited at 488.0 nm and 528.7 nm.

strongest bands in these spectra, contributing around 1530 cm^{-1} (referred to as ν_1), arises from stretching vibrations of the C = C bonds of the carotenoid. The frequency of this band is sensitive to the extent of the conjugated system of the scattering carotenoid and to its molecular configuration (34, 35); it also exhibits intrinsic temperature dependence (36). Fig. 4 shows the resonance Raman spectra at 77 and 293 K of Ycf39-HliD excited at 488.0 and 528.7 nm, corresponding to the maximum absorption for each of the β-carotenes determined in Fig. 2. At 528.7-nm excitation, which should favor the contribution of the red-most absorbing β-carotene (β-car$_2$), this band is observed at about 1516.9 cm^{-1} at 77 K and about 1514.3 cm^{-1} at room temperature. The bandwidth at 77 K is 12 cm^{-1} (FWHM), as it is expected for single carotenoid molecules. When moving the excitation to 488.0 nm, where resonance is expected with the blue-absorbing β-carotene (β-car$_1$), the frequency of this band shifts to 1523.8 and 1522.4 cm^{-1} at 77 K and room temperature, respectively. However, it is also clear that the band becomes much broader in these conditions of excitation (nearly 20 cm^{-1}, FWHM), revealing the presence of more than one carotenoid species contributing at this wavelength. Fig. 5*a* focuses on the 1500–1545 cm^{-1} region at 77 K for excitations at 488.0, 496.5, 501.7, 514.5, and 528.7 nm. These spectra can all be fitted with a linear combination of only two peaks, with maxima represented by *dashed red lines* at 1516.9 and 1526.9 cm^{-1} (data not shown). Hence, it can be concluded that there are only two β-carotene populations associated with the putative HliD dimer as suggested in Ref. 19 and that one of them displays an exceptionally red-shifted absorption. The 528.7 nm excitation fits with the 0–0 transition of β-car$_2$, and is lying far from the β-car$_1$. Shifting the excitation to the blue will result in a decrease of β-car$_2$ contributions, and an increase of those from β-car$_1$. However, the maximum 0–0 transition of the β-car$_1$ (~489 nm; Fig. 2) lies close to the expected position for the 0–1 transition of β-car$_2$ (33 nm from 522 nm). This will result in significant contributions of β-car$_2$ at 488.0 nm, as observed in Figs. 4 and 5.

The intense contributions around 1160 cm^{-1}, termed ν_2, arise from stretching vibrations of C-C single bonds coupled
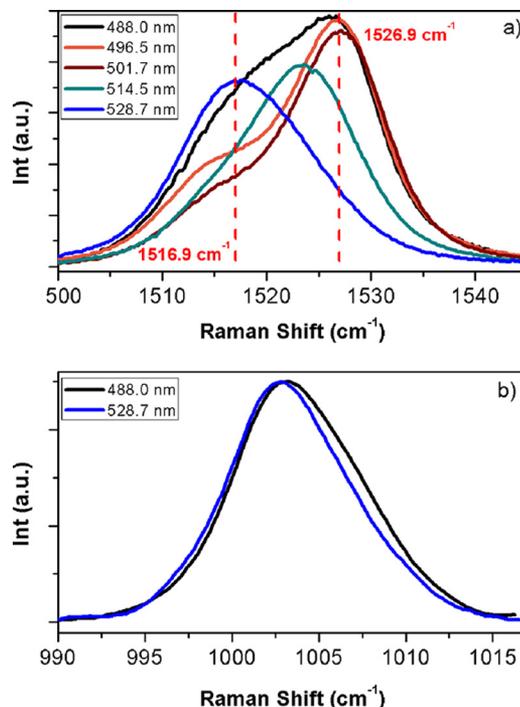
with C-H in-plane bending modes. This region is a fingerprint for the assignment of carotenoid configurations, *i.e.* isomerization states occurring in the conjugated C = C chain (34, 37). At room temperature, this region exhibits a main peak at 1155.2–1156.6 cm^{-1} with three satellite bands at 1171.6, 1190.2, and 1213.3 cm^{-1}, whereas at 77 K the main peak appears at 1157.9 cm^{-1} with the satellite bands at 1174.2, 1189.6, and 1214.8 cm^{-1}. These features do not present any difference from all-*trans* β-carotene in solution (34), and hence it may be safely concluded that the conjugated chain of both carotenoids present in HliD are in an all-*trans* configuration.

The next important set of bands appears around 1000 cm^{-1} (ν_3), arising from in-plane rocking vibrations of the methyl groups attached to the conjugated chain, coupled with the adjacent C-H in-plane bending modes (38, 39). It was proposed to be a fingerprint of the conjugated end cycle configuration (38), a hypothesis that was recently confirmed by theoretical modeling (39). For β-carotene in solvents, the band in ν_3 was shown as a doublet, and it was concluded that the presence of these two components revealed the out-of-plane configuration of the β-carotene end cycles (38). In Ycf39-HliD, this band (zoom-in Fig. 5*b*) displays mostly one component, located at 1003.2 cm^{-1}, when exciting at 528.7 nm, whereas two components are clearly observable upon 488.0 nm excitation, at 1002.7, and a shoulder at 1007.5 cm^{-1}, as observed for β-carotene free in solution (39, 40). Finally, around 960 cm^{-1} is found in the band termed ν_4, which arises from C-H out-of-plane wagging motions coupled with C=C torsional modes (out-of-plane twists of the carbon backbone) (41). When the carotenoid-conjugated system is planar, these out-of-plane modes will not be coupled with the electronic transition, and these bands will not
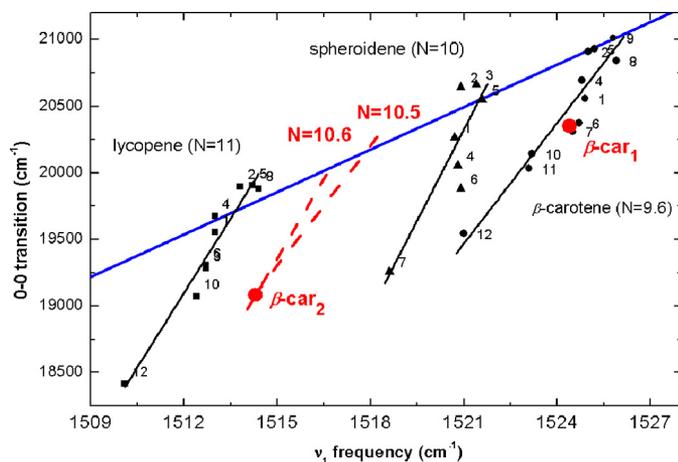
50

FIGURE 6. **Correlation between the position of the $S_0 \rightarrow S_2$ electronic transition and the ν_1 band frequency, as a function of solvent polarizability, for β-carotene (black circles), spheroidene (black triangles), and lycopene (black squares).** *1*, tetrahydrofuran; *2*, *n*-hexane; *3*, dichloroethane; *4*, cyclohexane; *5*, diethyl ether; *6*, toluene; *7*, chloroform; *8*, acetonitrile; *9*, methanol; *10*, pyridine; *11*, nitrobenzene; *12*, carbon disulfide. For comparison, the relationship between carotenoids of different conjugation lengths in the same solvent (*n*-hexane) is indicated by the *blue line*. The values for β-Car$_1$ and β-Car$_2$ in HLiD are indicated by *red dots*. All values were measured at room temperature.

be resonance-enhanced. However, distortions around C-C single bonds will increase the coupling of these modes with the electronic transition, resulting in an increase in their intensity, but also in their structure as these distortions will partially lift the degeneracy between the many ν_4 modes. In Fig. 4, it clearly appears that the ν_4 band displays a structure when exciting at both wavelengths: 488.0 nm (β-car$_1$) and 528.7 nm (β-car$_2$), indicating that both carotenoids are twisted. It is noteworthy that the structure observed for these bands is different. β-Car$_1$ presents an intense peak at 961 cm^{-1} slightly more enhanced than the peak at this position for β-car$_2$.

To obtain further insight in the two β-carotenes attached to HLiD, we plotted the energy of the electronic transitions of the two bound carotenes against the frequency of their ν_1 Raman band. Comparing simple, unsubstituted carotenoids on such a plot gives a linear relationship, where the position on the line depends on the effective conjugation length (42). Cyclic carotenoids such as β-carotene generally exhibit a shorter effective conjugation length than expected from their chemical structure, with the C-5,6 (and C-5′,6′) double bond(s) in the β-ring(s) adding only 0.3 to the *effective* conjugation length, N_{eff}, in each case, so that $N_{eff} = 9.6$ for β-carotene (42). On the other hand, for each carotenoid, the results obtained in different solvents fit with a different linear relationship, with the position on the line depending on the polarizability of their environment (42). This plot may thus give direct access to the effective conjugation length of a given carotenoid and the polarizability of its environment (42). In Fig. 6, the correlation between the position of the $S_0 \rightarrow S_2$ transition and the ν_1 band frequency, as a function of solvent polarizability was plotted for β-carotene (*black circles*, $N_{eff} = 9.6$), spheroidene (*black triangles*, $N_{eff} = 10$), and lycopene (*black squares*, $N_{eff} = 11$) in solution. The *blue line* represents the relationship between carotenoids of different conjugation length in the same solvent (*n*-hexane) (42). For each of these carotenoids, the correlation

between $S_0 \rightarrow S_2$ electronic transition and the ν_1 band frequency according to solvent polarizability was also plotted, represented as *solid black lines*. This correlation is similar for all carotenoid molecules, although it could be slightly less steep for β-carotene. When two β-carotenes present in Ycf39-HliD are placed on the plot (*red points*), β-Car$_1$ fits on the line obtained for β-carotene according to solvent polarizability. This indicates that this molecule adopts the same configuration as in solvent, in an environment with moderate polarizability (similar to toluene). This conclusion is consistent with the analysis of the ν_3 components, where two components are observed at 488.0 nm, as for β-carotene in solution. Conversely, β-Car$_2$ clearly deviates from this line, and the relationship obtained between its absorption position and its ν_1 can only be interpreted by assuming that this molecule displays a longer effective conjugated length, and it is sitting in a relatively high polarizability environment. As the correlation according to solvent polarizability is not exactly the same for every carotenoid, taking into account the two extreme slopes (shown by the *two red lines*), we may propose that the effective length of β-Car$_2$ lies between 10.5 and 10.6 C=C, and the polarizability of its binding site is either (in the first case) very high, similar to carbon disulfide, or similar to toluene in the second case.

In solvent, β-carotene displays an effective conjugation length of 9.6, shorter than its 11 C=C-conjugated chain, and this was attributed to out-of-plane positions of its conjugated end-cycles due to torsional twisting of the terminal rings of carotenoids that contain conjugated C=C bonds (43, 44). We may thus further conclude that β-Car$_1$ in Ycf39-HliD displays a configuration close to that observed in solvents, and is bound in a moderate polarizability binding site, whereas β-Car$_2$ have its C-5,6 (and C-5′,6′) double bonds in the β-rings clearly more conjugated to the π electronic system, and thus that its rings must be maintained close to the plane of the conjugated carbon chain. Its effective conjugation is close to that of its theoretically maximum ($n = 11$), and it is furthermore, bound to a binding site of high polarizability (comparable with carbon disulfide). It is well known that for terminal conjugated rings, the interaction of end groups with the polyene chain leads to steric deformations of around 45° for β-carotene (44). This deformation at the ends of the polyene chains together with the influence of end CH$_3$ groups or β-rings in carotenes causes smaller participation of π orbitals from C$_5$ and C$_6$ atoms in HOMO and LUMO of the polyene chain, diminishing the effective conjugation length (44) as we observe for β-Car$_1$. On the other hand, the effective conjugation length of β-Car$_2$ (which is still lower that its theoretical conjugation length of 11) is determined in Fig. 6 by the ν_1 band position, which is 8 cm^{-1} shifted from ν_1 band of β-Car$_1$. Bringing the aryl rings back into the plane of the β-carotene molecule would result in an increase of the effective conjugation length of up to 1.4. This effect has been observed for theoretical studies that prove that the change in dihedral angle of the terminal aryl ring in the ground state have an important effect in the effective conjugation length (43) and at the same time it has been observed for protein-bound carotenoids, where larger twists can be achieved depending on the design of the carotenoid binding pocket (45, 46). We thus propose that HLiD is able to tune the absorption of the red-absorbing β-carotene

51

via the rotation of its conjugated end-cycles toward the conjugated plane of the molecule, this rotation being imposed by its binding pocket through steric hindrance.

Discussion

The approach we use in this paper to address the structure and properties of the binding site of carotenoids, using a plot relating to energy of the electronic transition to the frequency of the C=C stretching mode, has already been widely applied to carotenoids bound to proteins (38, 42). It was shown, using this plot, that the absorption of carotenoid molecules in light-harvesting proteins from purple bacteria can be explained by the polarizability of their binding site alone. In that case, points corresponding to the LH-bound carotenoid in the plot obey the linear relationship due to solvent polarizability (38). In the case of the two luteins bound to LHCII and the two β-carotenes in Photosystem II reaction centers, polarizability alone can also explain the properties of the carotenoid molecule with absorption transitions to the blue. On the other hand, polarizability cannot explain the properties of the red-shifted carotenoid in either case, and an effect of the protein on their effective conjugation length had to be considered to account for the experimental results. Specific alterations of their equilibrium end-cycle conformations were concluded for the two red-absorbing carotenoids, in line with their ν_3 structure. It is important to emphasize that these conclusions were fully confirmed by analysis of the crystal structures of both proteins. However, for Photosystem II reaction centers, this effect is rather limited as the effective conjugation length reached by β-carotene is only 10 (38). It seems that the same phenomenon occurs for the HliD-bound β-Car_2, where the conjugation length increase up to about 10.5; the ν_3 band shows a clear shoulder indicating the twisting of both end rings and the shape of the ν_4 band when compared both carotenoids resembles that observed for the red-shifted β-carotene in Photosystem II reaction centers (38). Based on these similarities, it is possible to propose a model when the end rings of β-Car_2 are in a flat conjugated conformation, which has as a consequence the extension of the effective conjugation length.

HliD is a permanently quenched protein, and it has been clearly demonstrated that energy dissipation occurs via energy transfer from the Chl *a* Q_y state to β-carotene S_1 (19). Hence, these results suggest that this particularly extended conformation of the β-carotene molecule plays a role in the high efficiency of this singlet-singlet energy transfer.

The overall picture that emerges from this study is that the HliD binds two β-carotene molecules, both in S-cis configuration. The first one (β-Car_1) exhibits the same effective conjugation length as β-carotene in solution having moderate polarizability, whereas the second (β-Car_2) adopts an extended conformation that in turn confers to a molecule having lower energy of the S_0-S_2 transition. It is known that increase of the conjugation length leads to a decrease of energy of both the S_2 and S_1 states (47). Hence, it is proposed that this torsional conformation, which leads to an extension of effective conjugation, pushes the S_1 energy low enough to open a permanent dissipation channel for the excitation energy in this protein.

As shown previously the conformation of red-shifted β-carotene appears sensitive to the surrounding environment; the dissociation of Ycf39 from HliD changes the β-carotene absorption to be slightly less red-shifted (19). We, however, do not expect that the role Ycf39 is to modulate the HliD quenching mechanism. The firm binding of Ycf39 to HliD might rather localize this putative enzyme to a membrane compartment where it can regulate chlorophyll biosynthesis (17) and/or Photosystem II assembly (16). Structural details of the Ycf39 and HliD interaction are not known but the only feasible model is the Ycf39 binds to the N-terminal segment of HliD at the stromal side of the membrane (16). Indeed, the interaction with relatively large Ycf39 protein (40 kDa) will shape the HliD structure and probably also the β-carotene binding pocket.

We do not yet know whether there is an effect of Ycf39 on the efficiency of HliD quenching. However, the pure HliD clearly exhibits a quenching of chlorophyll fluorescence (19). Thus this quenching mechanism seems to be robust and not affected by small changes of carotenoid configuration. Nonetheless, the fact that the configuration of the quenching carotenoid in HliD can be affected by interactions with other proteins, or perhaps lipids, might play an important role during the evolution of eukaryotic antenna. A simple quenching mechanism in HliD seems adapted to a protein acting only for photoprotection. In LHCII from higher plants, which can oscillate from a light-harvesting mode to a quenching photoprotective mode, the dissipation mechanism is more complex, as it has to be tuned according to photosynthetic activity.

Experimental Procedures

Sample Preparation—Construction of *Synechocystis* strains and purification of the Ycf39-HliD complex were completed as described in Ref. 19.

Absorption Spectroscopy—Absorption spectra were collected using a Varian Cary E5 Double-beam scanning spectrophotometer.

Raman Spectroscopy—Resonance Raman spectra were recorded with a 90° signal collection using a two-stage monochromator (U1000, Jobin Yvon, Longjumeau, France) equipped with a front-illuminated, deep-depleted CCD detector (Jobin Yvon, Longjumeau, France). Excitation wavelengths were provided by a 24-watt Sabre Argon laser (Coherent, Palo Alto, CA), except for 413.1 and 406.7 nm, which were provided by an Innova 90 Krypton laser (Coherent). Unless otherwise indicated, less than 2 milliwatts reached the sample, and the sample integrity was verified by following resonance Raman spectral evolution during the experiment. These experiments were done at 77 K in an LN2 flow cryostat (Air Liquide), and room temperature and the spectral resolution of the Raman spectrometer was 0.5 cm^{-1}.

References

1. Blankenship, R. E. (2014) *Molecular Mechanisms of Photosynthesis*, Blackwell Science, Oxford, United Kingdom

2. Gust, D., Kramer, D., Moore, A., Moore, T. A., and Vermaas, W. (2008) Engineered and artificial photosynthesis: human ingenuity enters the game. *MRS Bull.* **33,** 383–387

3. Demmig-Adams, B., Garab, G., Adams Iii, W., and Govindjee. (2014) *Non-Photochemical Quenching and Energy Dissipation in Plants, Algae and Cyanobacteria*, Springer, The Netherlands

4. Ruban, A. V. (2016) Nonphotochemical chlorophyll fluorescence quenching: mechanism and effectiveness in protecting plants from photodamage. *Plant Physiol.* **170,** 1903–1916

5. Müller, M. G., Lambrev, P., Reus, M., Wientjes, E., Croce, R., and Holzwarth, A. R. (2010) Singlet energy dissipation in the photosystem II light-harvesting complex does not involve energy transfer to carotenoids. *ChemPhysChem* **11,** 1289–1296

6. Holt, N. E., Zigmantas, D., Valkunas, L., Li, X.-P., Niyogi, K. K., and Fleming, G. R. (2005) Carotenoid cation formation and the regulation of photosynthetic light harvesting. *Science* **307,** 433–436

7. Ruban, A. V., Berera, R., Ilioaia, C., van Stokkum, I. H., Kennis, J. T., Pascal, A. A., van Amerongen, H., Robert, B., Horton, P., and van Grondelle, R. (2007) Identification of a mechanism of photoprotective energy dissipation in higher plants. *Nature* **450,** 575–578

8. Bode, S., Quentmeier, C. C., Liao, P.-N., Hafi, N., Barros, T., Wilk, L., Bittner, F., and Walla, P. J. (2009) On the regulation of photosynthesis by excitonic interactions between carotenoids and chlorophylls. *Proc. Natl. Acad. Sci. U.S.A.* **106,** 12311–12316

9. Dolganov, N. A., Bhaya, D., and Grossman, A. R. (1995) Cyanobacterial protein with similarity to the chlorophyll *a/b* binding proteins of higher plants: evolution and regulation. *Proc. Natl. Acad. Sci. U.S.A.* **92,** 636–640

10. Neilson, J. A., and Durnford, D. G. (2010) Structural and functional diversification of the light-harvesting complexes in photosynthetic eukaryotes. *Photosynth. Res.* **106,** 57–71

11. Engelken, J., Brinkmann, H., and Adamska, I. (2010) Taxonomic distribution and origins of the extended LHC (light-harvesting complex) antenna protein superfamily. *BMC Evol. Biol.* **10,** 233

12. Bhaya, D., Dufresne, A., Vaulot, D., and Grossman, A. (2002) Analysis of the *hli* gene family in marine and freshwater cyanobacteria. *FEMS Microbiol. Lett.* **215,** 209–219

13. He, Q., Dolganov, N., Bjorkman, O., and Grossman, A. R. (2001) The high light-inducible polypeptides in *Synechocystis* PCC6803: expression and function in high light. *J. Biol. Chem.* **276,** 306–314

14. Komenda, J., and Sobotka, R. (2016) Cyanobacterial high-light-inducible proteins: protectors of chlorophyll: protein synthesis and assembly. *Biochim. Biophys. Acta* **1857,** 288–295

15. Yao, D., Kieselbach, T., Komenda, J., Promnares, K., Prieto, M. A., Tichy, M., Vermaas, W., and Funk, C. (2007) Localization of the small CAB-like proteins in photosystem II. *J. Biol. Chem.* **282,** 267–276

16. Knoppová, J., Sobotka, R., Tichy, M., Yu, J., Konik, P., Halada, P., Nixon, P. J., and Komenda, J. (2014) Discovery of a chlorophyll binding protein complex involved in the early steps of photosystem II assembly in *Synechocystis*. *Plant Cell* **26,** 1200–1212

17. Chidgey, J. W., Linhartová, M., Komenda, J., Jackson, P. J., Dickman, M. J., Canniffe, D. P., Koník, P., Pilný, J., Hunter, C. N., and Sobotka, R. (2014) A cyanobacterial chlorophyll synthase-HliD complex associates with the Ycf39 protein and the YidC/Alb3 insertase. *Plant Cell* **26,** 1267–1279

18. Niedzwiedzki, D. M., Tronina, T., Liu, H., Staleva, H., Komenda, J., Sobotka, R., Blankenship, R. E., and Polívka, T. (2016) Carotenoid-induced non-photochemical quenching in the cyanobacterial chlorophyll synthase-HliC/D complex. *Biochim. Biophys. Acta* **1857,** 1430–1439

19. Staleva, H., Komenda, J., Shukla, M. K., Šlouf, V., Kaňa, R., Polívka, T., and Sobotka, R. (2015) Mechanism of photoprotection in the cyanobacterial ancestor of plant antenna proteins. *Nat. Chem. Biol.* **11,** 287–291

20. Ruban, A. V., Lee, P. J., Wentworth, M., Young, A. J., and Horton, P. (1999) Determination of the stoichiometry and strength of binding of xanthophylls to the photosystem II light harvesting complexes. *J. Biol. Chem.* **274,** 10458–10465

21. Ruban, A. V., Pascal, A. A., Robert, B., and Horton, P. (2001) Configuration and dynamics of xanthophylls in light-harvesting antennae of higher plants: spectroscopic analysis of isolated light-harvesting complex of photosystem II and thylakoid membranes. *J. Biol. Chem.* **276,** 24862–24870

22. Ruban, A. V., Pascal, A., Lee, P. J., Robert, B., and Horton, P. (2002) Molecular configuration of xanthophyll cycle carotenoids in photosystem II antenna complexes. *J. Biol. Chem.* **277,** 42937–42942

23. Robert, B. (1996) Resonance Raman studies in photosynthesis: chlorophyll and carotenoid molecules. in *Biophysical Techniques in Photosynthesis* (Amesz, J., and Hoff, A., eds) pp. 161–176, Springer, The Netherlands

24. Pascal, A. A., Ruban, A. V., and Robert, B. (2014) Antenna protein conformational changes revealed by resonance Raman spectroscopy. in *Non-Photochemical Quenching and Energy Dissipation in Plants, Algae and Cyanobacteria* (Demmig-Adams, B., Garab, G., Adams, Iii, W., and Govindjee, eds) pp. 245–257, Springer, The Netherlands

25. Lutz, M. (1977) Antenna chlorophyll in photosynthetic membranes: a study by resonance Raman spectroscopy. *Biochim. Biophys. Acta* **460,** 408–430

26. Fujiwara, M., and Tasumi, M. (1986) Metal-sensitive bands in the Raman and infrared spectra of intact and metal-substituted chlorophyll *a*. *J. Phys. Chem.* **90,** 5646–5650

27. Lutz, M., and Mäntele, W. (1991) in *The Chlorophylls* (Scheer, H., ed) pp. 855–902, CRC Press Inc., Boca Raton, FL

28. Näveke, A., Lapouge, K., Sturgis, J. N., Hartwich, G., Simonin, I., Scheer, H., and Robert, B. (1997) Resonance Raman spectroscopy of metal-substituted bacteriochlorophylls: characterization of Raman bands sensitive to bacteriochlorin conformation. *J. Raman Spectrosc.* **28,** 599–604

29. Feiler, U., Mattioli, T. A., Katheder, I., Scheer, H., Lutz, M., and Robert, B. (1994) Effects of vinyl substitutions on resonance Raman spectra of (bacterio)chlorophylls. *J. Raman Spectrosc.* **25,** 365–370

30. Lapouge, K., Näveke, A., Sturgis, J. N., Hartwich, G., Renaud, D., Simonin, I., Lutz, M., Scheer, H., and Robert, B. (1998) Non-bonding molecular factors influencing the stretching wavenumbers of the conjugated carbonyl groups of bacteriochlorophyll *a*. *J. Raman Spectrosc.* **29,** 977–981

31. Pascal, A., Wacker, U., Irrgang, K.-D., Horton, P., Renger, G., and Robert, B. (2000) Pigment binding site properties of two photosystem II antenna proteins: a resonance Raman investigation. *J. Biol. Chem.* **275,** 22031–22036

32. Liu, Z., Yan, H., Wang, K., Kuang, T., Zhang, J., Gui, L., An, X., and Chang, W. (2004) Crystal structure of spinach major light-harvesting complex at 2.72-Å resolution. *Nature* **428,** 287–292

33. Standfuss, J., Terwisscha van Scheltinga, A. C., Lamborghini, M., and Kühlbrandt, W. (2005) Mechanisms of photoprotection and nonphotochemical quenching in pea light-harvesting complex at 2.5-Å resolution. *The EMBO J.* **24,** 919–928

34. Robert, B. (1999) The electronic structure, stereochemistry and resonance Raman spectroscopy of carotenoids. in *The Photochemistry of Carotenoids* (Frank, H. A., Young, A. J., Britton, G., and Cogdell, R. J., eds) pp. 189–201, Springer, The Netherlands

35. Koyama, Y., and Fujii, R. (1999) Cis-trans carotenoids in photosynthesis: configurations, excited-state properties and physiological functions. in *The Photochemistry of Carotenoids* (Frank, H. A., Young, A. J., Britton, G., and Cogdell, R. J., eds) pp. 161–188, Springer, The Netherlands

36. Andreeva, A., Apostolova, I., and Velitchkova, M. (2011) Temperature dependence of resonance Raman spectra of carotenoids. *Spectrochim. Acta A Mol. Biomol. Spectrosc.* **78,** 1261–1265

37. Koyama, Y., Takii, T., Saiki, K., and Tsukida, K. (1983) Configuration of the carotenoid in the reaction centers of photosynthetic bacteria: 2. comparison of the resonance Raman lines of the reaction centers with those of the 14 different cis-trans isomers of β-carotene. *Photochem. Photobiol.* **5,** 139–150

38. Mendes-Pinto, M. M., Galzerano, D., Telfer, A., Pascal, A. A., Robert, B., and Ilioaia, C. (2013) Mechanisms underlying carotenoid absorption in oxygenic photosynthetic proteins. *J. Biol. Chem.* **288,** 18758–18765

39. Macernis, M., Galzerano, D., Sulskus, J., Kish, E., Kim, Y.-H., Koo, S., Valkunas, L., and Robert, B. (2015) Resonance Raman spectra of carotenoid molecules: influence of methyl substitutions. *J. Phys. Chem. A* **119,** 56–66

53

40. Telfer, A., Frolov, D., Barber, J., Robert, B., and Pascal, A. (2003) Oxidation of the two β-carotene molecules in the photosystem II reaction center. *Biochemistry* **42,** 1008–1015

41. Lutz, M., Szponarski, W., Berger, G., Robert, B., and Neumann, J.-M. (1987) The stereoisomerization of bacterial, reaction-center-bound carotenoids revisited: an electronic absorption, resonance Raman and NMR study. *Biochim. Biophys. Acta* **894,** 423–433

42. Mendes-Pinto, M. M., Sansiaume, E., Hashimoto, H., Pascal, A. A., Gall, A., and Robert, B. (2013) Electronic absorption and ground state structure of carotenoid molecules. *J. Phys. Chem. B* **117,** 11015–11021

43. Fuciman, M., Keşan, G., LaFountain, A. M., Frank, H. A., and Polívka, T. (2015) Tuning the spectroscopic properties of aryl carotenoids by slight changes in structure. *J. Phys. Chem. B* **119,** 1457–1467

44. Macernis, M., Sulskus, J., Malickaja, S., Robert, B., and Valkunas, L. (2014) Resonance Raman spectra and electronic transitions in carotenoids: a density functional theory study. *J. Phys. Chem. A* **118,** 1817–1825

45. Polívka, T., Kerfeld, C. A., Pascher, T., and Sundström, V. (2005) Spectroscopic properties of the carotenoid 3′-hydroxyechinenone in the orange carotenoid protein from the cyanobacterium *Arthrospira maxima*. *Biochemistry* **44,** 3994–4003

46. Polívka, T., Balashov, S. P., Chábera, P., Imasheva, E. S., Yartsev, A., Sundström, V., and Lanyi, J. K. (2009) Femtosecond carotenoid to retinal energy transfer in xanthorhodopsin. *Biophys. J.* **96,** 2268–2277

47. Polívka, T., and Sundström, V. (2004) Ultrafast dynamics of carotenoid excited states: from solution to natural and artificial systems. *Chem. Rev.* **104,** 2021–2071

54

3.3   Result III

Binding of pigments to the cyanobacterial high-light-inducible protein HliC

Shukla, M.K., Llansola-Portoles, M.J., Tichý, M., Pascal, A.A., Robert, B., Sobotka, R.

ORIGINAL ARTICLE

CrossMark

Binding of pigments to the cyanobacterial high-light-inducible protein HliC

Mahendra Kumar Shukla[1,2] · Manuel J. Llansola-Portoles[3] · Martin Tichý[1] · Andrew A. Pascal[3] · Bruno Robert[3] · Roman Sobotka[1,2]

Abstract

Cyanobacteria possess a family of one-helix high-light-inducible proteins (HLIPs) that are widely viewed as ancestors of the light-harvesting antenna of plants and algae. HLIPs are essential for viability under various stress conditions, although their exact role is not fully understood. The unicellular cyanobacterium *Synechocystis* sp. PCC 6803 contains four HLIPs named HliA–D, and HliD has recently been isolated in a small protein complex and shown to bind chlorophyll and β-carotene. However, no HLIP has been isolated and characterized in a pure form up to now. We have developed a protocol to purify large quantities of His-tagged HliC from an engineered *Synechocystis* strain. Purified His-HliC is a pigmented homo-oligomer and is associated with chlorophyll and β-carotene with a 2:1 ratio. This differs from the 3:1 ratio reported for HliD. Comparison of these two HLIPs by resonance Raman spectroscopy revealed a similar conformation for their bound β-carotenes, but clear differences in their chlorophylls. We present and discuss a structural model of HliC, in which a dimeric protein binds four chlorophyll molecules and two β-carotenes.

Keywords *Synechocystis* · HLIPs · HliC · Raman spectroscopy · Chlorophyll · β-Carotene

Abbreviations

HLIPs	High-light-inducible proteins
Chl	Chlorophyll *a*
β-car	β-Carotene
LHC	Light-harvesting complex
PSII	Photosystem II

Mahendra Kumar Shukla and Manuel J. Llansola-Portoles have contributed equally to this work.

Electronic supplementary material The online version of this article (https://doi.org/10.1007/s11120-017-0475-7) contains supplementary material, which is available to authorized users.

✉ Roman Sobotka
sobotka@alga.cz

1   Centre Algatech, Institute of Microbiology, Academy of Sciences of the Czech Republic, 379 81 Třeboň, Czech Republic

2   Faculty of Science, University of South Bohemia, 370 01 České Budějovice, Czech Republic

3   Institute for Integrative Biology of the Cell (I2BC), CEA, CNRS, Université Paris-Saclay, 91198 Gif-sur-Yvette cedex, France

Introduction

Oxygenic photosynthesis evolved in cyanobacteria about three billion years ago (Holland 2006), and roughly one billion years ago, an endosymbiotic event between a eukaryotic cell and a cyanobacterium created the first ancestor of algae and plants. Although the original engulfed cyanobacterium was drastically reduced and modified during the process that resulted in modern chloroplasts, the photosynthetic apparatus remained remarkably preserved in cyanobacteria and plants despite the amount of time that has passed since this primary endosymbiosis. However, there is a striking difference in the structure of light-harvesting complexes (LHCs) used by cyanobacteria and plants to collect photons for photosynthesis.

During evolution, the green lineage of algae replaced the extrinsic cyanobacterial phycobilisome antenna, which collects light using phycobilin chromophores, with a family of chlorophyll (Chl)- and carotenoid-containing membrane proteins. Modern LHCs of algae and plants are sophisticated nano-devices that can switch from a light-harvesting mode, where energy input is optimized in low-light conditions, to a dissipative (protective) mode in high light, thus avoiding light-induced damage (Ruban 2016). Although the LHC

🙂 Springer

proteins are not present in cyanobacteria, a cyanobacterial family of single-helix proteins possessing a typical LHC-like Chl-binding motif—the high-light-inducible proteins (HLIPs)—was discovered more than 20 years ago (Dolganov et al. 1995). Similar small one-helix proteins (OHPs) have been discovered in eukaryotic phototrophs, together with two- (SEP, LIL), three- (ELIPs) and four- (PsbS) helix proteins. The functions of these LHC-like proteins are apparently not in light harvesting but rather in photoprotection, biogenesis and regulation of the photosynthetic apparatus (Beck et al. 2017; Hutin et al. 2003; Lohscheider et al. 2015; Peers et al. 2009). The 'true' light-harvesting LHCs thus form only a branch of the extended LHC superfamily, and members are recognizable by the conserved Chl-binding motif on the stromal side of one or more of their transmembrane α-helices (Fig. S1).

HLIPs are now widely accepted as ancestors of the whole LHC superfamily (Neilson and Durnford 2010), but their exact role is still a matter of debate. Cyanobacterial mutants lacking HLIPs are generally stress sensitive, and there is accumulating evidence that HLIPs assist during biogenesis and repair of Photosystem II (PSII), particularly under stress conditions (reviewed in Komenda and Sobotka 2016). The function of HLIPs is best studied in the model cyanobacterium *Synechocystis* sp. PCC 6803 (hereafter *Synechocystis*), which contains four small HLIPs, HliA–D. All four proteins bind to newly synthesized PSII core proteins. A sub-complex of the putative alcohol dehydrogenase (Ycf39) with HliD and HliC tightly associates with the newly synthesized D1 subunit of PSII (Knoppová et al. 2014), whereas HliA, HliB and HliC bind to the CP47 assembly module (Yao et al. 2007). In addition, HliD and HliC also form a complex with Chl synthase, the last enzyme of Chl biosynthesis (ChlG; Chidgey et al. 2014; Niedzwiedzki et al. 2016).

The finding that HLIPs are essential for long Chl half-life (days) in *Synechocystis* cells led to the speculation that they facilitate Chl recycling (Chl dephytylation–phytylation cycle) by providing a shuttle for Chl molecules between the site of PSII repair and the ChlG enzyme (Vavilin et al. 2007). However, it was not clear that HLIPs were able to bind pigments until fairly recently. Purification of HliD in a complex with Ycf39 or ChlG demonstrated binding of Chl and β-carotene (β-car; Niedzwiedzki et al. 2016; Staleva et al. 2015). Moreover, HliD binds these pigments in a dissipative configuration, converting absorbed light energy to heat via Chl-to-β-car energy transfer (Staleva et al. 2015), mirroring the mechanism observed for the dissipative mode in plant LHCII (Ruban et al. 2007).

Current knowledge about pigment binding to HLIPs is limited to the HliD protein, which has been purified in complex with other proteins only, by expensive immuno-affinity chromatography. Here we report a *Synechocystis* HliC preparation devoid of other proteins, using a cheap His-tag

approach and in quantities and purity sufficient for biophysical and biochemical studies. The isolated His-HliC oligomers bind Chl and β-car but in a different ratio than reported for HliD. Based on detailed characterization, we provide a structural model of dimeric HliC with its bound pigments.

Materials and methods

Construction of His-HliC-expressing Synechocystis strain

To generate a *Synechocystis* strain expressing HliC with an 8xHis tag on its N terminus, we adopted an analogous approach to that described previously for the preparation of His-HliB (ScpDHis; Promnares et al. 2006). The method takes advantage of an engineered strain expressing the *sacB* gene from the *psbA2* promoter (Lagarde et al. 2000). *sacB* encodes a levansucrase, which converts sucrose to a toxic substance, leading to sucrose sensitivity. The designed His-HliC construct with overlapping *psbA2* upstream and downstream regions was transformed into the strain with *sacB*; sucrose was added for negative selection. In the resulting marker-less strain expressing His-tagged HliC under the control of the *psbA2* promoter, the native *hliC, psbB* and *hliD* genes were subsequently inactivated using available constructs (Eaton-Rye and Vermaas 1991; Xu et al. 2004). The resulting His-HliC/Δ*hliC*/Δ*psbB*/Δ*hliD* strain was grown at 28 °C in liquid BG11 medium supplemented with 5 mM glucose under high-light conditions (300 μmol of photons/m^2/s), in 1-L cylinders bubbled with air.

Purification of His-HliC by nickel affinity chromatography

For the purification of His-HliC, 4 L of HliC/Δ*hliC*/Δ*psbB*/Δ*hliD* cells were broken using glass beads (0.1 mm diameter) in buffer A containing 25 mM MES/NaOH, pH 6.5, 10 mM CaCl$_2$, 10 mM MgCl$_2$, 25% glycerol and EDTA-free protease inhibitor (Roche). The pelleted membrane fraction, prepared essentially as described in Kopečná et al. (2012), was resuspended in buffer A (~ 0.5 mg Chl/mL) and solubilized for 30 min at 10 °C with 1% dodecyl-β-maltoside. Finally, insoluble contaminants were removed by centrifugation (65,000×*g*, 25 min), and the supernatant was loaded on a nickel affinity chromatography column (0.5 mL Protino Ni–NTA agarose, Macherey-Nagel, Germany). Proteins bound to the column were washed with 15 mL of buffer A containing 0.04% dodecyl-β-maltoside (A-DDM), with 2 mL of 40 mM imidazole in A-DDM, and finally with 1 mL of 80 mM imidazole in A-DDM. His-HliC was eluted using 2 mL A-DDM containing 150 mM imidazole and

Two-dimensional electrophoresis

For native electrophoresis, 50 μL of the concentrated His-HliC elution was separated on a 4–12% clear-native gel (Wittig et al. 2007). Chl fluorescence emitted by separated Chl proteins was detected by a Fuji LAS 4000 upon excitation with blue light. For the second dimension, the gel strip was incubated in 2% SDS and 1% dithiothreitol for 30 min at room temperature, and proteins were separated by SDS electrophoresis in a denaturing 12–20% polyacrylamide gel containing 7 M urea (Dobáková et al. 2009). Proteins were stained by Coomassie Brilliant Blue or transferred to a PVDF membrane; this membrane was incubated with a specific primary antibody against HliC and then with secondary antibody conjugated with horseradish peroxidase (Sigma-Aldrich). The anti-HliC antibody was raised in rabbits against a synthetic peptide corresponding to unique HliC residues 1–17.

Anion exchange chromatography and pigment HPLC

0.4 mL of the concentrated His-HliC elution from the nickel column was injected onto a MonoQ anion exchange column (1.6 mL volume, GE Healthcare) and separated by a NaCl gradient in HEPES/NaOH buffer, pH 8.1, 5 mM $MgCl_2$ and 0.04% dodecyl-β-maltoside. The NaCl concentration was zero for the first 15 min, then gradually increased to 0.2 M in 5 min and then to 0.6 M in 40 min (flow rate 0.4 mL/min, 8 °C). Eluted proteins were monitored by a diode array detector (Agilent 1260). The His-HliC eluted as a peak at ~ 11 mL and was concentrated to 25 μL in Amicon 3 kDa micro-concentrators (Millipore). Pigments were extracted with an excess of methanol and separated on a reverse-phase column (Zorbax Eclipse plus C18, 3.5 μm particle size, 4.6 × 100 mm; Agilent) using an Agilent 1200 HPLC. The extract was loaded with 35% methanol and 15% acetonitrile in 0.25 M pyridine (solvent A), and pigments were eluted with a linear gradient of solvent B (20% methanol, 20% acetone in acetonitrile; 30–95% gradient over 25 min), followed by 95% solvent B (flow rate 0.8 ml/min, 40 °C).

Room-temperature and low-temperature absorption spectroscopy

Absorption spectra of the purified His-HliC were measured at room temperature with a UV 3000 spectrophotometer (Shimadzu) and at 4.5 K in a helium bath cryostat (Utreks) using a Varian Cary E5 double-beam scanning spectrophotometer. Glycerol was added to the low-temperature sample (70%, v/v) to prevent devitrification.

Raman spectroscopy

Resonance Raman spectra were recorded at 90° signal collection using a Jobin Yvon U1000 two-stage monochromator equipped with a front-illuminated, deep-depleted CCD detector (Jobin Yvon, Longjumeau, France). Excitation wavelengths in the blue-green region were provided by a 24-W Sabre Argon laser (Coherent, Palo Alto, California) and those in the violet region by an Innova 90 Krypton laser (Coherent, Palo Alto, California). Less than 2 mW reached the sample, and sample integrity was verified by following RR spectral evolution during the experiment. 77 K measurements were performed in an SMC-TBT flow cryostat (Air Liquide, Sassenage, France).

Results and discussion

Purification of Synechocystis His-HliC and pigment analysis

We have generated a *Synechocystis* strain expressing 8xHis-tagged HliC under the control of the *psbAII* promoter and lacking the native *hliC* gene. To facilitate isolation of pure His-HliC, this strain was further modified by deletion of the genes coding for proteins known to interact with HliC—the PSII CP47 subunit (Yao et al. 2007) and HliD (Knoppová et al. 2014; Niedzwiedzki et al. 2016). His-HliC was purified using nickel affinity chromatography from thylakoid membranes prepared from this His-HliC/Δ*hliC*/Δ*psbB*/Δ*hliD* strain.

The eluted fraction was yellow-orange and its absorbance spectrum indicated the presence of Chl and carotenoids (Fig. S2). The eluate was separated by clear-native electrophoresis and then in a second dimension on a denaturing SDS gel. After Coomassie blue staining, we observed one intensely stained band at ~ 6 kDa, along with a weaker one at ~ 15 kDa (i.e. roughly two times the size), and both were identified as HliC by immunodetection (Fig. S3). Thus, a small but significant proportion of the isolated HliC ran as a dimer even on the denaturing SDS gel (Fig. 1a; Fig. S3), indicating the remarkable stability of this dimeric form. On clear-native electrophoresis, the purified His-HliC tends to aggregate yielding oligomers with a mass of greater than 100 kDa—note that freshly prepared His-HliC (Fig. 3a) appeared less aggregated on the native gel than the identical sample after storing at − 80 °C (Fig. 1a), but still exhibited significant oligomerization. These different His-HliC multimers exhibit essentially the same absorption spectra (Fig. S3b). Chl fluorescence of the purified His-HliC, as detected using blue-light excitation in the native gel, was apparently very
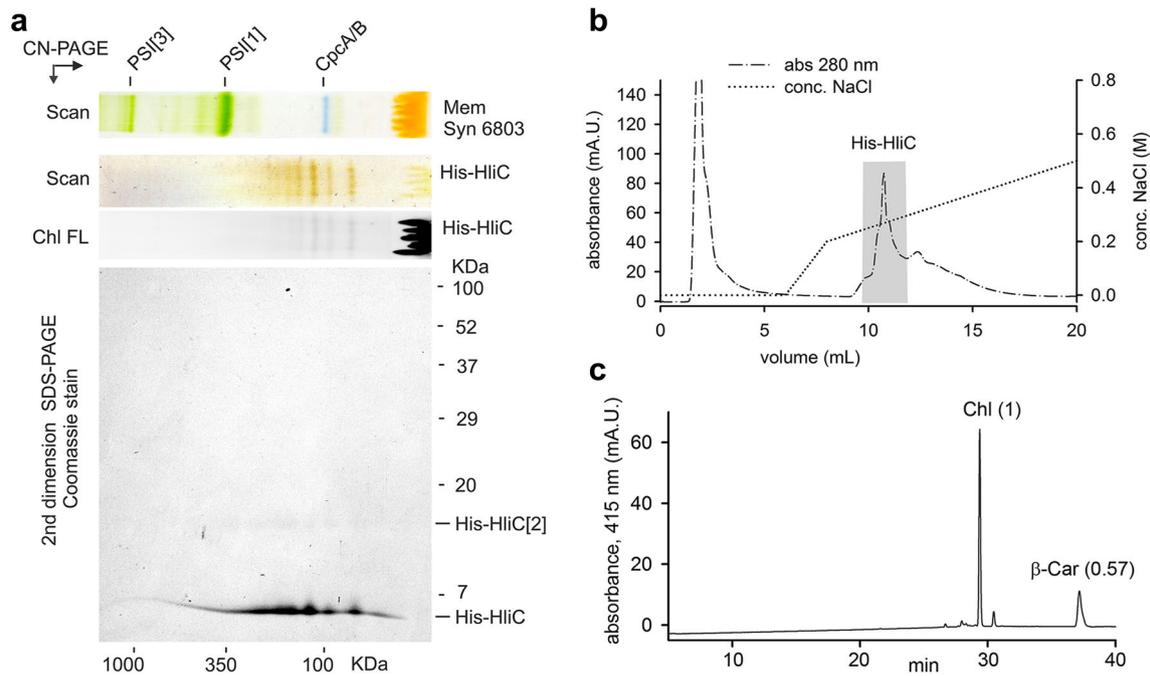
Fig. 1 Two-dimensional electrophoresis and pigment analysis of the purified His-HliC protein. **a** The His-HliC protein eluted from a nickel column was separated by clear-native electrophoresis (CN-PAGE), together with solubilized thylakoid membranes from *Synechocystis* (Mem Syn 6803). PSI[1] and PSI[3] indicate the monomer and trimer of Photosystem I with masses of ~ 1 MDa and ~ 350 kDa, respectively. CpcA/B marks ~ 100 kDa heterohexamer of CpcA and CpcB phycobiliproteins. The obtained gel strip from CN-PAGE with separated His-HliC was scanned for Chl fluorescence (Chl FL) and then further separated in a second dimension by SDS electrophoresis. This gel was stained by Coomassie blue. **b** A second purification step using anion exchange (MonoQ) chromatography. A fraction of His-HliC that binds to the MonoQ column was collected (indicated by a grey box) and concentrated for pigment analysis. The absorbance spectrum of the collected peak is shown in Fig. S1. **c** HPLC chromatogram of pigments extracted from the His-HliC protein after anion exchange chromatography. The calculated molar stoichiometry of Chl and β-car is shown in parentheses

low when compared to unbound pigments (Fig. 1a). This suggests that HliC binds pigments in an energy-dissipative conformation.

To remove any unbound pigments, the His-HliC eluate was further separated on a MonoQ anion exchange column. Although in the buffer system used most of His-HliC did not bind to the column, a bound sub-fraction was eluted with higher salt concentration and collected (Fig. 1b). The absorbance spectrum of the collected His-HliC was essentially identical to the 'crude' preparation of His-HliC obtained from the nickel column (Fig. S2). It is not clear why only a fraction of His-HliC bound to the anion exchange column but it might be related to the different oligomeric states observed. Pigments in the His-HliC fraction (a peak over ~ 11 mL; Fig. 1b) were extracted with methanol and analysed by HPLC. This revealed that His-HliC contains Chl and β-car in a 2:1 ratio. The Chl:carotenoid ratio is lower than that reported for the HliD protein (Staleva et al. 2015). Indeed, the increase in β-car per Chl in His-HliC is clearly observed when

comparing the absorption spectra of the two preparations (Staleva et al. 2015). The spectrum of the ChlG–HliC/D complex exhibiting ~ 1:1 Chl-to-carotenoid ratio (Chidgey et al. 2014) is also included for comparison (Fig. 2a).

It has been shown recently that HliD binds at least two different populations of β-car, one of which displays a very red-shifted absorption (Llansola-Portoles et al. 2017b). At room temperature, in the blue-green region corresponding to carotenoid 0–0 absorption transitions, His-HliC exhibits two absorption peaks around 487 and 521 nm—resembling ChlG–HliC/D more closely than does HliD (Fig. 2a). Second derivative analysis resolved two potential β-car populations bound to His-HliC (inset to Fig. 2a). Upon lowering the temperature to 4.5 K, both β-car populations in His-HliC appear to red-shift further, peaking at 492 and 527 nm (Fig. 2b). Note that this is not due to the use of 70% glycerol for the low-temperature spectra, as at room temperature this glycerol sample had the same spectrum as without glycerol (data not shown).

Fig. 2 Absorption spectra of His-HliC. **a** Room-temperature absorption spectrum of purified His-HliC compared with the spectra of HliD and ChlG–HliD/C. Second derivative is shown for His-HliC in the inset, to identify the two β-car peak positions. **b** 4.5 K absorption spectrum of the same His-HliC sample
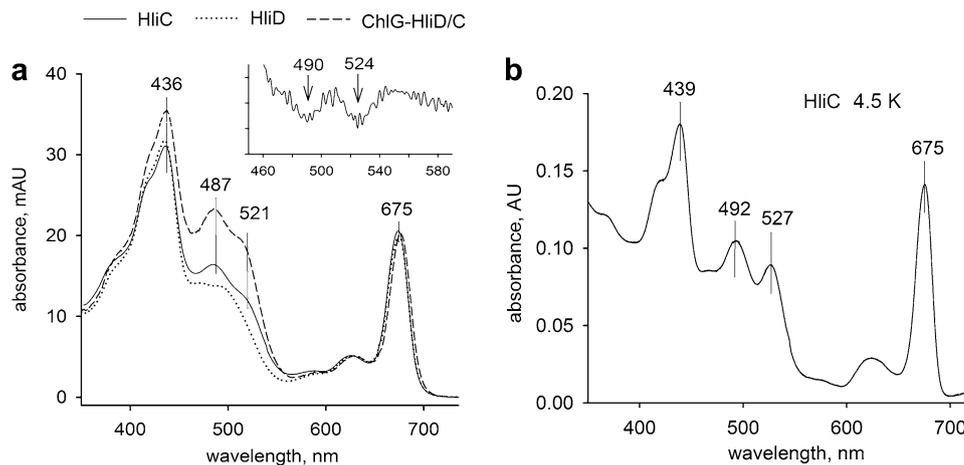
Resonance Raman spectroscopy of Chl molecules bound to HliC

To gain further insight into the configuration and stoichiometry of HliC-bound pigments, we employed resonance Raman spectroscopy. Raman spectra under resonance conditions contain bands arising from those vibrational modes that are coupled with the electronic transition used to produce the resonance effect (i.e. corresponding to the excitation wavelength). In the case of Chl molecules, resonance Raman spectroscopy is most easily performed by excitation in the highest-energy Soret transition (Lutz 1977). The majority of bands arise from vibrations that are delocalized on the Chl macrocycle. Modes in the high-frequency region (1500–1615 cm^{-1}) are of particular interest in assessing the conformation and state of interaction of protein-bound Chl molecules. The band around 1550 cm^{-1}, attributed to complex vibrational modes of the macrocycle, is primarily sensitive to macrocycle distortions (Fujiwara and Tasumi 1986; Näveke et al. 1997)—for example, it is located at 1550 and 1540 cm^{-1} when the central Mg is five- or six-coordinated, respectively. A second band, mainly arising from the methane bridge stretching modes, appears around 1600 cm^{-1} when the central magnesium is six-coordinated, and is up-shifted to 1610–1615 cm^{-1} for five-coordinated magnesium (Fujiwara et al. 1985; Näveke et al. 1997). Additionally, the stretching modes of conjugated C=O groups (keto carbonyl for Chl *a*), observed above 1630 cm^{-1}, can be used to determine the state of interactions of this group with its environment (Feiler et al. 1994). These modes contribute at *ca* 1700 cm^{-1} for a Chl keto group free from interactions in a non-polar environment (Lapouge et al. 1998). This frequency downshifts by up to 40 cm^{-1} according to the strength of intermolecular interactions (H-bonds) that these groups are involved in, while smaller downshifts (5–10 cm^{-1}) are induced when the C=O is present in a polar environment (Lapouge et al. 1998).

Figure 3a shows the 77 K resonance Raman spectra of pure His-HliC excited at 406.7 and 413.1 nm, compared to that of the Ycf39–HliD complex (Llansola-Portoles et al. 2017b). As described above, the two bands around 1550 and 1600 cm^{-1} are highly sensitive to distortions of the Chl macrocycle (Fujiwara and Tasumi 1986; Näveke et al. 1997). For LHCII and CP29, these modes were observed around 1550 and 1612 cm^{-1}, and were non-homogeneously broadened (FWHM 12 cm^{-1}), indicating that the central magnesium atoms of most if not all Chl molecules are five-coordinated in each case. In Ycf39–HliD, the band around 1550 cm^{-1} showed a main component peaking at 1552 cm^{-1} with an additional shoulder at 1558 cm^{-1} (Llansola-Portoles et al. 2017b), whereas His-HliC shows a wide plateau corresponding to one band at 1552 cm^{-1} and another around 1560 cm^{-1}. We can therefore conclude that for HliC, at least one, if not two Chls are present with a distorted macrocycle. It should be noted that the change in coordination number of the central Mg from 6 to 5 induces an up-shift of this band by *ca* 12 cm^{-1} (Fujiwara and Tasumi 1986)—i.e. more than that observed here. This, along with the frequency of the methine bridge mode at 1612 cm^{-1}, indicates that this distorted Chl in HliC is nevertheless five-coordinated. It is not possible to determine the exact kind of distortion of the macrocycle, but it probably concerns only a partial subset of the macrocycle angles between the pyrrole rings.

In the region corresponding to bands arising from the stretching modes of the keto carbonyl groups, there are also clear differences between the Ycf39–HliD complex and His-HliC. HliD presents a wide, congested cluster of peaks at 1666–1675 and 1682 cm^{-1}, and possibly one at 1695 cm^{-1}. Considering the intensity of the two latter bands, we concluded that at least four carbonyl modes contribute in the 1666–1675 cm^{-1} region, leading to a stoichiometry of at least six Chl molecules, in agreement with the pigment analysis (Staleva et al. 2015). The His-HliC resonance Raman spectra upon 406.7 and 413.1 nm excitation (Fig. 3a) display
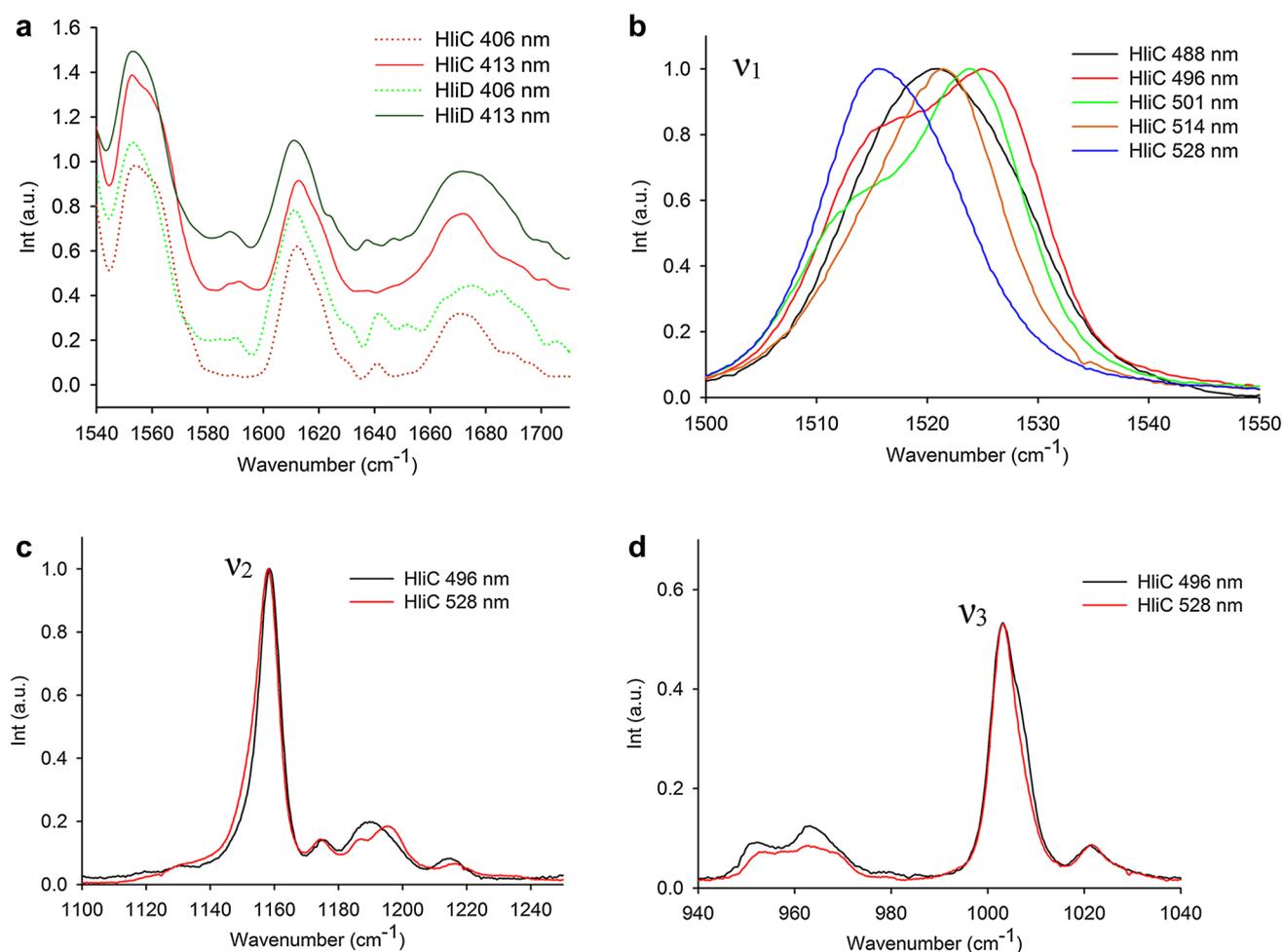
Fig. 3 77 K resonance Raman spectra of purified His-HliC and Ycf39–HliD. **a** Chl excitation at 406.7 and 413.1 nm, for His-HliC and Ycf39–HliD (HliD). **b–d** Carotenoid excitation for His-HliC at 488.0, 496.5, 501.7, 514.5 and 528.7 nm. See text for description of ν_{1-4} bands

a narrower distribution of frequencies, suggesting that most Chls in HliC have a strongly H-bonded keto C=O, with one being either weakly H-bonded, or free from interactions in a polar environment. It is worth noting that the relative intensities of the macrocycle modes discussed above, and the envelope of keto C=O modes, are significantly different than those for HliD, suggesting significant changes in resonance conditions.

Resonance Raman spectroscopy of β-car bound to HliC

The resonance Raman spectra of carotenoid molecules present four main groups of intense bands that can be used to obtain information on their conformation and configuration. The major contribution around 1520 cm^{-1}, referred to as ν_1, arises from stretching vibrations of the conjugated C=C bonds of the carotenoid. The position of this band is sensitive to the extent of the conjugated system and to the

molecular configuration of the scattering carotenoid (Koyama and Fujii 1999; Robert 1999), in addition to being temperature dependent (Andreeva et al. 2011). Figure 3b shows the resonance Raman spectra at 77 K of HliC excited at 488.0, 496.5, 501.7, 514.5 and 528.7 nm. These excitations were chosen to span the (0,0) absorption bands of the two apparent carotenoid populations observed in Fig. 2 (490 and 524 nm). For excitation at 528.7 nm, which should favour contributions of the red-most absorbing β-car (β-car$_2$), ν_1 is observed at ca 1515 cm^{-1}. Its bandwidth (~ 15 cm^{-1} FWHM) corresponds to that expected for a single population of carotenoid molecules. Shifting the excitation to 488.0 nm, an additional contribution is observed at 1525 cm^{-1}, which can be attributed to the blue-absorbing β-car (β-car$_1$). The 528.7 nm excitation fits with the 0–0 transition of β-car$_2$ and is lying quite far from that of β-car$_1$. Shifting the excitation to the blue will result in a decrease of β-car$_2$ contributions and an increase of those from β-car$_1$. However, the maximum of the 0–0 transition of the latter nearly fits with the

0–1 transition of the former. This explains why, although 488.0 nm excitation matches with the 0–0 transition of β-car$_1$, its 1525 cm^{-1} contributions at this excitation remain mixed with those of β-car$_2$ (1515 cm^{-1}). Figure 3b shows the evolution of this mode for excitations throughout this region. It can be explained by a linear combination of the peaks at 1515 and at 1525 cm^{-1} (not shown), consistent with two carotenoid species in the HliC preparation—β-car$_1$ with an absorption peak at 487 nm and β-car$_2$ absorbing at 521 nm. Therefore, only the bluest and reddest excitations matching the main absorption peaks for each carotenoid population will be considered in the analysis of the remaining carotenoid Raman modes.

Another important region in carotenoid resonance Raman spectra is the intense group of bands around 1160 cm^{-1}. This ν_2 region arises from stretching vibrations of C–C single bonds coupled with C–H in-plane bending modes. It can be used as a fingerprint for the assignment of carotenoid configurations, i.e. isomerization states occurring along the conjugated C=C chain (Koyama et al. 1983; Robert 1999). Figure 3c shows the resonance Raman spectra of HliC at 77 K in this region. Upon 528.7 nm excitation, the main peak appears at 1157 cm^{-1} with satellite bands at 1174 and 1214 cm^{-1}. For 496.5 nm excitation, this region is essentially the same, except the two bands at 1186 and 1195 cm^{-1} that are replaced by a broad feature peaking at 1189 cm^{-1}. The spectra do not exhibit significant difference from *all-trans* β-car in solution (Robert 1999), and hence it may be safely concluded that the conjugated chain of both carotenoid populations present in His-HliC are in an *all-trans* configuration.

The bands around 1000 cm^{-1} (ν_3) arise from in-plane rocking vibrations of the methyl groups attached to the conjugated chain, coupled with in-plane bending modes of the adjacent C–H's (Macernis et al. 2015; Mendes-Pinto et al. 2013a). They were proposed to be a fingerprint of the conjugated end-cycle configuration (Mendes-Pinto et al. 2013a), a hypothesis that was recently confirmed by theoretical modelling (Macernis et al. 2015). For β-car in solvents, the band in ν_3 was shown as a doublet, and it was concluded that the presence of these two components reflected the out-of-plane configuration of the β-car end-cycles (Mendes-Pinto et al. 2013b). In His-HliC, the signal obtained at 528.7 nm displays one principal component located at 1003.2 cm^{-1}, while two components are clearly observable at 1003.2 and 1007.6 cm^{-1} upon 496.5 nm excitation (Fig. 3d)—the latter as observed for β-car in solution (Macernis et al. 2015). These data bear striking resemblance to the results previously reported for Ycf39–HliD (Staleva et al. 2015), as well as those for the blue- and red-absorbing β-cars in PSII reaction centres (Mendes-Pinto et al. 2013b), implying that one or both end-cycles of the red-absorbing β-car$_2$ are pushed back towards the plane of the conjugated carbon backbone.

Finally, at around 960 cm^{-1} the band termed ν_4 arises from C–H out-of-plane wagging motions coupled with C=C torsional modes (out-of-plane twists of the carbon backbone; Lutz et al. 1987). When the carotenoid conjugated system is planar, these out-of-plane modes will not be coupled with the electronic transition, and these bands are not resonance enhanced. However, distortions around C–C single bonds increase the coupling of these modes with the electronic transition, resulting in an increase not only in their intensity, but also in their structure, as these distortions will partially lift the degeneracy between the many ν_4 modes. In Fig. 3d, it appears that the ν_4 band gains structure when exciting at 496.5 nm (β-car$_1$), indicating that the carbon backbone of this carotenoid is slightly more twisted or distorted than β-car$_2$, again as observed for Ycf39–HliD (Staleva et al. 2015), and is consistent with the apparent twisting of its end-cycle(s) into the plane.

Absorption red-shifts of monomer carotenoids, including β-cars, can generally be explained by increases in environment polarizability, lengthening of their effective conjugation (N_{eff}) and/or by excitonic interactions. Plotting the energy of the absorption transition of carotenoid molecules according to the frequency of their ν_1 Raman band at room temperature can help disentangle the relative importance of these effects (Llansola-Portoles et al. 2017a). This so-called MP graph was described first by Mendes-Pinto et al. using the values for lycopene, β-car, spirilloxanthin, spheroidene and neurosporene in different solvents (Mendes-Pinto et al. 2013b). Figure 4 displays such a graph where the blue line represents the relationship between carotenoids of differing
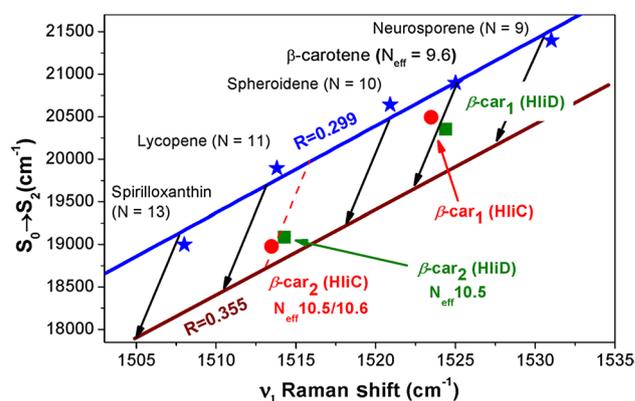

Fig. 4 Correlation between the position of the S0→S2 electronic transition and the ν_1 Raman band for β-cars in His-HliC (red circles) and HliD (Ycf39–HliD complex; green squares) (Llansola-Portoles et al. 2017b). Also shown is the relationship between carotenoids of different conjugation lengths in the same solvent (*n*-hexane in blue, carbon disulfide in maroon), as well as the relationship for individual carotenoids as a function of solvent polarizability (black arrows; Mendes-Pinto et al. 2013b). The room temperature values for β-car$_1$ and β-car$_2$ in HliC and HliD are indicated by red dots and green squares, respectively

N_{eff} in *n*-hexane, a solvent with low polarizability (0.299). The parallel maroon line shows the same relationship for the range of carotenoids in carbon disulfide, which is a solvent with high polarizability (0.355). A linear relationship is also observed when considering a single carotenoid in solvents of differing polarizability, but the slope is different—represented in Fig. 4 as arrows going from the blue *n*-hexane line towards the maroon carbon disulfide one. In this graph, we have inserted the values obtained for each of the carotenoids present in HliD (green symbols) and His-HliC (red symbols). The positions of the absorption peaks and ν_1 Raman bands at room temperature for each His-HliC carotenoid are (498 nm, 1523 cm^{-1}) for β-car$_1$ and (527 nm, 1513 cm^{-1}) for β-car$_2$. It clearly appears that the two carotenoids in His-HliC fall very close to those observed in HliD, within experimental error. It can thus be deduced for His-HliC, as is the case for HliD, that the effective conjugation length of β-car$_2$ increases to 10.5, while the properties of β-car$_1$ can be explained by polarizability effects alone. It is worth noting that increasing the conjugation length may induce a diminution of the energy gap S_1–S_0 (Christensen 1999) and hence lowering the S_1 state to an energy level where it may accept excitation energy from Chl.

A structural model of HliC

To our knowledge, HliC is the smallest protein (47 amino acids) known to bind Chl and carotenoids. Our data suggest that at least four Chls and two β-cars are associated with His-HliC and, regarding the conserved Chl-binding motif in HliC (Fig. S1), it is feasible to predict a model of how a small protein like HliC binds Chl. However, one has to be aware that the spectrum of potential ligands to the Chl central Mg atom is broad. It includes the imidazole group of His, the charge-compensated carboxyl group of Glu, the amide group of Asn and Gln or the carbonyl group of a peptide bond. Moreover, Chl can be coordinated by proteins via a water bridge or ligated by a protein-associated lipid (Hoober et al. 2007; Pan et al. 2011).

Importantly, HLIPs contain conserved residues that are crucial for Chl binding in all LHC antenna proteins for which the structures have been solved to date (Liu et al. 2004; Pan et al. 2011; Standfuss et al. 2005). In the crystallized LHCII from pea, Chls *a*1 and *a*4 are ligated by ion pairs between Glu-65 (helix 1) and Arg-185 (helix 3), and Glu-180 (helix 3) and Arg-70 (helix 1), respectively (Fig. S1). Asn-183 and His-68 positioned between Glu-65/180 and Arg-70/185 ligate another two Chl molecules (*a*2, *a*5; Fig. S1). The Glu carboxyl group alone is too negative to serve as a Chl ligand and needs to be charge-compensated by an Arg side-chain (Hoober et al. 2007). Although these Glu–Arg moieties may be intra- as well as inter-helix ion pairs (e.g. binding of Chl-609 in CP29; Pan et al. 2011), the conserved Glu and Arg residues in the ExxNxR Chl-binding motif are spatially too far apart to form such a pair on a single helix. Together, it strongly suggests that two HLIP helices must dimerize via Glu–Arg salt bridges to create a functional four-Chl-binding motif resembling LHCII (Fig. S1).

To assess the theoretical ability of HliC to dimerize via Glu–Arg ion pairs, we predicted the HliC structure using I-TASSER server (Yang et al. 2015). The best scored structure (C-score = − 0.67) was very similar to helix 1 of the PsbS protein (Fig. S4; Fan et al. 2015), and we therefore created a putative HliC dimer using PsbS as a template. Indeed, the HliC Glu-15 and Arg-20 residues were in almost identical positions as the Glu–Arg ion pairs in PsbS and LHCII (Fig. S4) and the putative Gln-18 ligands are positioned similarly to their Gln/His counterparts in LHCII (not shown). The HliC dimer model can be decorated with four Chls and two β-cars, following the typical LHCII pattern (Fig. 5). However, residues forming carotenoid binding pocket(s) in LHC proteins are much less conserved than the Chl-binding residues, and more sophisticated approaches (e.g. molecular dynamics) would be needed to examine β-car binding to HLIPs.

Dimerization of HliC via two ion pairs is supported by the observed stability of His-HliC dimers during SDS electrophoresis (Fig. S3). All higher-mass His-HliC oligomers are totally disrupted by SDS, and it is possible that the aggregation of the His-HliC dimer is facilitated by carotenoids, as demonstrated for plant LHCII complexes (Ruban et al. 1997), and/or that it might involve hydrophobic interaction between helices as observed between two PsbS proteins (Fan et al. 2015). We are however aware that the present HliC model cannot be completely correct, since spectroscopic data suggest that pigments are not bound with fully 2-dimensional symmetry. The two β-car molecules should differ in the rotation of their end-cycles, with at least one end-cycle of the red-shifted β-car$_2$ rotated back into the plane (Mendes-Pinto et al. 2013a). In addition, at least one of the four Chls appears to have a distorted macrocycle, and one exhibits a weaker H-bond to its keto C=O than the others (whether this is the same Chl, we cannot determine). How such asymmetry is achieved is not clear. In LHCII, one of the two central luteins is red-shifted by trimerization—in LHCII monomers, where this lutein conformation is relaxed, the absorption of both luteins are similar (Ruban et al. 2000). We therefore hypothesize that the distortion of β-car in HliC requires the formation of a higher order structure. Given the very small size of HLIPs and the presence of detergent molecules, it is practically impossible to distinguish the number of units by standard methods like size-exclusion chromatography. The Ycf39–HliD complex contains two different pools of β-car as well, but the oligomerization state of HliD is also unclear (Staleva et al. 2015). An alternative explanation is that a strong association between HliC and a lipid molecule(s)
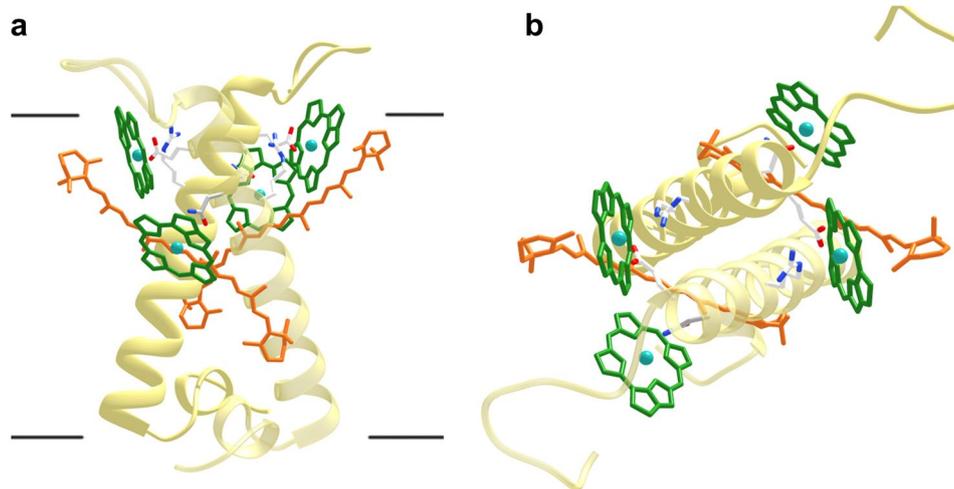
Fig. 5 A structural model of the putative HliC dimer. **a** Side view along the membrane plane; **b** view from the stromal side. The structure was predicted using I-TASSER (Yang et al. 2015) and two identical HliC helices 'dimerized' and loaded with pigments in Chimera software (Pettersen et al. 2004) using PsbS (Fan et al. 2015) and LHCII (Standfuss et al. 2005) structures as templates. Conformations of protein side chains were manually adjusted using a rotamer library (Dunbrack 2002). For clarity, only porphyrin rings of Chl molecules are shown

affects the local environment, altering the hydrogen-bond network around a Chl and increasing the effective conjugation length of one of the two β-cars. It is worth noting that the Ycf39–HliD complex exhibits a different red-shifted carotenoid absorbance than the HliD protein alone (Staleva et al. 2015), indicating that the local environment around β-car molecules in HLIPs is readily perturbed.

The different Chl:β-car ratios in His-HliC (2:1) and HliD (3:1) implies that the HliD helix contains an extra Chl ligand not present in HliC. This Chl-binding site is probably also not present in the LHC proteins with solved structures, as the Gln-197 residue ligating Chl a3 in LHCII is not conserved in HLIPs (Fig. S1). A candidate for an HliD-specific Chl ligand could be Asn-47, or alternatively Chl binding could occur on the N-terminal stromal segment that is longer and differs from the HliC N terminus (Fig. S1). Despite containing less Chl, HliC seems to be the crucial HLIP for Chl recycling as the elimination of this protein in the *Synechocystis* Photosystem I-less strain reduced the Chl half-life to ~40%, whereas it dropped to only ~70% after deletion of both *hliA* and *hliB* genes and the deletion of *hliD* gene has only a subtle effect (Vavilin et al. 2007). We propose that the HliD protein is primarily connected to the function/regulation of Chl synthase because the stability and oligomerization of this enzyme are impaired in the Δ*hliD* strain (Chidgey et al. 2014).

The role of HliC differs from that of HliD as the loss of HliC does not affect the Chl synthase (Chidgey et al. 2014), and the expression of these two HLIPs is regulated differently in *Synechocystis*. For instance, HliC is strongly up-regulated under high-temperature or low nitrogen, whereas the three other HLIPs are down-regulated under such conditions (Kopf et al. 2014). In addition, it appears that only HliC can interact with all other HLIPs (Knoppová et al. 2014; Yao et al. 2007), potentially forming a network to facilitate Chl reutilization. Whether at least some Chl molecules trapped by HLIPs can later be released and transferred to Chl synthase is still an open question that needs to be addressed in the future. There is also the interesting possibility that the binding of pigments to HliC/D generates a signal that modulates the tetrapyrrole pathway (Xu et al. 2002). Such a link between the pool of Chl molecules released from degraded proteins (sensed by HliC/D) and de novo Chl formation could control the minute amount of Chl that is necessary for the synthesis of Chl-binding proteins (Sobotka 2014).

References

Andreeva A, Apostolova I, Velitchkova M (2011) Temperature dependence of resonance Raman spectra of carotenoids. Spectrochim Acta A 78:1261–1265

Beck J et al (2017) Small one-helix proteins are essential for photosynthesis in Arabidopsis. Front Plant Sci 8:7. https://doi.org/10.3389/fpls.2017.00007

Chidgey JW et al (2014) A cyanobacterial chlorophyll synthase-HliD complex associates with the Ycf39 protein and the YidC/Alb3 insertase. Plant Cell 26:1267–1279. https://doi.org/10.1105/tpc.114.124495

Christensen RL (1999) The electronic states of carotenoids. In: Frank HA, Young AJ, Britton G, Cogdell RJ (eds) The photochemistry of carotenoids. Springer Netherlands, Dordrecht, pp 137–159

Dobáková M, Sobotka R, Tichý M, Komenda J (2009) Psb28 protein is involved in the biogenesis of the photosystem II inner antenna CP47 (PsbB) in the cyanobacterium *Synechocystis* sp. PCC 6803. Plant Physiol 149:1076–1086. https://doi.org/10.1104/pp.108.130039

Dolganov NA, Bhaya D, Grossman AR (1995) Cyanobacterial protein with similarity to the chlorophyll a/b binding proteins of higher plants: evolution and regulation. Proc Natl Acad Sci USA 92:636–640

Dunbrack RL Jr (2002) Rotamer libraries in the 21st century. Curr Opin Struct Biol 12:431–440

Eaton-Rye JJ, Vermaas WFJ (1991) Oligonucleotide-directed mutagenesis of psbB, the gene encoding CP47, employing a deletion mutant strain of the cyanobacterium *Synechocystis* sp. PCC 6803. Plant Mol Biol 17:1165–1177

Fan M et al (2015) Crystal structures of the PsbS protein essential for photoprotection in plants. Nat Struct Mol Biol 22:729–735. https://doi.org/10.1038/nsmb.3068

Feiler U, Mattioli TA, Katheder I, Scheer H, Lutz M, Robert B (1994) Effects of vinyl substitutions on resonance Raman spectra of (bacterio)chlorophylls. J Raman Spectrosc 25:365–370

Fujiwara M, Tasumi M (1986) Metal-sensitive bands in the Raman and infrared spectra of intact and metal-substituted chlorophyll *a*. J Phys Chem 90:5646–5650

Holland HD (2006) The oxygenation of the atmosphere and oceans. Philos Trans R Soc Lond B Biol Sci 361:903–915. https://doi.org/10.1098/rstb.2006.1838

Hoober JK, Eggink LL, Chen M (2007) Chlorophylls, ligands and assembly of light-harvesting complexes in chloroplasts. Photosynth Res 94:387–400. https://doi.org/10.1007/s11120-007-9181-1

Hutin C, Nussaume L, Moise N, Moya I, Kloppstech K, Havaux M (2003) Early light-induced proteins protect Arabidopsis from photooxidative stress. Proc Natl Acad Sci USA 100:4921–4926. https://doi.org/10.1073/pnas.0736939100

Knoppová J et al (2014) Discovery of a chlorophyll binding protein complex involved in the early steps of photosystem II assembly in *Synechocystis*. Plant Cell 26:1200–1212. https://doi.org/10.1105/tpc.114.123919

Komenda J, Sobotka R (2016) Cyanobacterial high-light-inducible proteins–Protectors of chlorophyll-protein synthesis and assembly. Biochim Biophys Acta 1857:288–295. https://doi.org/10.1016/j.bbabio.2015.08.011

Kopečná J, Komenda J, Bučinská L, Sobotka R (2012) Long-term acclimation of the cyanobacterium *Synechocystis* sp. PCC 6803 to high light is accompanied by an enhanced production of chlorophyll that is preferentially channeled to trimeric photosystem I. Plant Physiol 160:2239–2250. https://doi.org/10.1104/pp.112.207274

Kopf M, Klahn S, Scholz I, Matthiessen JK, Hess WR, Voss B (2014) Comparative analysis of the primary transcriptome of *Synechocystis* sp. PCC 6803. DNA Res 21:527–539. https://doi.org/10.1093/dnares/dsu018

Koyama Y, Fujii R (1999) Cis-trans carotenoids in photosynthesis: configurations, excited-state properties and physiological functions. In: Frank HA, Young AJ, Britton G, Cogdell RJ (eds) The photochemistry of carotenoids. Springer, Netherlands, pp 161–188

Koyama Y, Takii T, Saiki K, Tsukida K (1983) Configuration of the carotenoid in the reaction centers of photosynthetic bacteria. 2. Comparison of the resonance Raman lines of the reaction centers with those of the 14 different cis-trans isomers of β-carotene. Photobiochem Photobiophys 5

Lagarde D, Beuf L, Vermaas WFJ (2000) Increased production of zeaxanthin and other pigments by application of genetic engineering techniques to *Synechocystis* sp. strain PCC 6803. Appl Environ Microbiol 66:64–72

Lapouge K et al (1998) Non-bonding molecular factors influencing the stretching wavenumbers of the conjugated carbonyl groups of bacteriochlorophyll *a*. J Raman Spectrosc 29:977–981

Liu Z et al (2004) Crystal structure of spinach major light-harvesting complex at 2.72 A resolution. Nature 428:287–292. https://doi.org/10.1038/nature02373

Llansola-Portoles MJ, Pascal AA, Robert B (2017a) Electronic and vibrational properties of carotenoids: from in vitro to in vivo. J R Soc Interface. https://doi.org/10.1098/rsif.2017.0504

Llansola-Portoles MJ, Sobotka R, Kish E, Shukla MK, Pascal AA, Polívka T, Robert B (2017b) Twisting a beta-carotene, an adaptive trick from nature for dissipating energy during photoprotection. J Biol Chem 292:1396–1403. https://doi.org/10.1074/jbc.M116.753723

Lohscheider JN et al (2015) Altered levels of LIL3 isoforms in Arabidopsis lead to disturbed pigment-protein assembly and chlorophyll synthesis, chlorotic phenotype and impaired photosynthetic performance. Plant Cell Environ 38:2115–2127. https://doi.org/10.1111/pce.12540

Lutz M (1977) Antenna chlorophyll in photosynthetic membranes. A study by resonance Raman spectroscopy. Biochim Biophys Acta 460:408–430

Lutz M, Szponarski W, Berger G, Robert B, Neumann J-M (1987) The stereoisomerization of bacterial, reaction-center-bound carotenoids revisited: an electronic absorption, resonance Raman and NMR study. Biochim Biophys Acta 894:423–433

Macernis M et al (2015) Resonance Raman spectra of carotenoid molecules: influence of methyl substitutions. J Phys Chem A 119:56–66. https://doi.org/10.1021/jp510426m

Mendes-Pinto MM, Galzerano D, Telfer A, Pascal AA, Robert B, Ilioaia C (2013a) Mechanisms underlying carotenoid absorption in oxygenic photosynthetic proteins. J Biol Chem 288:18758–18765. https://doi.org/10.1074/jbc.M112.423681

Mendes-Pinto MM, Sansiaume E, Hashimoto H, Pascal AA, Gall A, Robert B (2013b) Electronic absorption and ground state structure of carotenoid molecules. J Phys Chem B 117:11015–11021. https://doi.org/10.1021/jp309908r

Näveke A, Lapouge K, Sturgis JN, Hartwich G, Simonin I, Scheer H, Robert B (1997) Resonance Raman spectroscopy of metal-substituted bacteriochlorophylls: characterization of Raman bands sensitive to bacteriochlorin conformation. J Raman Spectrosc 28:599–604

Neilson JA, Durnford DG (2010) Structural and functional diversification of the light-harvesting complexes in photosynthetic eukaryotes. Photosynth Res 106:57–71. https://doi.org/10.1007/s11120-010-9576-2

Niedzwiedzki DM et al (2016) Carotenoid-induced non-photochemical quenching in the cyanobacterial chlorophyll synthase-HliC/D complex. Biochim Biophys Acta 1857:1430–1439. https://doi.org/10.1016/j.bbabio.2016.04.280

Pan X et al (2011) Structural insights into energy regulation of light-harvesting complex CP29 from spinach. Nat Struct Mol Biol 18:309–315. https://doi.org/10.1038/nsmb.2008

Peers G et al (2009) An ancient light-harvesting protein is critical for the regulation of algal photosynthesis. Nature 462:518–521. https://doi.org/10.1038/nature08587

Pettersen EF, Goddard TD, Huang CC, Couch GS, Greenblatt DM, Meng EC, Ferrin TE (2004) UCSF Chimera—a visualization

system for exploratory research and analysis. J Comput Chem 25:1605–1612. https://doi.org/10.1002/jcc.20084

Promnares K, Komenda J, Bumba L, Nebesářová J, Vácha F, Tichý M (2006) Cyanobacterial small chlorophyll-binding protein ScpD (HliB) is located on the periphery of photosystem II in the vicinity of PsbH and CP47 subunits. J Biol Chem 281:32705–32713. https://doi.org/10.1074/jbc.M606360200

Robert B (1999) The electronic structure, stereochemistry and resonance Raman spectroscopy of carotenoids. In: Frank HA, Young AJ, Britton G, Cogdell RJ (eds) The photochemistry of carotenoids. Springer, Netherlands, pp 189–201

Ruban AV (2016) Nonphotochemical chlorophyll fluorescence quenching: mechanism and effectiveness in protecting plants from photodamage. Plant Physiol 170:1903–1916. https://doi.org/10.1104/pp.15.01935

Ruban AV, Phillip D, Young AJ, Horton P (1997) Carotenoid-dependent oligomerization of the major chlorophyll a/b light harvesting complex of photosystem II of plants. Biochemistry 36:7855–7859. https://doi.org/10.1021/bi9630725

Ruban AV, Pascal AA, Robert B (2000) Xanthophylls of the major photosynthetic light-harvesting complex of plants: identification, conformation and dynamics. FEBS Lett 477:181–185

Ruban AV et al (2007) Identification of a mechanism of photoprotective energy dissipation in higher plants. Nature 450:575–578. https://doi.org/10.1038/nature06262

Sobotka R (2014) Making proteins green; biosynthesis of chlorophyll-binding proteins in cyanobacteria. Photosynth Res 119:223–232. https://doi.org/10.1007/s11120-013-9797-2

Staleva H, Komenda J, Shukla MK, Šlouf V, Kaňa R, Polívka T, Sobotka R (2015) Mechanism of photoprotection in the cyanobacterial ancestor of plant antenna proteins. Nat Chem Biol 11:287–291. https://doi.org/10.1038/nchembio.1755

Standfuss J, Terwisscha van Scheltinga AC, Lamborghini M, Kuhlbrandt W (2005) Mechanisms of photoprotection and nonphotochemical quenching in pea light-harvesting complex at 2.5 A resolution. EMBO J 24:919–928. https://doi.org/10.1038/sj.emboj.7600585

Vavilin D, Yao D, Vermaas WFJ (2007) Small Cab-like proteins retard degradation of photosystem II-associated chlorophyll in *Synechocystis* sp. PCC 6803: kinetic analysis of pigment labeling with 15N and 13C. J Biol Chem 282:37660–37668. https://doi.org/10.1074/jbc.M707133200

Wittig I, Karas M, Schägger H (2007) High resolution clear native electrophoresis for in-gel functional assays and fluorescence studies of membrane protein complexes. Mol Cell Proteomics 6:1215–1225

Xu H, Vavilin D, Funk C, Vermaas WFJ (2002) Small Cab-like proteins regulating tetrapyrrole biosynthesis in the cyanobacterium *Synechocystis* sp. PCC 6803. Plant Mol Biol 49:149–160

Xu H, Vavilin D, Funk C, Vermaas WFJ (2004) Multiple deletions of small Cab-like proteins in the cyanobacterium *Synechocystis* sp. PCC 6803: consequences for pigment biosynthesis and accumulation. J Biol Chem 279:27971–27979. https://doi.org/10.1074/jbc.M403307200

Yang J, Yan R, Roy A, Xu D, Poisson J, Zhang Y (2015) The I-TASSER suite: protein structure and function prediction. Nat Methods 12:7–8. https://doi.org/10.1038/nmeth.3213

Yao D et al (2007) Localization of the small CAB-like proteins in photosystem II. J Biol Chem 282:267–276. https://doi.org/10.1074/jbc.M605463200

Supplementary Data

Binding of pigments to the cyanobacterial High-light-inducible protein HliC

Mahendra Kumar Shukla[a,b], Manuel J. Llansola-Portoles[c], Martin Tichý[a], Andrew A. Pascal[c], Bruno Robert[c] and Roman Sobotka[a,b]

[a] Centre Algatech, Institute of Microbiology, Czech Academy of Sciences, Třeboň, 379 81, Czech Republic

[b] Faculty of Science, University of South Bohemia, České Budějovice, 370 01, Czech Republic.

[c] Institute for Integrative Biology of the Cell (I2BC), CEA, CNRS, Université Paris-Saclay, F-91198, Gif-sur-Yvette cedex, France.
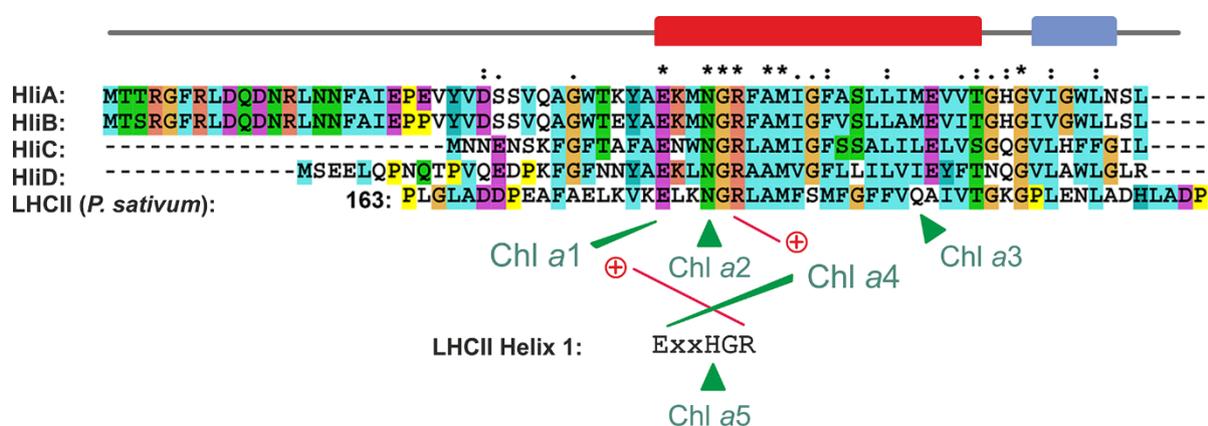
Figure S1. Amino acid sequence alignment of *Synechocystis* HLIPs and the third trans-membrane helix of the LHCII protein. Chl-binding sites within the conserved Chl-binding motif are highlighted; Chls are named according to nomenclature from Standfuss et al. (2005). Chl *a*1 and *a*4 are ligated by charge-compensated ion-pairs between a Glu sidechain carboxylate of one LHCII helix and an Arg guanidinium group of another (Kuhlbrandt et al. 1994; Hoober et al. 2007) – note that these are conserved in HLIPs. On the other hand, Chl *a*3 is ligated by a Gln residue that is not conserved in HLIPs. Boxes above the alignment indicate trans-membrane (red) and amphipathic (blue) α-helices.
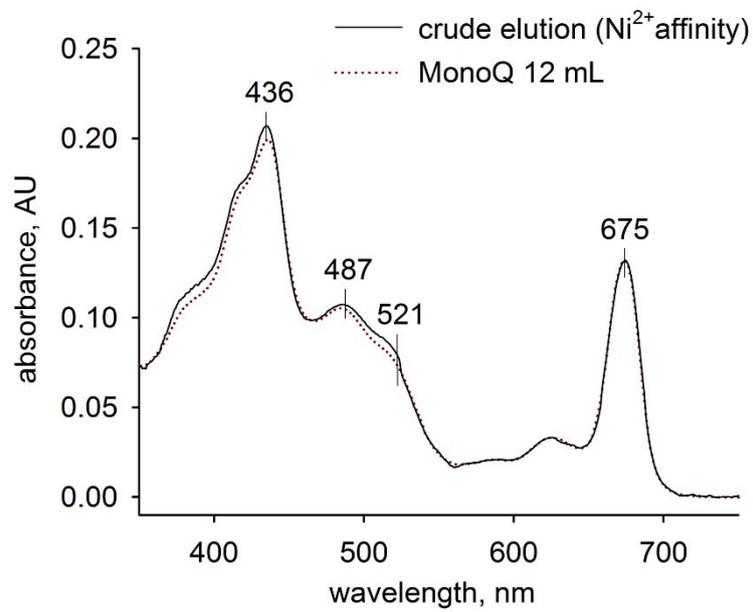
Figure S2: Absorbance spectrum of the His-HliC eluate obtained from the nickel-affinity chromatography (crude elution) and after further purification on an anion-exchange column (MonoQ 12 mL).
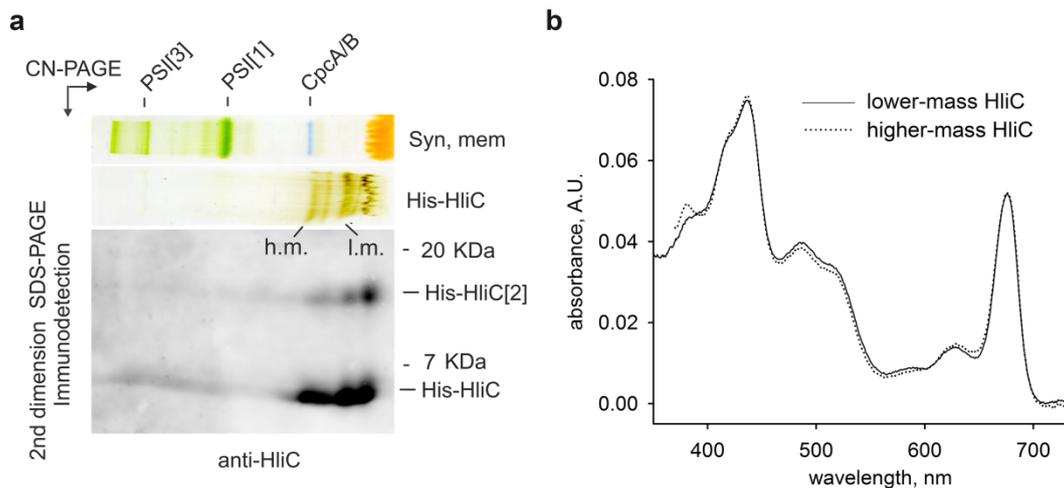
Figure S3: Two-dimensional clear-native/SDS electrophoresis and blot of the purified His-HliC. **a**) The His-HliC protein eluted from a nickel column was separated by clear-native-electrophoresis (CN-PAGE) together with solubilized thylakoid membranes from *Synechocystis* (Syn, mem). PSI[1] and PSI[3] indicate monomer and trimer of Photosystem I with masses ~1 MDa and ~350 KDa, respectively. CpcA/B marks ~100 KDa heterohexamer of CpcA and CpcB phycobiliproteins. A gel strip CN-PAGE with separated His-HliC was further separated in a second dimension by SDS-electrophoresis, blotted and the His-HliC immunodetected by a specific anti-HliC antibody. His-HliC[2] indicates a dimeric form of His-HliC. **b**) Absorbance spectra of His-HliC multimers with different masses. Spectra were measured in a small piece of gel cut in positions indicated by h.m. (higher mass) and l.m. (lower mass) in (**a**).
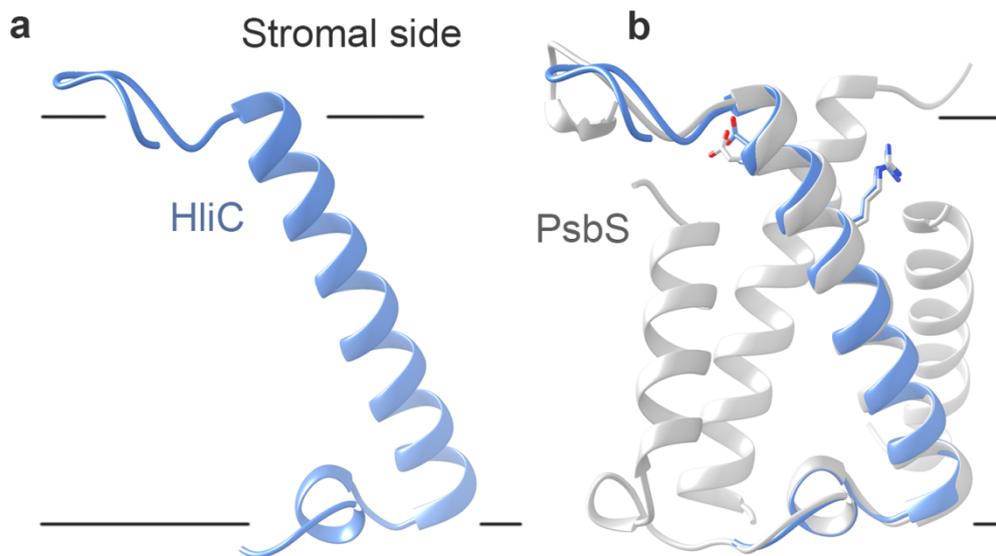
Figure S4: Prediction of monomeric HliC structure and comparison with PsbS. a) Side view of predicted HliC structure using I-TASSER (Yang et al. 2015). Position of HliC in lipid bilayer is indicated. **b**) Structure alignment between predicted HliC structure (blue) and plant PsbS (white; Fan et al. 2015). Glu-15 and Arg-20 residues of HliC (see Fig. S1) are visualized together with their PsbS counterparts.

References

Fan M et al. (2015) Crystal structures of the PsBS protein essential for photoprotection in plants. Nat Struct Mol Biol 22:729-735 doi:10.1038/nsmb.3068

Hoober JK, Eggink LL, Chen M (2007) Chlorophylls, ligands and assembly of light-harvesting complexes in chloroplasts. Photosynth Res 94:387-400 doi:10.1007/s11120-007-9181-1

Kuhlbrandt W, Wang DN, Fujiyoshi Y (1994) Atomic model of plant light-harvesting complex by electron crystallography. Nature 367:614-621 doi:10.1038/367614a0

Standfuss J, Terwisscha van Scheltinga AC, Lamborghini M, Kuhlbrandt W (2005) Mechanisms of photoprotection and nonphotochemical quenching in pea light-harvesting complex at 2.5 A resolution. EMBO J 24:919-928 doi:10.1038/sj.emboj.7600585

Yang J, Yan R, Roy A, Xu D, Poisson J, Zhang Y (2015) The I-TASSER Suite: protein structure and function prediction. Nat Methods 12:7-8 doi:10.1038/nmeth.3213

3.4   Result IV

Cyanobacterial LHC-like proteins control formation of the chlorophyll-synthase-Ycf39 complex

Shukla, M.K., Jackson, P.J., Moravcová, L., Zdvihalová, B., Brindley, A.A., Hunter, C.N., Sobotka, R. *Unsubmitted manuscript*

Cyanobacterial LHC-like proteins control formation of the chlorophyll-synthase-Ycf39 complex

Mahendra K. Shukla[a,b], Philip J. Jackson[c,d], Lenka Moravcová[a,b], Barbora Zdvihalová[a], Amanda A. Brindley[c], C. Neil Hunter[c], Roman Sobotka[a,b,*]

[a] Centre Algatech, Institute of Microbiology, Academy of Sciences of the Czech Republic, Třeboň, 379 81, Czech Republic

[b] Faculty of Science, University of South Bohemia, České Budějovice, 370 01, Czech Republic.

[c] Department of Molecular Biology and Biotechnology, University of Sheffield, Sheffield S10 2TN, UK.

[d] ChELSI Institute, Department of Chemical and Biological Engineering, University of Sheffield, Sheffield S1 3JD, UK.

Abstract

Plant light harvesting complexes (LHCs) evolved from cyanobacterial high-light-inducible proteins (Hlips) – a family of small one-helix proteins, which contain a chlorophyll-binding motif conserved in the whole LHC protein superfamily[1]. Hlips are essential under stress conditions; however their function is not explained. The cyanobacterium *Synechocystis* PCC 6803 contains four Hlips (HliA-D). While HliA/B/C proteins accumulate only after exposure to stress conditions, the HliD is constantly present in the cell where it associates with chlorophyll synthase (ChlG) and with a putative alcohol dehydrogenase Ycf39, a protein factor implicated in the assembly of Photosystem II (PSII)[2]. The large Ycf39-ChlG-HliD assemblies have been also reported[3]. Here, we demonstrated that the stress-induced HliC forms heterodimers with HliD, which integrate into ChlG complexes, destabilize ChlG oligomers and release Ycf39. The formed HliC/D pairs bind also to Ycf39 and, together, they associate with an early PSII assembly intermediate, which appears as a critical event for the maintaining of

29   active PSII under harsh conditions. Our results demonstrate that two Hlips control the
30   ChlG - Ycf39 interaction to facilitate the synthesis/repair of PSII.

Results and Discussion

32   Although only plants and some groups of algae capture photons using LHC-based
33   systems, all oxygenic phototrophs contain light harvesting-like (LHC-like) proteins
34   characterized by a conserved chlorophyll (Chl) binding motif identified first in a 'true'
35   light-harvesting LHC protein[4]. The LHC antennae thus form only a branch of the
36   extended LHC superfamily, which includes also cyanobacterial Hlips and similar
37   eukaryotic One Helix Proteins[5] (OHPs; Supplementary Fig. 1). Hlips are required for
38   viability under stress conditions[6] and the expression of *hli* genes coding for these proteins
39   is highly induced by high-light (HL), low temperature as well as by various nutrient
40   deficiencies[7]. Hlips generally quickly accumulate (in minutes) after shift to harsh
41   conditions but they also relatively promptly disappear once the stress passes[6].

42   Annotated cyanobacteria genomes virtually always contain more different copies of *hli*
43   genes[8] and it is clear now these are not redundant copies but they have specialized
44   functions[3,9,10]. The sequences of four Hlips (HliA-D) of the cyanobacterium
45   *Synechocystis* PCC 6803 (hereafter *Synechocystis*) are shown in Supplementary Fig. 1.
46   In contrast to HliA/B/C proteins, which expression follows the 'canonical' fast up-and-
47   down pattern[6], the HliD appears to be permanently present in the cell as it is required for
48   the proper functioning of ChlG, the final enzyme of Chl biosynthesis[3]. Intriguingly, the
49   ChlG-HliD-HliC complex has been also identified[11] but its biological role is unknown.

50   Apart of ChlG, the HliD associates with a putative alcohol dehydrogenase Ycf39[2], a
51   protein implicated in the assembly of PSII in cyanobacteria[2] as well as in plants[12,13]. How
52   the Ycf39 facilitates PSII biogenesis is not clear yet. The Ycf39 can assemble into a
53   complex with ChlG and HliD[3] or be attached, together with HliD and HliC, to the
54   reaction core assembly intermediate of PSII named RCII[2,14]. Its formation is an early step
55   in the assembly of PSII and it is composed of Chl-binding D1 and D2 subunits subjoined
56   with a few small subunits and lumenal assembly factor Ycf48[15]. Both HliC and HliD
57   proteins have been shown to bind Chl and β-carotene molecules in an energy-dissipative
58   configuration[14,16] and the docking of HliC/D to RCII is able to quench the absorbed
59   energy of the whole complex[2]. It let to hypothesis that the attachment of Hlips to RCII

60 photoprotects the PSII assembly[2,9]; however a role of Hlips in Chl reutilization/delivery[17]

61 and/or in the regulation of Chl biosynthesis has been also proposed[10].

62 In order to explain the biological role of described interactions between HliC/D, ChlG

63 and Ycf39, we checked first the levels of these proteins under low stress (normal light,

64 NL) and under stressful conditions (HL). The result confirmed that the HliC is detectable

65 only in stress-treated cells. Although the levels of ChlG, Ycf39 and HliD were elevated

66 by HL, these proteins are most likely constitutive components of the cell (Supplementary

67 Fig. 2a). The HliC protein, as the most variable component, could have an effect on the

68 organization of ChlG complexes. In order to check, we expressed 3xFlag-tagged ChlG

69 (f.ChlG) against wild type (WT) and Δ*hliC* backgrounds. As shown in Supplementary

70 Fig. 2b the presence of f.ChlG had no significant effect on the levels of HliD, Ycf39 and

71 HliC. Then we immunoprecipitated f.ChlG from the cells grown under NL and HL and

72 quantified the expected interacting partners by specific antibodies. Indeed, the HliD and

73 YidC insertase, which is physically attached to ChlG to connect Chl biosynthesis and

74 proteosynthesis[3], were equally present regardless the genetic background or grown

75 conditions used (Supplementary Fig. 2c). However, specifically under stress conditions,

76 the amount of native (non-tagged) ChlG co-eluted with f.ChlG from the Δ*hliC* strain was

77 much higher than in the absence of HliC. It suggested that the accumulation of HliC

78 protein hampers the assembly of ChlG oligomers. Interestingly, this lack of ChlG

79 oligomers was accompanied by markedly more co-eluted Ycf39 protein (Supplementary

80 Fig. 2c).

81 To confirm that the HliC remodels ChlG complexes, we grew WT cells under NL and

82 then shifted the cell culture to HL for 2 hours. Isolated membrane proteins were separated

83 by 2D blue-native/SDS electrophoresis (BN/SDS-PAGE), blotted and the ChlG and HliD

84 visualized by antibodies. Under low stress two ChlG-HliD complexes can be detected,

85 which we tentatively assigned as monomeric and dimeric ChlG associated with a HliD

86 oligomer[3] (Fig. 1a). Notably, the larger ChlG-HliD almost disappeared in light-stressed

87 WT cells but it remained preserved after deletion of *hliC*. The provided HL pulse was

88 apparently sufficient to induce a stress response as both strains almost completely lost

89 dimeric PSII (see Supplementary Fig. 2 and 3). Rather weak cross-reactivity of the

90 available HliC antibody did not allow us to detect HliC on 2D blot. We therefore purified

91 the f.ChlG complexes from light-stressed cells possessing or lacking HliC; for this

92 experiment the native *chlG* gene was deleted to simplify the spectrum of ChlG

complexes. As the obtained f.ChlG pulldown were pigmented (green-yellowish) we used clear-native electrophoresis (CN-PAGE) to visualize pigmented complexes, though the HliD shows a tendency to dissociate from ChlG on this gel system[3]. It should be noted that Hlips need to form a dimeric structure to bind pigments[16] and the f.ChlG protein alone appears colourless[3].

The only f.ChlG-Hlips complex purified from the WT ($\Delta chlG$) background contained a comparable amount of HliD and HliC and had mass < 100 KDa (Fig. 2b); the Ycf39 was not detectable in this pulldown on 2D gel even by immunodetection (Supplementary Fig. 5). In the absence of HliC the f.ChlG was however pulled down mostly as an oligomer with mass >100 KDa (Fig. 2b). Also consistent with the co-immunoprecipitation experiment (Supplementary Fig. 2c), the f.ChlG/$\Delta hliC$ eluate contained Ycf39, which dissociated on the CN-gel as a pigmented Ycf39-HliD subcomplex (Fig. 2b). Its observed mass (>100 KDa) was too large for a monomeric Ycf39-HliD complex characterized previously[2]. As it is known that the Ycf39 can dimerize[2] we expect that the large f.ChlG-HliD-Ycf39 assembly contains a dimeric Ycf39.

Remarkably, both f.ChlG and f.ChlG/$\Delta hliC$ pulldowns contained a high amount of Photosystem I complexes (PSI); certainly much more than could be explained by a contamination of pulldown assay (Fig. 2b). Moreover, PSI[1]* - an enigmatic PSI monomer that has been already reported to interact with ChlG[3], was pulled down only if the HliC was present (Fig. 2b). These data indicate that the ChlG is rather firmly attached to PSI and there is a low abundant form of PSI (PSI[1]*), presumably with a specialized function, to which the stress-induced ChlG-HliC/D complexes bind preferentially.

To further explore the organization of ChlG complexes, we determined molar quantities of f.ChlG, HliD and Ycf39 in f.ChlG pulldowns by mass spectrometry (using ^{15}N-labeled internal standards; Supplementary Table 1). As shown in Table 1, the f.ChlG pulldown isolated from NL–grown cells contained f.ChlG and HliD proteins in a ratio of about 1:1.5, which would agree with a mixture of ChlG[2]-HliD[2] and ChlG[1]-HliD[2] complexes. In light-stressed cells the ratio between f.ChlG and HliD decreased to 1: 1.1 and this shift depends on HliC. Given the roughly similar amounts of HliC and HliD in f.ChlG pulldowns isolated from the HL-stressed cells (Fig. 2b), the obtained values correspond to a ChlG[1]-HliC/D[1,1] stoichiometry (Table 1). This measurement confirmed the dramatic effect of HliC on the interaction between Ycf39 and the f.ChlG.

125 Whereas the Ycf39 protein practically did not stably associate with the f.ChlG complex

126 when the HliC was expressed, the binding capacity of the f.ChlG-HliD for Ycf39 looked

127 close to a full saturation (0.7 Ycf39 per ChlG) after elimination of HliC. It is however

128 not clear why much less of Ycf39 binds to the ChlG-HliD in non-stressed cells (Table

129 1). It is possible that a stress-induced factor, e.g. a substrate of this putative enzyme,

130 promotes dimerization of Ycf39 and thus increases affinity to ChlG-HliD complexes.

131 Although HliD and HliC are similar, small proteins, the HliC has a shorter N-terminus

132 and differs in a few charged residues (Supplementary Fig. 1). As a next step, we therefore

133 analysed the ability of the HliC to interact directly with ChlG and with Ycf39 (RCII).

134 We expressed His-HliC in a genetic background engineered to accumulate RCII

135 assembly intermediate (see Material and Methods) and purify this protein using metal-

136 affinity chromatography. The analysis of co-eluted proteins revealed the presence HliD,

137 ChlG as well as the RCII components Ycf39 and Ycf48 (Fig. 3). However, additional

138 deletion of the *hliD* gene yielded a strain possessing a lowered level of ChlG and the

139 ChlG protein was undetectable in His-HliC elution. In contrast, the interaction between

140 His-HliC with RCII complex was preserved even if the HliD protein was absent (Fig. 3).

141 One has to be however careful to interpret these data as an evidence that the putative

142 HliC dimer[16] has the same affinity to Ycf39 as an HliC/D oligomer observed before[2].

143 According to this work the absence of either HliC or HliD weakens the binding of Ycf39

144 to RCII. Together it indicates that, although the HliC (most likely a dimer) alone is able

145 to interact with Ycf39, the HliC/D structure is best tuned to integrate via Ycf39 into the

146 assembling PSII.

147 The *Synechocystis* Δ*hliC* mutant grown on agar plates exhibited no significant defect

148 under HL; however it grew poorly under more severe conditions such as intermitted light

149 (5 min HL/5 min dark) and showed an unexpected sensitivity to cold stress (20°C; Fig.

150 3a). The growth of the mutant in liquid culture was completely inhibited by a

151 combination of cold (16°C) and HL (600 μmols photons s^{-1} m^{-2}) whereas WT cells were

152 still able to proliferate (Fig. 3b). After 18 hours under these severe conditions the mutant

153 lost most of its Chl and carotenoid pigments, which implies a massive oxidative damage

154 (Fig. 3b,c). Analysis of membrane complexes of bleached mutant cells revealed low level

155 of PSII and as well as the RC47 complex - a partially disassembled monomeric PSII in

156 the process of repair[18]. The affected capacity of the mutant to synthesize and repair PSII

157 is most likely the reason of its arrested growth (Fig. 3d). It is worth noting that the

158 expression of the *ycf39* gene is particularly strongly upregulated by cold stress[7].

159 We summarized our results in a working model (Fig. 4). In fluctuating environments the

160 cellular machinery responsible for the synthesis of Chl-proteins must be reorganized to

161 stop the synthesis of PSI (note the lack of PSI trimers in stressed cells, Fig. 4d) but to

162 continue in the synthesis of short-lived D1/D2 subunits of PSII[19]. The synthesis of D1/D2

163 does not strictly require de novo produced Chl molecules and can rely on Chl released

164 from degraded proteins[20]. The ChlG is involved in the process of Chl recycling but, in

165 this case, the proposed connection with the preceding enzymes of Chl biosynthetic

166 pathway is not needed[21]. We suggest that the HliC serves as a (dummy) copy of HliD,

167 which does not interact with ChlG and might have also weaker affinity to Ycf39

168 preventing its dimerization. On the other hand, the ChlG-HliC/D complexes can localize

169 in the vicinity of PSI[1]*, which might be a complex involved in the PSII repair, e.g. by

170 storing Chl molecules. The HliC protein further mobilizes cellular pool of Ycf39 to be

171 available for the PSII biogenesis to maintain a sufficient amount of active PSII

172 complexes. The Ycf39 promotes D1 synthesis under conditions when the de novo Chl

173 biosynthesis is restricted[2]. It is thus possible that it is not just photoprotection but mainly

174 the efficiency of Chl re-utilization that the HliC executes in the cell. As the HliC probably

175 interacts also with HliA/B proteins[22], there might be another set of protein interactions

176 modulated by HliC. The plant OHP2 protein exists in a complex with the Ycf39

177 homologue (HCF136)[13] and, indeed, has much longer N-terminus than OHP1

178 (Supplementary Fig. 1). This indicates that the OHP1 and OHP2 proteins act as

179 regulatory couple similarly to their cyanobacterial counterparts.

180

181

182 **Materials and methods**

183 *Synechocystis strains and growth conditions*

184 The ΔhliC strain and the f.ChlG/(ΔchlG) strain expressing the 3xFlag-tagged ChlG have

185 been described previously[3] as well as the His-HliC/ΔhliC/ΔpsbB and His-

186 HliC/ΔhliC/ΔpsbB/ΔhliD mutants[16]. For the preparation of f.ChlG/ΔchlG/ΔhliC strain

187 the native *hliC* was inactivated using the available construct[23]. If not stated otherwise,

188   the cells were grown in a rotary shaker under 40 μmol of photons m^{-2} s^{-1} (normal light)

189   or 300 μmol of photons m^{-2} s^{-1} (high light) at 28 °C in liquid BG11 medium.

190   For the purification of f.ChlG the cells were grown at 28 °C in liquid BG11 medium

191   under normal light or high light conditions in 1 L cylinders bubbled with air. The same

192   conditions were used for the purification of His-HliC, only the His-

193   HliC/ΔhliC/ΔpsbB(/ΔhliD) strains were supplemented with 5 mM glucose. For the cold

194   stress conditions (16 °C) combined with high light (600 μmol of photons m^{-2} s^{-1}), the

195   cells were grown in air-bubbled 100 mL cylinders in a water-tempered growth chamber.

196

Preparation of cellular membranes and isolation of protein complexes

198   Cells were harvested and broken using glass beads (0.1 mm diameter) in a buffer A

199   containing 25 mM MES/NaOH, pH 6.5, 10 mM CaCl$_2$, 10 mM MgCl$_2$, 25% glycerol and

200   EDTA-free Protease Inhibitor (Roche). The broken cells were pelleted (20 000 x g, 15

201   min), the supernatant discarded while the sediment was resuspended in the excess

202   volume of the thylakoid buffer and pelleted again. For the purification of Flag-tagged

203   ChlG or His-HliC complexes the membrane fractions prepared from 4 L of cells were

204   resuspended in the buffer A (~ 0.5 mg Chl/mL) and solubilised for 30 min at 10 °C with

205   1 % dodecyl-β-maltoside. Finally, insoluble contaminants were removed by

206   centrifugation (65,000 x g, 25 min), and the supernatant loaded either on an anti-Flag M2

207   agarose column (0.4 mL, Sigma, Germany) or on a nickel-column (0.5 mL Protino Ni–

208   NTA-agarose, Macherey-Nagel, Germany). To remove contaminants the anti-Flag-resin

209   was washed with 20 resin volumes of buffer A containing 0.04% dodecyl-β-maltoside

210   (A-DDM). The Flag-tagged ChlG was eluted with 2 resin volumes of A-DDM containing

211   150 μg/ml 3xFlag peptide (Sigma-Aldrich, Germany). For the purification of His-HliC,

212   the nickel column was washed with 15 mL of A-DDM and with 2 mL of 40 mM

213   imidazole in A-DDM, and the His-HliC protein was eluted using 2 mL A-DDM

214   containing 300 mM imidazole.

215

Protein electrophoresis and immunoblotting

217   For native electrophoresis, solubilized membrane proteins or isolated complexes were

218   separated on 4-12% clear native gel[24] or blue native gel[25]. Individual components of

219 protein complexes were resolved by incubating the gel strip from the first dimension in

220 2% (w/v) SDS and 1% (w/v) dithiothreitol for 30 min at room temperature, and proteins

221 were separated in the second dimension by SDS-electrophoresis in a denaturing 12 to

222 20% (w/v) polyacrylamide gel containing 7 M urea[26]. For standard single dimension

223 SDS-PAGE, membrane proteins from cyanobacteria were denatured at room temperature

224 for 30 min with 2% (w/v) SDS and 1% (w/v) dithiothreitol before loading to the gel.

225 Proteins were stained by Coomassie Brilliant Blue or by SYPRO Orange; and in the latter

226 case, they were subsequently transferred onto a PVDF membrane. Membranes were

227 incubated with specific primary antibodies and then with secondary antibody conjugated

228 with horseradish peroxidase (Sigma-Aldrich, Germany). The following primary

229 antibodies were used in the study: anti-ChlG[3], Ycf39[2], anti-HliC antibody raised in

230 rabbits against a synthetic peptide corresponding to unique HliC residues 1-17 and anti-

231 Ycf48 raised in rabbit against recombinant *Synechocystis* Ycf48. Antibody against the

232 HliD were purchased from Agrisera (Sweden). The antibody raised against the

233 recombinant fragment Arg117-Ser384 of the *Synechocystis* YidC was kindly provided

234 by Jörg Nickelsen (Ludwig-Maximilians-University, Munich, Germany).

235

236 *Quantitative protein mass-spectrometry*

237 The eluate from the immobilized anti-FLAG antibody resin was mixed with 30 pmol of

238 an ^{15}N-labeled internal standard in the form of an artificial protein sequence[27]. This

239 protein contained concatenated proteotypic tryptic peptide sequences belonging to ChlG,

240 HliD and Ycf39 (see Supplementary Table 1) and was expressed in *E. coli* as described

241 previously[28]. The mixed immuno-captured and standard proteins were precipitated using

242 a 2-D clean-up kit (GE Healthcare) and redissolved in 8M urea, 100 mM Tris-HCl pH

243 8.5. Subsequent processing, including digestion with a combination of endoproteinase

244 Lys-C and trypsin followed by analysis using nano-flow liquid chromatography coupled

245 to mass spectrometry was carried out according to[29]. Proteotypic peptides, both ^{14}N from

246 the FLAG eluates and ^{15}N from the internal standard were identified in the mass spectra

247 by searching a *Synechocystis* PCC 6803 proteome database

248 (http://genome.annotation.jp/cyanobase/Synechocystis/genes.faa) using Mascot

249 Daemon v. 2.5.1 running with Mascot Server v. 2.5.1 (Matrix Science). Picomolar

amounts of f.ChlG, HliD and Ycf39 were calculated from the relative intensities of the ^{14}N and ^{15}N isotopomers of their respective proteotypic peptide ions.

Funding

References

1. Engelken, J., Brinkmann, H. & Adamska, I. Taxonomic distribution and origins of the extended LHC (light-harvesting complex) antenna protein superfamily. *BMC Evol. Biol.* **10** (2010).

2. Knoppová, J. *et al.* Discovery of a chlorophyll binding protein complex involved in the early steps of photosystem II assembly in *Synechocystis*. *Plant Cell* **26**, 1200-1212 (2014).

3. Chidgey, J. W. *et al.* A cyanobacterial chlorophyll synthase-HliD complex associates with the Ycf39 protein and the YidC/Alb3 insertase. *Plant Cell* **26**, 1267-1279 (2014).

4. Kuhlbrandt, W., Wang, D. N. & Fujiyoshi, Y. Atomic model of plant light-harvesting complex by electron crystallography. *Nature* **367**, 614-621 (1994).

5. Beck, J. *et al.* Small One-Helix Proteins are essential for photosynthesis in *Arabidopsis*. *Front. Plant Sci.* **8** (2017).

6. He, Q., Dolganov, N., Bjorkman, O. & Grossman, A. R. The high light-inducible polypeptides in *Synechocystis* PCC 6803. Expression and function in high light. *J. Biol. Chem.* **276**, 306-314 (2001).

7. Kopf, M. *et al.* Comparative analysis of the primary transcriptome of *Synechocystis* sp. PCC 6803. *DNA Res* **21**, 527-539 (2014).

8. Bhaya, D., Dufresne, A., Vaulot, D. & Grossman, A. Analysis of the hli gene family in marine and freshwater cyanobacteria. *FEMS Microbiol. Lett.* **215**, 209-219 (2002).

9. Promnares, K. *et al.* Cyanobacterial small chlorophyll-binding protein ScpD (HliB) is located on the periphery of photosystem II in the vicinity of PsbH and CP47 subunits. *J. Biol. Chem.* **281**, 32705-32713 (2006).

10. Xu, H., Vavilin, D., Funk, C. & Vermaas, W. Small Cab-like proteins regulating tetrapyrrole biosynthesis in the cyanobacterium Synechocystis sp PCC 6803. *Plant Mol. Biol.* **49**, 149-160 (2002).

11. Niedzwiedzki, D. M. *et al.* Carotenoid-induced non-photochemical quenching in the cyanobacterial chlorophyll synthase-HliC/D complex. *Biochim. Biophys. Acta* **1857**, 1430-1439 (2016).

12. Link, S., Engelmann, K., Meierhoff, K. & Westhoff, P. The atypical short-chain dehydrogenases HCF173 and HCF244 are jointly involved in translational

290 initiation of the psbA mRNA of Arabidopsis. *Plant Physiol.* **160**, 2202-2218
291 (2012).

292 13. Myouga, F. *et al.* Stable accumulation of photosystem II requires ONE-HELIX
293 PROTEIN1 (OHP1) of the light harvesting-like family. *Plant*
294 *Physiol.*doi:10.1104/pp.17.01782 (2018).

295 14. Staleva, H. *et al.* Mechanism of photoprotection in the cyanobacterial ancestor of
296 plant antenna proteins. *Nat. Chem. Biol.* **11**, 287-291 (2015).

297 15. Komenda, J. *et al.* The cyanobacterial homologue of HCF136/YCF48 is a
298 component of an early photosystem II assembly complex and is important for
299 both the efficient assembly and repair of photosystem II in *Synechocystis* sp PCC
300 6803. *J. Biol. Chem.* **283**, 22390-22399 (2008).

301 16. Shukla, M. K. *et al.* Binding of pigments to the cyanobacterial high-light-
302 inducible protein HliC. *Photosynth. Res.*doi: 10.1007/s11120-017-0475-7 (2017).

303 17. Vavilin, D., Yao, D. & Vermaas, W. F. J. Small cab-like proteins retard
304 degradation of photosystem II-associated chlorophyll in *Synechocystis* sp PCC
305 6803 - Kinetic analysis of pigment labeling with N-15 and C-13. *J. Biol. Chem.*
306 **282**, 37660-37668 (2007).

307 18. Komenda, J., Sobotka, R. & Nixon, P. J. Assembling and maintaining the
308 Photosystem II complex in chloroplasts and cyanobacteria. *Curr. Opin. Plant*
309 *Biol.* **15**, 245-251 (2012).

310 19. Kopečná, J., Komenda, J., Bučinská, L. & Sobotka, R. Long-term acclimation of
311 the cyanobacterium *Synechocystis* sp PCC 6803 to high light is accompanied by
312 an enhanced production of chlorophyll that is preferentially channeled to trimeric
313 Photosystem I. *Plant Physiol.* **160**, 2239-2250 (2012).

314 20. Hollingshead, S. *et al.* Synthesis of chlorophyll-binding proteins in a fully
315 segregated Δ*ycf54* strain of the cyanobacterium *Synechocystis* PCC 6803. *Front.*
316 *Plant Sci.* **7**, 292 (2016).

317 21. Sobotka, R. Making proteins green; biosynthesis of chlorophyll-binding proteins
318 in cyanobacteria. *Photosynth. Res.* **119**, 223-232 (2014).

319 22. Yao, D. *et al.* Localization of the small CAB-like proteins in photosystem II. *J.*
320 *Biol. Chem.* **282**, 267-276 (2007).

321 23. Xu, H., Vavilin, D., Funk, C. & Vermaas, W. F. J. Multiple deletions of small
322 Cab-like proteins in the cyanobacterium *Synechocystis* sp. PCC 6803:
323 consequences for pigment biosynthesis and accumulation. *J. Biol. Chem.* **279**,
324 27971-27979 (2004).

325 24. Wittig, I., Karas, M. & Schagger, H. High resolution clear native electrophoresis
326 for in-gel functional assays and fluorescence studies of membrane protein
327 complexes. *Mol. Cell. Proteomics* **6**, 1215-1225 (2007).

328 25. Schagger, H. & von Jagow, G. Blue native electrophoresis for isolation of
329 membrane protein complexes in enzymatically active form. *Anal. Biochem.* **199**,
330 223-231 (1991).

331 26. Dobáková, M., Sobotka, R., Tichý, M. & Komenda, J. Psb28 protein is involved
332 in the biogenesis of the photosystem II inner antenna CP47 (PsbB) in the

333   cyanobacterium *Synechocystis* sp PCC 6803. *Plant Physiol.* **149**, 1076-1086
334   (2009).

335   27.   Pratt, J. M. *et al.* Multiplexed absolute quantification for proteomics using
336   concatenated signature peptides encoded by QconCAT genes. *Nat Protoc* **1**,
337   1029-1043 (2006).

338   28.   Qian, P. *et al.* Three-dimensional structure of the Rhodobacter sphaeroides RC-
339   LH1-PufX complex: dimerization and quinone channels promoted by PufX.
340   *Biochemistry* **52**, 7575-7585 (2013).

341   29.   Hitchcock, A. *et al.* Biosynthesis of Chlorophyll a in a Purple Bacterial
342   Phototroph and Assembly into a Plant Chlorophyll-Protein Complex. *ACS Synth*
343   *Biol* **5**, 948-954 (2016).

344

345

346

Table 1. Quantification of f.ChlG, HliD and Ycf39 proteins in f.ChlG pulldowns. *Synechocystis* cells expressing f.ChlG against a Δ*chlG* background were grown under NL and HL conditions, both with and without the additional deletion of *hliC*. Membrane fractions were used in pulldown experiments (see Material and Methods) and proteins were quantified as described in Supplementary Information. Please note that these are different pulldown samples than shown in Fig. 1b.

| Experiment	Protein	Quantity (pmols ± SD)	Stoichiometry (ratio per 1 ChlG ± propagated SD)
f.ChlG/Δ*chlG* **Normal light**	ChlG	60.33 ± 0.14	**1**
	HliD	92.79 ± 0.74	**1.54 ± 0.013**
	Ycf39	2.58 ± 0.47	**0.04 ± 0.008**
f.ChlG/Δ*chlG*/Δ*hliC* **Normal light**	ChlG	37.19 ± 0.96	**1**
	HliD	54.74 ± 3.15	**1.47 ± 0.093**
	Ycf39	2.02 ± 0.34	**0.05 ± 0.009**
f.ChlG/Δ*chlG* **High light**	ChlG	32.06 ± 0.59	**1**
	HliD	35.96 ± 3.14	**1.12 ± 0.010**
	Ycf39	0.12 ± 0.02	**0.004 ± 0.001**
f.ChlG/Δ*chlG*/Δ*hliC* **High light**	ChlG	6.92± 0.07	**1**
	HliD	10.46 ± 0.78	**1.51 ± 0.11**
	Ycf39	4.98 ± 1.55	**0.72 ± 0.22**
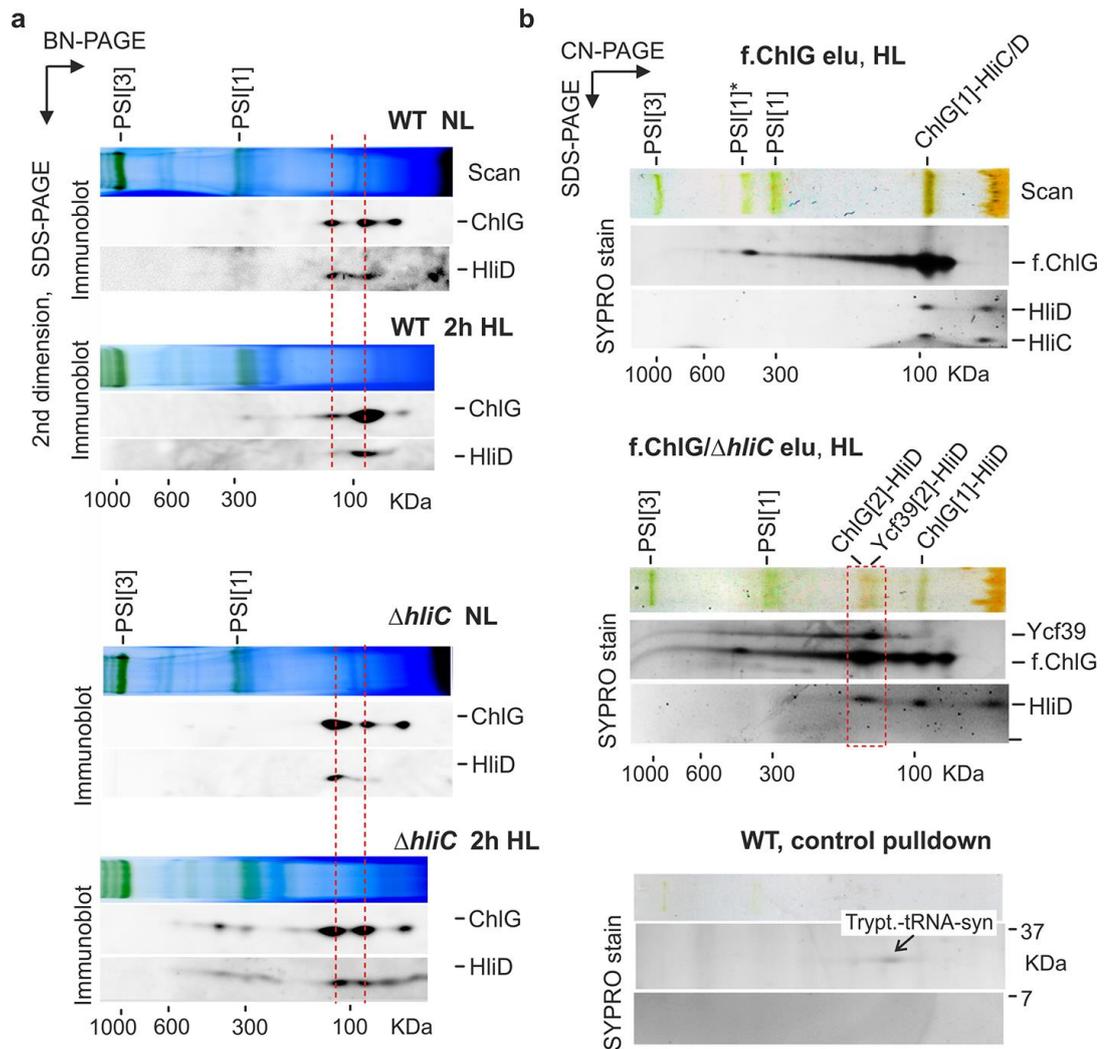
Figure 1. The HliC protein integrates into ChlG-HliD complex and disrupts its oligomeric structure. a) *Synechocystis* WT and Δ*hliC* strains were grown under NL (low-stress) conditions and then shifted to HL (300 µmol photons s^{-1} m^{-2}) for 2 hours. Membrane proteins isolated from these cell cultures were separated by 2D BN/SDS-PAGE, blotted and the blot was sequentially probed with ChlG and HliD antibodies. The separate segments of the blot with individual antibody signals are shown. PSI[3], PSI[1] – trimer and monomer of PSI. Dashed red lines indicate higher- and lower-mass ChlG-HliD complexes. The whole stained gels are shown as Supplementary figures 3 and 4. b) f.ChlG complexes were isolated using anti-Flag resin from f.*chlG*/Δ*chlG* and f.*chlG*/Δ*chlG*/Δ*hliC* strains grown under HL conditions. Obtained pulldowns were separated by 2D CN/SDS-PAGE and stained by SYPRO Orange (see also Supplementary figure 5 for immunoblotting). A control WT pulldown is also included. The separate segments of the stained gels are shown; red-box indicates higher-mass HliD complexes (~ 150 KDa), tentatively assigned to contain dimeric ChlG and Ycf39. PSI[1]* - an uncharacterized form of monomeric PSI. Dimeric f.ChlG lacking HliD is marked by asterisk. Tryptophanyl-tRNA synthetase is a standard unspecific interactor of the Flag resin (REF).

369
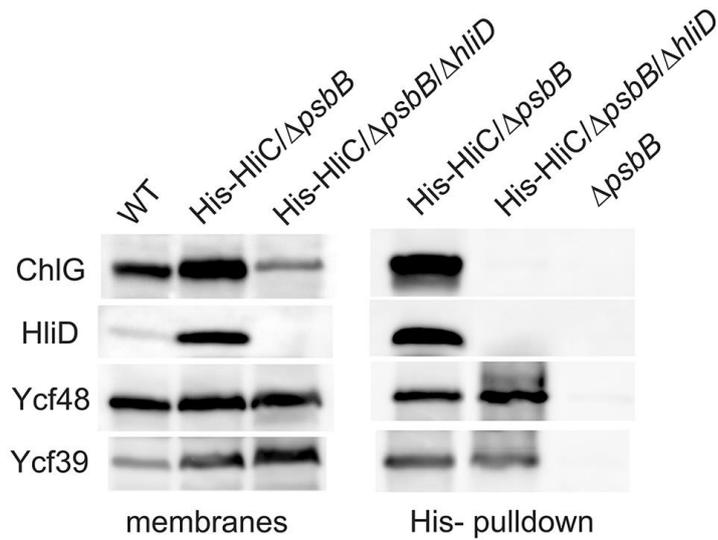
Figure 2. Interactions between His-HliC, ChlG and the RCII complex (Ycf39). The His-HliC protein was expressed under the *psbAII* promoter against a genetic background lacking the original *hliC* gene and the CP47 subunit of PSII (Δ*psbB*). A strain with additional deletion of *hliD* gene was also made to distinguish what interactions are provided by HliD. The levels of ChlG, HliD, Ycf48 and Ycf39 proteins in isolated membranes were assessed by immunodetection after separation by SDS-PAGE (left side). The right side shows the levels of the same proteins as co-eluted with His-HliC from a nickel-affinity column.

377

378
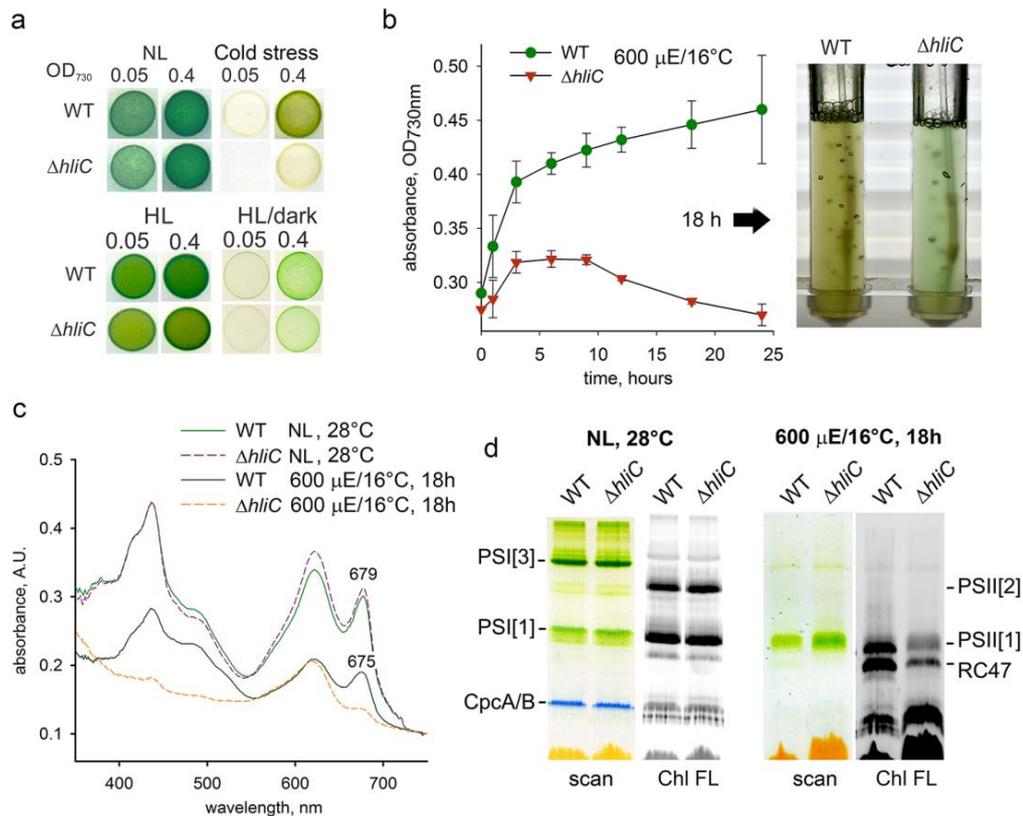
Figure 3. The HliC protein is required for the stability of PSII under stress conditions. a) Autotrophic growth of the WT and Δ*hliC* strains for 5 days on agar plates under NL/28°C, cold stress (NL/20°C), HL (28°C/300 μmol photons s^{-1} m^{-2}) and fluctuating light-dark conditions (5 min HL/5 min dark; 28°C). b) A growth curve of WT and Δ*hliC* strains in liquid culture kept under a combination of cold stress and HL (16°C/600 μmol photons s^{-1} m^{-2}). After 18 hours in these conditions the mutant cells were bluish and, as shown by the whole cell absorbance spectra (c), they lost most of Chl and carotenoid pigments. d) Cellular membranes were isolated from the WT and Δ*hliC* cells before and after 18 h of cold/HL stress, solubilized and separated by CN-PAGE. PSI[3], PSI[1] – trimer and monomer of PSI, PSII[1], PSII[2] - monomer and dimer of PSII, respectively. RC47 marks the PSII assembly core complex lacking CP43, CpcA/B[6], heterohexamer of CpcA and CpcB phycobiliproteins.

390
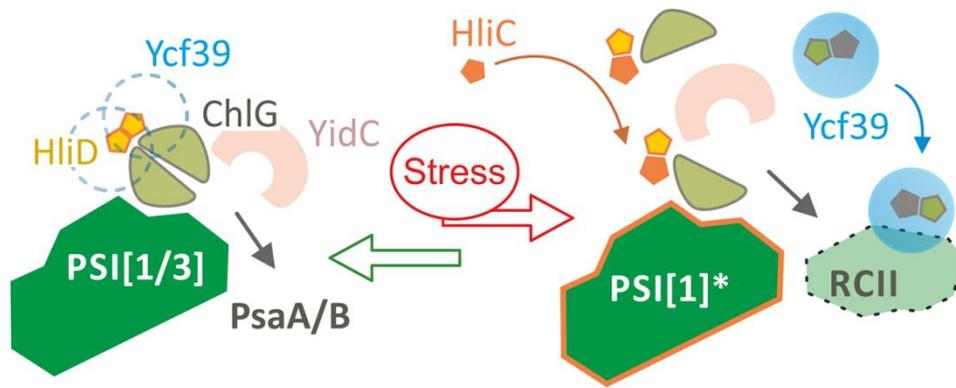
Figure 4. Remodelling of ChlG-Ycf39 complexes under stress conditions. Under low stress, the produced Chl molecules are partitioned mostly into the synthesized PsaA/B subunits of PSI[19]. ChlG-HliD complexes are organized as oligomers docked to trimeric or to monomeric PSI and can be also associate with Ycf39, most likely with its dimeric form. The HliC protein quickly accumulates if the growth conditions become challenging and the formed HliC/D heterodimers replace HliD homodimers in ChlG complexes. HliC however does not physically interact with ChlG, which causes melting of ChlG oligomers and releasing of the Ycf39 protein. On the other hand, the resulting monomeric ChlG-HliC/D complexes can be attached to a low abundant form of PSI (PSI[1]*)[3], which might participate in Chl re-utilization. The HliC/D pairs associate also with Ycf39 and, via this PSII assembly factor, are docked to the newly synthesized RCII assembly intermediates. We hypothesize that during intensive PSII repair this mechanism ensures a sufficient production of the Hlip-protected D1/D2 assembly modules by utilizing Chl molecules from degraded proteins.

SUPPLEMENTARY TABLE AND FIGURES

Cyanobacterial LHC-like proteins control formation of the chlorophyll-synthase-Ycf39 complex

Mahendra K. Shukla, Philip J. Jackson, Lenka Moravcová, Barbora Zdvihalová, Amanda A. Brindley, C. Neil Hunter, Roman Sobotka

Supplementary Table 1. Proteotypic tryptic peptide sequences used to construct the artificial ^{15}N-labeled internal standard protein. The sequence elements were incorporated into the ^{15}N-labeled artificial internal standard protein in the order specified. Proteotypic peptides that were used in the quantification of the target proteins are highlighted in bold. Peptides were selected on the basis of their frequent identification in proteomic analyses of *Synechocystis* thylakoid membranes. N- and C-side flanking sequences were included where indicated to mimic the cleavage sites in the natural protein.. Although selection of ≥2 peptides per protein is advisable, in the case of ChlG only GAA-IWK is consistently detectable. Additional peptides not relevant to this study were also present, making a total molecular mass of 40963 Da for this artificial protein.

| Sequence element	Tryptic peptide	Notes
pET-14b N-terminal extension	MGSSHHHHHHSSGLVPRGSH	His-tag for purification by immobilized Ni^{2+} ion affinity chromatography
2 x W insertion	AWSWK	Additional Trp-containing sequence to increase A_{280} for protein concentration measurement
ChlG spacer	LGMK	N-side flanking sequence to GAA-IWK
ChlG-1	GAAPGESSIWK	Peptide used for quantification
ChlG spacer	IRLQ	C-side flanking sequence to GAA-IWK

|		
ChlG spacer	YFLR	N-side flanking sequence to NPL-DVK
ChlG-2	NPLENDVK	Peptide with low recovery not used for quantification
HliD-1	SEELQPNQTPVQEDPK	Peptide used for quantification
HliD-2	FGFNNYAEK	Peptide used for quantification
HliD spacer	LNGR	C-side flanking sequence to FGF-AEK
Ycf39 spacer	MR	N-side flanking sequence to VLV-LGR
Ycf39-1	VLVVGGTGTLGR	Peptide used for quantification
Ycf39 spacer	QIVR	C-side flanking sequence to VLV-LGR
Ycf39 spacer	FAVR	N-side flanking sequence to AVE-VAR
Ycf39-2	AVELDSVAR	Peptide used for quantification
Ycf39 spacer	KTYP	C-side flanking sequence to AVE-VAR
Ycf39 spacer	ASDR	N-side flanking sequence to LAF-SGK
Ycf39-3	LAFSEVLASGK	Peptide with low recovery not used for quantification
Ycf39 spacer	ALTA	C-side flanking sequence to LAF-SGK

Supplementary Figure 1. Amino acid sequence alignment of *Synechocystis* Hlips, *Arabidopsis* OHPs and the third trans-membrane helix of the pea LHCII protein. The conserved Chl-binding motif (ExxNxR) [1] is highlighted by a green bar. The sequences of OHPs are shown without the predicted targeting peptide.
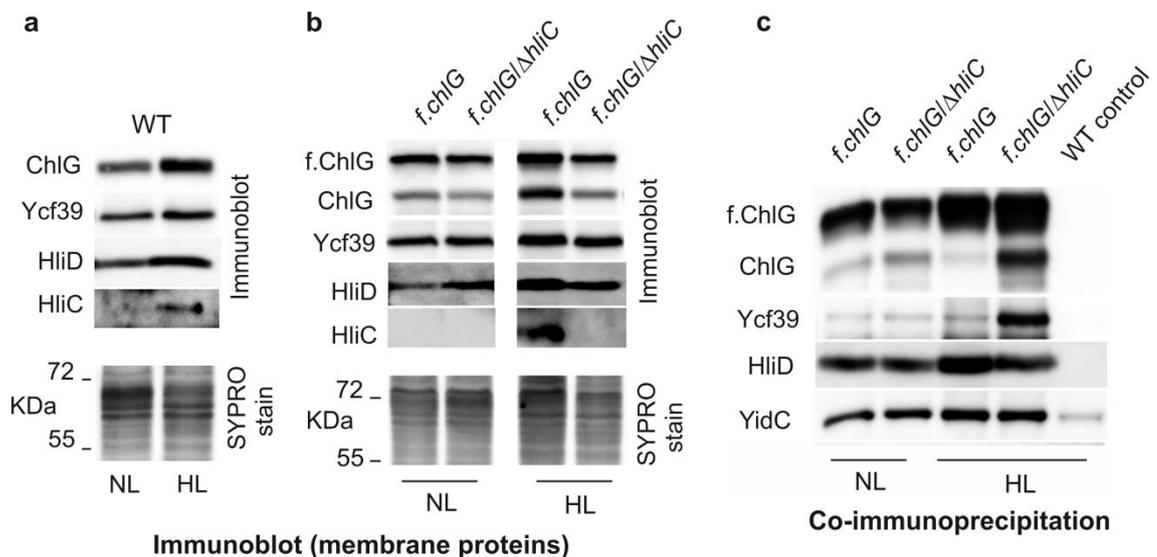

Supplementary Figure 2. Stress-induced expression of HliC prevents oligomerization of ChlG. Membrane proteins from WT (a) and from *f.chlG* and *f.chlG/ΔhliC* strains (b) grown under normal light (NL) and high light (HL) were separated by SDS-PAGE, blotted and sequentially probed by indicated antibodies. A part of the SYPRO Orange stained gel is shown as loading control. c) Solubilized membranes isolated from the *f.chlG*, *f.chlG/ΔhliC* strains and from a control WT cells were incubated with anti-Flag resin and, after an intensive washing, the eluted proteins were resolved by SDS-PAGE, blotted, and probed with indicated antibodies.
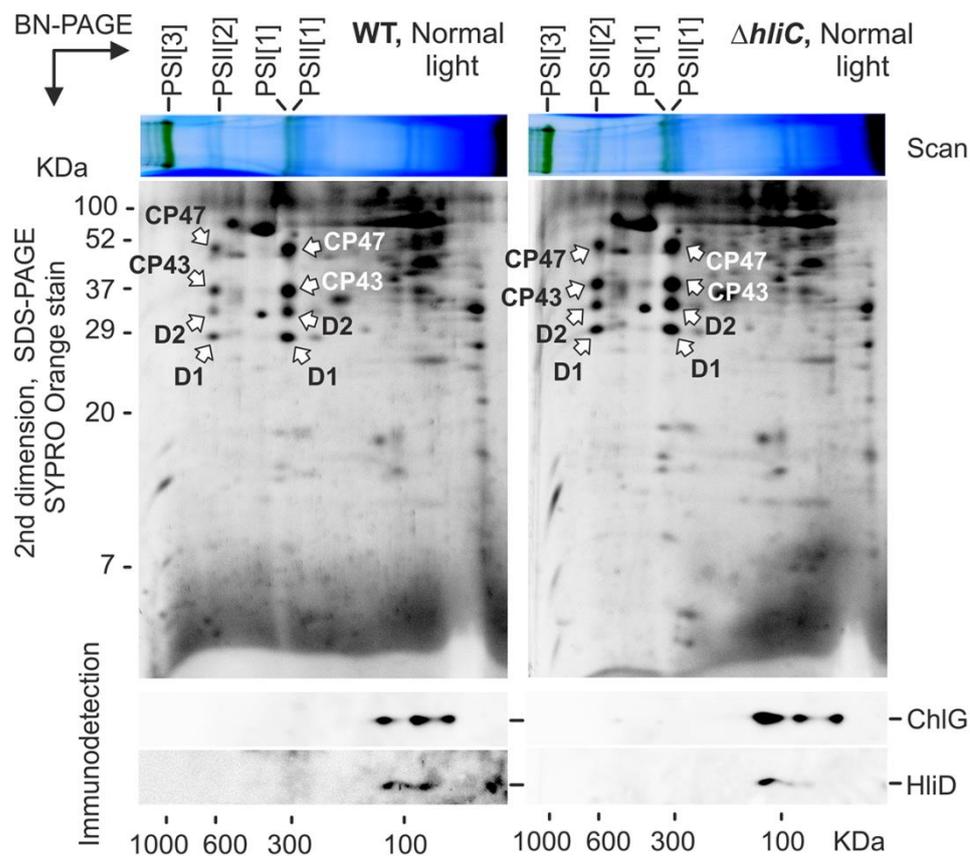
Supplementary Figure 3. Oligomeric state of the ChlG-HliD complexes in WT and Δ*hliC* cells grown under NL conditions. Isolated membrane proteins were separated by 4-14% BN-PAGE and then in a second dimension by 12-20 % SDS, stained by SYPRO Orange and blotted. The blot was sequentially probed with ChlG and HliD antibodies; the separate segments of the blot with individual antibody signals are shown. PSI[3], PSI[1] – trimer and monomer of PSI; PSII[2], PSII[1] - dimeric and monomeric PSII complexes, respectively. Chl-binding PSII subunits of PSII[2] and PSII[1] are indicated.
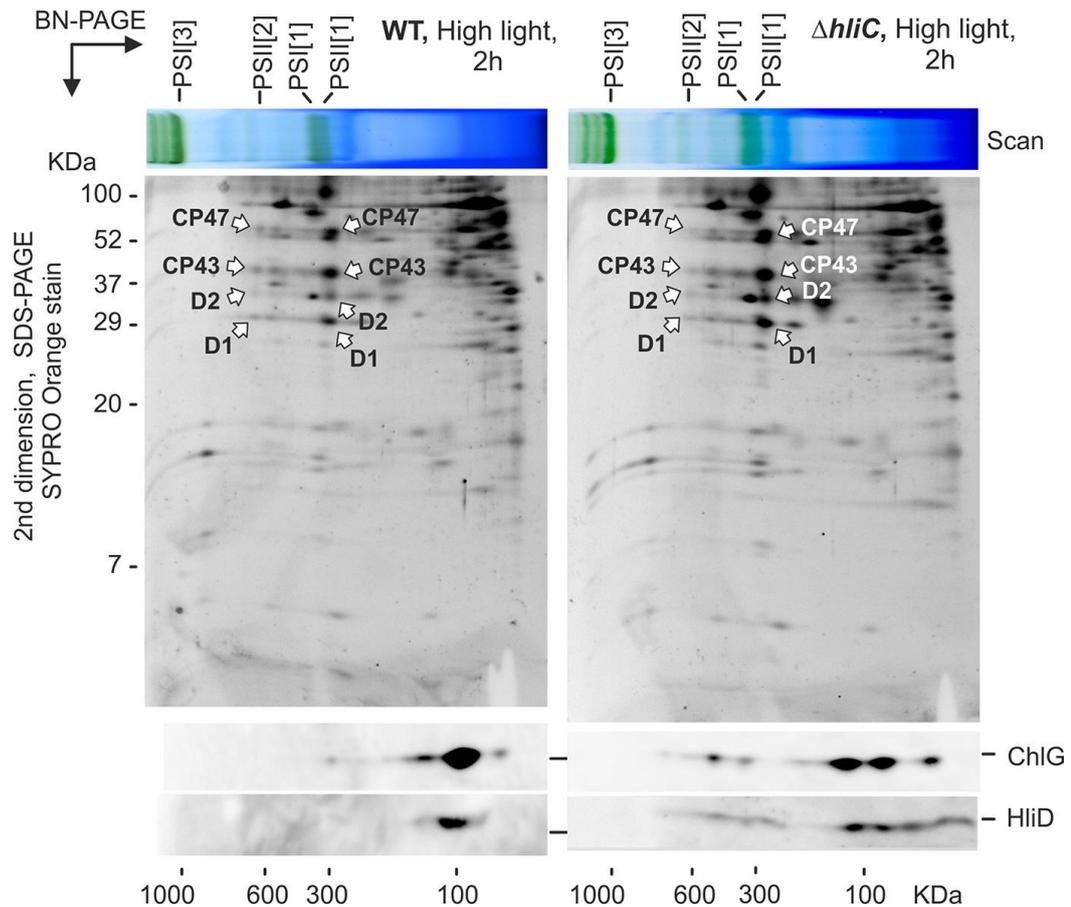
Supplementary Figure 4. Oligomeric state of the ChlG-HliD complexes in WT and Δ*hliC* cells harvested 2 hours after a shift from NL to HL. Isolated membrane proteins were separated by 4-14% BN-PAGE and then in a second dimension by 12-20 % SDS, stained by SYPRO Orange and blotted. The blot was sequentially probed with ChlG and HliD antibodies; the separate segments of the blot with individual antibody signals are shown. PSI[3], PSI[1] – trimer and monomer of PSI; PSII[2], PSII[1] - dimeric and monomeric PSII complexes, respectively. Chl-binding PSII subunits of PSII[2] and PSII[1] are indicated.
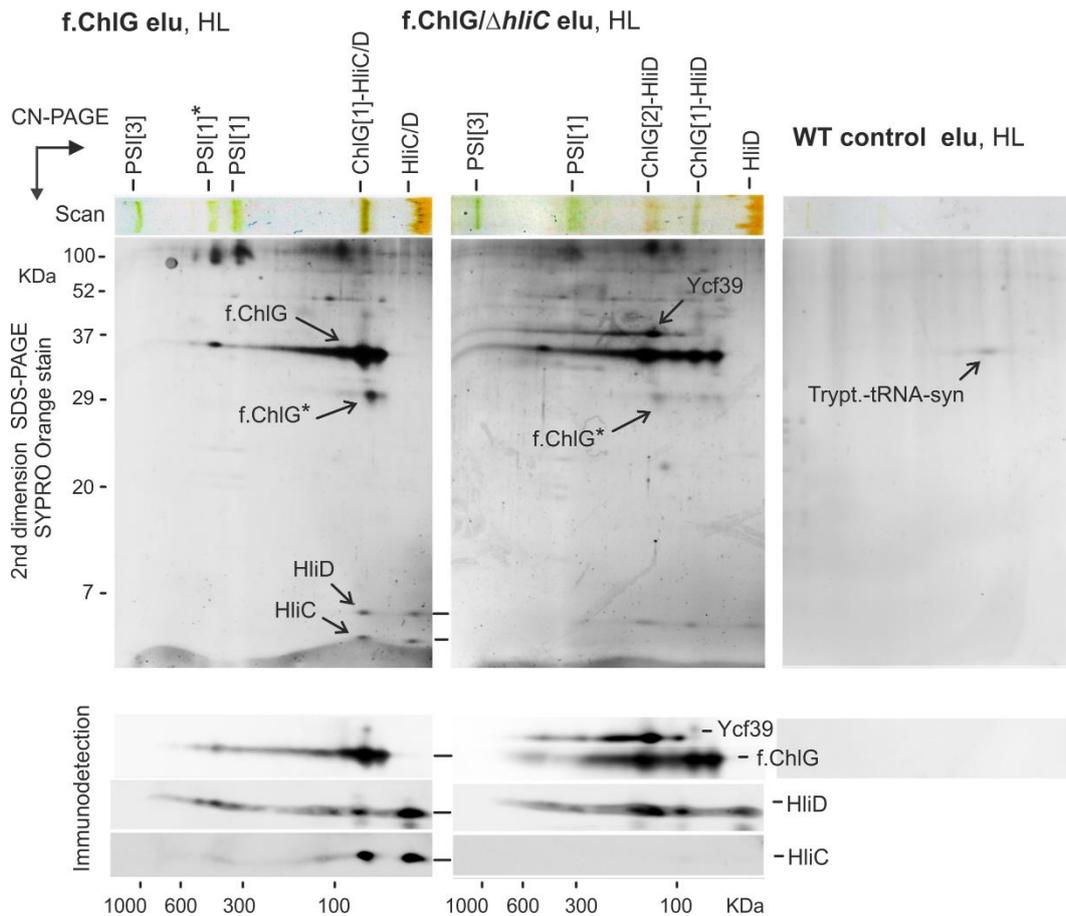
Supplementary Figure 5. Two-dimensional CN/SDS-PAGE of the f.ChlG eluates and the immunodetection of f.ChlG, Ycf39 and HliC/D proteins. Proteins eluted with f.ChlG used a bait from the *f.chlG/chlG*, *f.chlG/chlG/ΔhliC* and WT strains were separated by CN/SDS-PAGE, stained by SYPRO Orange and blotted. The blot was sequentially probed with the indicated antibodies; the separate segments of the blot with individual antibody signals are shown. Proteins shown by arrows on the stained gels were assigned according to[2,3]; tryptophanyl-tRNA synthetase Slr1884 is a standard unspecific interactor of the Flag resin[2]. f.ChlG* is a fragment of f.ChlG protein identified by protein mass spectrometry; ChlG[1] and ChlG[2] – monomer and dimer of ChlG; PSI[3], PSI[1] – trimer and monomer of PSI; PSI[1]* - an uncharacterized form of monomeric PSI.

Supplementary reference

1. Standfuss, J., Terwisscha van Scheltinga, A. C., Lamborghini, M. & Kuhlbrandt, W. Mechanisms of photoprotection and nonphotochemical quenching in pea light-harvesting complex at 2.5 A resolution. *EMBO J.* **24**, 919-928 (2005).

2. Knoppová, J. *et al.* Discovery of a chlorophyll binding protein complex involved in the early steps of photosystem II assembly in *Synechocystis*. *Plant Cell* **26**, 1200-1212 (2014).

3. Chidgey, J. W. *et al.* A cyanobacterial chlorophyll synthase-HliD complex associates with the Ycf39 protein and the YidC/Alb3 insertase. *Plant Cell* **26**, 1267-1279 (2014).

3.5   Result V

Molecular origin of photoprotection in oxygenic photosynthesis probed by femtosecond Raman spectroscopy

Hontani, Y., Kloz, M., Polívka, T., **Shukla, M.K.**, Sobotka, R., Kennis, J.T.M
Submitted manuscript - J. Phys Chem Lett.

Molecular Origin of Photoprotection in Oxygenic Photosynthesis Probed by Femtosecond Raman Spectroscopy

Yusaku Hontani,[1,‡] Miroslav Kloz,[1,2,‡] Tomáš Polívka,[3] Mahendra K. Shukla[4], Roman Sobotka[4] and John T.M. Kennis*[1]

[1]Department of Physics and Astronomy, Vrije Universiteit, Amsterdam, The Netherlands
[2]ELI, Prague, Czech Republic
[3]Institute of Physics and Biophysics, Faculty of Science, University of South Bohemia, České Budějovice, Czech Republic
[4]Centre Algatech, Institute of Microbiology, Academy of Sciences of the Czech Republic, Třeboň, 379 81, Ceske Budejovice, Czech Republic

corresponding author, e-mail: j.t.m.kennis@vu.nl
[‡]Y.H and M.K. contributed equally

Abstract

Photoprotection is fundamental in photosynthesis to avoid oxidative photodamage upon excess light exposure. Excited chlorophylls (Chl) are quenched by carotenoids but the precise molecular origin remains controversial. The cyanobacterial HliC protein belongs to the Hlip family ancestral to plant light-harvesting complexes, and binds Chl a and β-carotene in 2:1 ratio. We analyzed HliC by femtosecond stimulated Raman spectroscopy to follow the time evolution of its vibrational modes. We observed a 2-ps rise of the C=C stretch band of the $2A_g^-$ (S_1) state of β-carotene upon Chl a excitation, demonstrating energy transfer quenching and fast excess-energy dissipation. We detected two distinct β-carotene conformers but only the β-carotene whose $2A_g^-$ energy level is significantly lowered is involved in quenching. It implies that the low carotenoid S_1 energy that results from specific pigment-protein or pigment-pigment interactions is the key property for creating a dissipative energy channel.

Oxygenic photosynthetic organisms need to protect themselves from the consequences of excess sunlight, as the photosynthetic machinery easily gets overloaded even at moderate light intensities. To this end, elaborate photoprotection mechanisms have evolved, collectively known as nonphotochemical quenching (NPQ).[1,2] NPQ involves the active dissipation (quenching) of singlet excited states in the light harvesting antenna before they reach the reaction centers for photochemical conversion, and manifests itself in distinct ways in various oxygenic photosynthetic organisms. In plants and algae, NPQ involves specific interactions between carotenoids and chlorophylls in the light-harvesting complex (LHC) family, where the lifetime of Chl singlet excited states is quenched to hundreds of ps. The mechanism by which this process occurs has been controversially discussed in the literature: energy transfer,[3-5] electron transfer,[6,7] excitonic coupling,[8,9] and Chl-Chl charge transfer interactions[10] have been proposed.

Cyanobacterial photosynthesis is ancestral to that of plants and algae and although cyanobacteria do not use the plant-like LHC antenna system for light harvesting, they contain so called High Light-Inducible proteins (Hlips) that are homologues to 1st and 3rd helices of plant LHC proteins. Hlips are small single-helix polypeptides (5-7 kDa) ubiquitous in cyanobacteria, which play an important role during assembly and repair of photosystem II, particularly under stress conditions.[11] So far, only two members of the Hlip family, HliC and HliD, have been isolated and biochemically characterized.[4,12,13] Both these proteins, isolated from the cyanobacterium *Synechocystis* 6803, form oligomers and bind 4 Chl *a* (HliC) or 6 Chl *a* (HliD) and 2 β-carotenes per a putative dimer.[4,12,13]
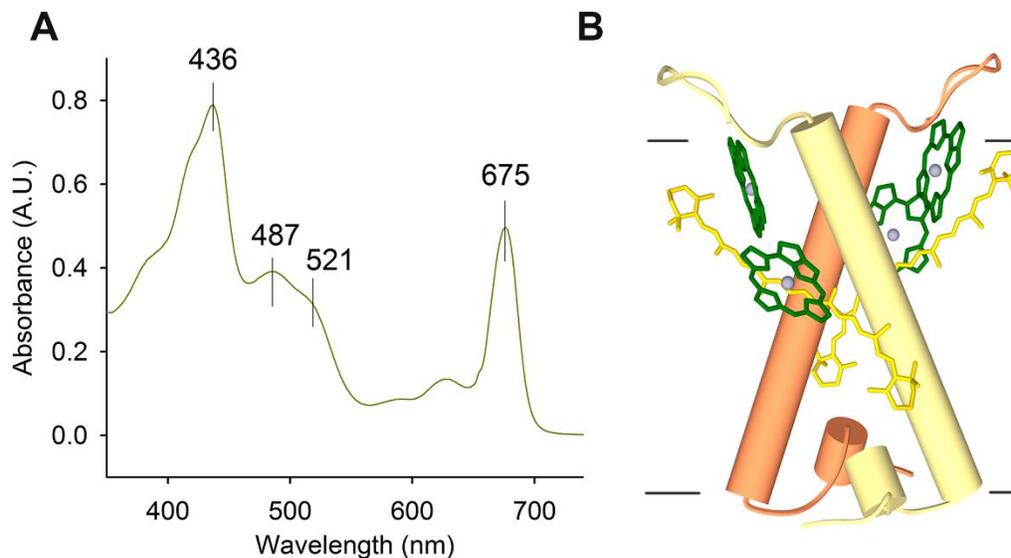
Figure 1. Steady-state absorption and a structural model of HliC. (**A**) Room-temperature absorbance spectrum of the purified HliC protein. (**B**) A structural model of the putative HliC dimer depicted as a side view along the membrane plane (modified from[12]).

62   Fig. 1 shows the absorption spectrum and a structural model of HliC[12]. Despite the apparent
63   two-fold symmetry in the proposed structure, resonance Raman spectroscopy demonstrated that
64   two distinct β-carotene conformers exist in HliC and also in HliD[13]: β-car$_1$ absorbs at higher energy
65   and exhibits a higher C=C stretch frequency at 1525 cm^{-1}, whereas β-car$_2$ absorbs at lower energy
66   and has a lower C=C stretch frequency at 1515 cm^{-1}. Strikingly, ultrafast transient absorption
67   spectroscopy showed that the HliD protein was highly quenched, with dominant Chl a lifetimes of
68   only 2 and 30 ps, and a minor unquenched fraction.[4] Moreover, it was shown that the quenching
69   of the Chl a excited state proceeded via energy transfer to the optically forbidden S$_1$ (A$_g^-$) state of
70   β-carotene.[4] This observation posed an important conundrum: close Chl-carotenoid positioning
71   that is a common motif in light-harvesting proteins is necessary to promote triplet-triplet transfer
72   from Chl to carotenoid upon Chl intersystem crossing. Yet, in most antenna complexes the Chl
73   singlet excited state is not quenched at all. Hence, unresolved questions remain about the
74   quenching mechanism with regard to electronic coupling to optically forbidden states and the
75   energetics of the states involved.[14] The latter is especially pressing because the energy level of the
76   optically forbidden S$_1$ state of carotenoids is largely insensitive to polarity and polarizability of the
77   environment.[15]

78   Femtosecond stimulated Raman spectroscopy (FSRS) is a powerful method to gain detailed
79   molecular information through transient vibrational spectra.[16] It features a high temporal
80   resolution of < 100 fs, high spectral resolution and high sensitivity with respect to time-resolved
81   resonance Raman methods. Recently, we have developed a watermarked FSRS method involving
82   shot-to-shot Raman pump modulation and wavelet transformation to successfully suppress the
83   large and unpredictable baseline fluctuations.[17-19] In this work, we make use of the ability of FSRS
84   to follow specific molecular vibrations with sub-100 fs time resolution to assess the mechanism,
85   pathways and energetics of excited-state energy quenching in HliC.

86   Fig. 2A shows the stimulated Raman spectrum of the HliC ground state with preresonant
87   800 nm pump. The two strongest bands at 1517 and 1156 cm^{-1} are due to the β-carotene C=C and
88   C-C stretches, respectively.[12,13] It furthermore features a shoulder near 1550 cm^{-1} and a band at
89   1671 cm^{-1}, which are both due to Chl a.[12,13] The amplitude of the β-carotene bands is much higher
90   than those of Chl a even though the 800 nm Raman pump is more preresonant with the Chl a Q$_y$
91   band than the β-carotene S$_2$ band, which relates to the higher Raman cross section of the latter
92   pigment. The bands at 1466, 1051 and 851 cm^{-1} are due to glycerol, which was added to stabilize
93   the sample and are conveniently used as an internal marker for the FSRS experiments.

94   Fig. 2B shows FSRS spectra at selected delays upon Chl a excitation at 675 nm. At very short
95   delays (300 fs), large bleaches of the β-carotene C=C stretch at 1515 cm^{-1} and C-C stretch at 1156
96   cm^{-1} are observed, as well as a bleach of the Chl a band at 1668 cm^{-1}. Importantly, the glycerol
97   solvent bands at 1465, 1047 and 851 cm^{-1} are bleached as well, which indicates that these are likely
98   spurious signals caused by partial absorption of the 800 nm Raman pump by Chl a excited-state
99   absorption,[20,21] $i.e.$ an inner filter effect that diminishes the Raman pump intensity and hence
100 results in a lower signal.[22] Thus, the bleaching signals associated with β-carotene stretches at early
101 delay times do not imply population of β-carotene excited states. This was confirmed by a FSRS
102 experiment on a Chl a – β-carotene mixture in organic solvent, where no close interactions exist
103 between the pigments. Here, selective Chl a excitation and population also lead to bleach of Chl a,
104 β-carotene and solvent modes (Fig. S1), confirming the inner filter effect.

105   In the ensuing evolution on the picosecond timescale, we observe the rise of a positive
106 band at 1774 cm^{-1}. This band is a unique marker of the optically forbidden S_1 ($2A_g^-$) state of
107 carotenoids, as it represents an upshifted C=C stretch frequency that results from strong vibronic
108 coupling between the S_0 ($1A_g^-$) and S_1 ($2A_g^-$) states.[23] Thus, FSRS data gives direct evidence of
109 energy transfer from the excited Chl *a* to the optically forbidden S_1 state of β-carotene in 2 ps,
110 consistent with transient absorption measurements (Fig. S2) where the β-carotene S_1 state has a
111 prominent absorption at 560 nm. The same quenching pathway has also been earlier reported by
112 ultrafast transient absorption experiments on HliD.[4] The 1774 cm^{-1} band disappears on a timescale
113 of 10 ps, which is assigned to the S_1-S_0 internal conversion (IC) of β-carotene.[15] In addition, a minor
114 slow phase of 30 ps is observed in the β-carotene S_1 decay (1774 cm^{-1}) in transient absorption as
115 well as in stimulated Raman. The Chl *a* bleach signal mainly decayed in 2.5 and 20 ps (Fig. S2). Given
116 that the IC time constant of β-carotene can hardly be longer than 15 ps due to the properties of its
117 conjugated π-electron system,[15] we interpret this to result from a slow 30 ps phase in the energy
118 transfer process from Chl *a* to β-carotene, which through inverted kinetics shows up as a 30 ps
119 lifetime component of β-carotene S_1.
120
121
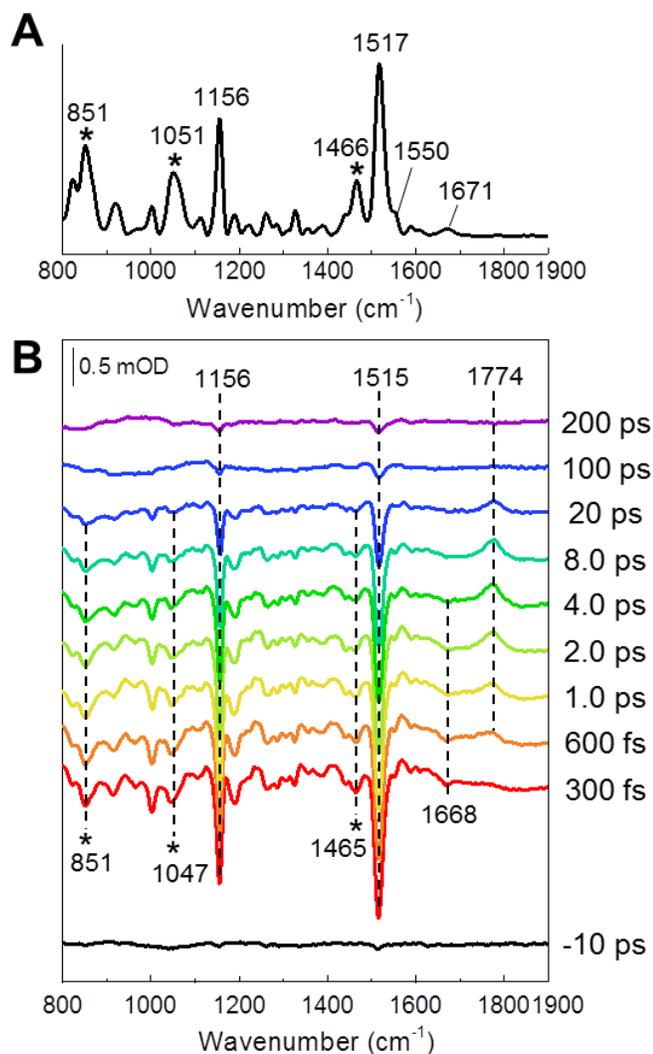
Figure 2. FSRS of HliC upon 675 nm excitation. (**A**) Ground-state Raman spectrum of HliC. (**B**) Selected time traces of difference spectra of FSRS. Asterisks (*) indicate signals originated from glycerol.

To gain additional information about the energy transfer processes and pathways, we performed FSRS experiments with direct excitation of β-carotene at 488 and 532 nm (Fig. S3). Here, the two β-carotene conformers, β-car$_1$ and β-car$_2$, are to a certain extent selectively excited. We observe that for both datasets upon 488- and 532-nm excitation, the high-frequency β-carotene S$_1$ marker band around 1775 cm^{-1} rises in about 300 fs and upshifts with approximately the same time constant, which is assigned to ultrafast IC from the optically allowed S$_2$ state, followed by intramolecular vibrational cooling.[17,24] For both datasets, the β-carotene S$_1$ marker band decays in ~10 ps, as shown in Fig. S4.
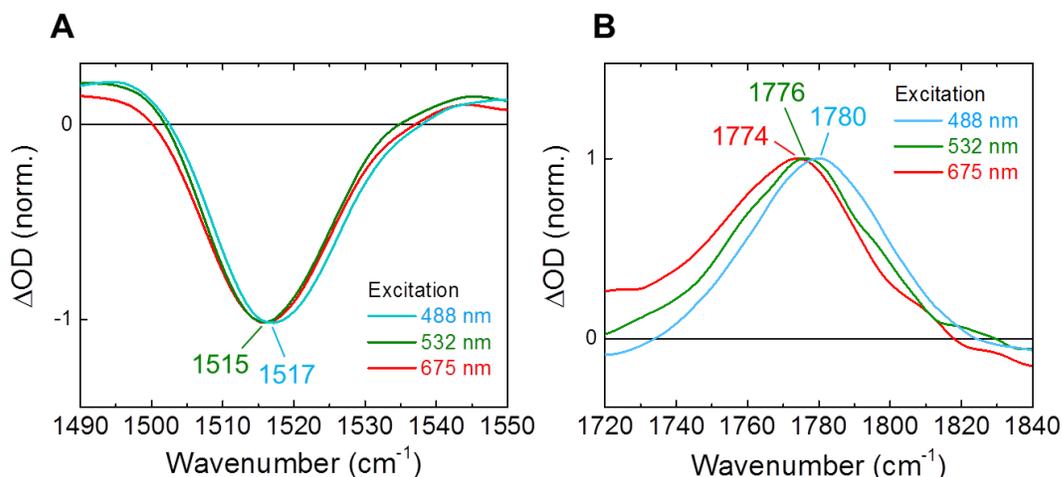
Figure 3. Comparison of FSRS peaks of HliC at 4 ps upon excitation at different wavelengths. (**A**) The bleaches of the C=C stretching and (**B**) the C=C stretching on the S_1 state of β-car. Signals upon excitation at 488, 532 and 675 nm are shown in cyan, green and red, respectively.

Although the spectral evolution is very similar between the two datasets, significant spectral differences are observed. Fig. 3 shows an overlap of the FSRS spectra at 4 ps in the C=C stretch regions of the S_0 state (panel A) and S_1 state (panel B) with excitation at 488 nm (cyan), 532 nm (green) and 675 nm (red). Strikingly, in the S_1 state (Fig. 3B) a 4 cm^{-1} difference is observed with 488 and 532 nm excitation, which demonstrates that the β-car$_1$ and β-car$_2$ conformers have distinct C=C stretch frequencies in the S_1 state. Note that selectivity is not 100% with either excitation wavelength,[13] so the difference in S_1 state frequency of β-car$_1$ and β-car$_2$ is probably larger than 4 cm^{-1}. Smaller, but observable shifts were observed in the ground state C=C stretch manifested as the S_0 state bleaching signal (Fig. 3A).

If we now compare the FSRS data with Chl *a* excitation at 675 nm (Fig 3B, red) with that at 488 nm excitation (Fig 3B, cyan), we find that the former has a frequency of 1774 cm^{-1}, which is lower by 6 cm^{-1} than the latter (Fig. 3B). This observation demonstrates beyond doubt that the β-car$_2$ conformer, and not β-car$_1$ acts as the energy acceptor that quenches the excited Chl *a*. In HliC and HliD, on the basis of the linear relationship between the ground state C=C stretch frequency and effective conjugation length,[25] the conjugation length of β-car$_2$ was estimated to be ~10.5, as opposed to ~9.6 for β-car$_1$,[12,13] which would result in an up to 800 cm^{-1} (0.1 eV) energy difference between β-car and β-car$_2$.[15] The 6 cm^{-1} shift of the C=C stretch frequency in the S_1 state observed here by FSRS corroborates this finding, though the precise relationship between the C=C stretch frequency in the S_1 state and effective conjugation has not been established yet. However, it is known that the S_1 C=C stretch frequency is much more sensitive to carotenoid-protein interaction than the ground state C=C stretch.[26] This implies that specific carotenoid-protein interactions induces asymmetry between the β-car molecules in HliC, making the β-car$_2$ the quenching site. Fig. 4 summarizes our findings. Application of FSRS allowed to follow the specific vibrational mode in the S_1 state, revealing that the β-carotene S_1 energy level tuning provides a key property in creating dissipative energy transfer pathways in closely confined Chl – carotenoid geometries. The carotenoid S_1 state energy is largely insensitive to environmental polarity and polarizability,[15] which

166 implies that specific pigment-protein or pigment-pigment interactions must be invoked to tune the
167 S_1 energy. One promising avenue is provided by specific in-plane tuning of the β-carotene β-rings,
168 which bring them in conjugation with the π-electron system of the polyene backbone, thereby
169 lowering the overall energy levels of the electronic excited states.[13] The ramifications of these
170 observations are very important indeed, as we demonstrate that the same type of carotenoid
171 molecule, β-carotene in this case, may assume a quenching and a non-quenching role in the same
172 LHC, a mechanism that has long been hypothesized for plant LHCs.[2,3,27]
173
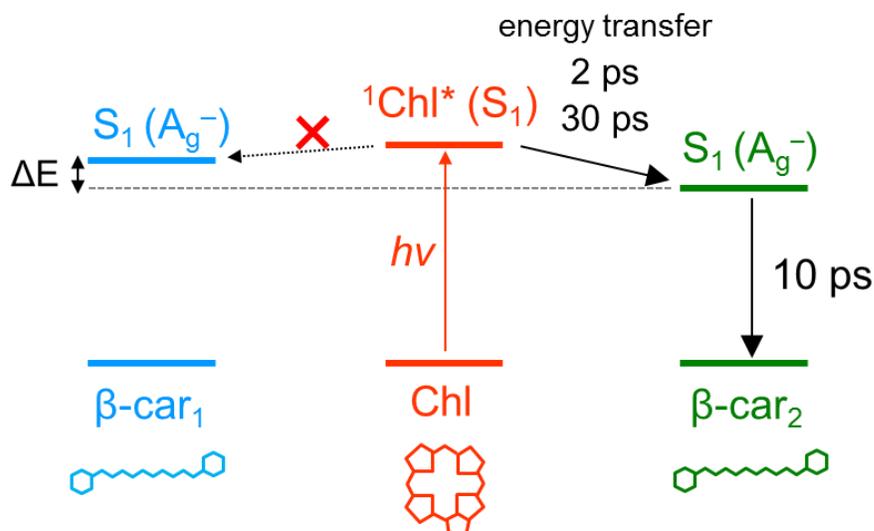
174

175 **Figure 4. Energy transfer model of HliC upon excitation of Chl.** After excitation of Chl, excited-state
176 energy transfer occurs specifically to the lower energy β-carotene (β-car$_2$) in 2 and 30 ps. The decay
177 of the S_1 state β-car$_2$ proceeds in 10 ps. The higher-energy β-car$_1$ is not populated because of
178 unfavorable energetics. See text for details.

179

185 **Author contributions**: M.K.S. and R.S. purified and prepared the protein samples. Y.H. and M.K.
186 performed femtosecond stimulated Raman spectroscopy. Y.H. conducted transient absorption
187 spectroscopy and global analysis. The manuscript was written by J.T.M.K, Y.H., T.P. and R.S. T.P. and
188 J.T.M.K. supervised the project. All authors contributed to discussion of the results and reviewed
189 the manuscript.

190 **Competing financial interests**: The authors declare no competing financial interests.

191 **References**

192   1   Croce, R. & van Amerongen, H. Natural strategies for photosynthetic light harvesting.
193   *Nature Chemical Biology* **10**, 492-501 (2014).
194   2   Ruban, A. V., Johnson, M. P. & Duffy, C. D. P. Natural light harvesting: principles and
195   environmental trends. *Energy Environ. Sci.* **4**, 1643-1650, doi:10.1039/c0ee00578a (2011).
196   3   Ruban, A. V. *et al.* Identification of a mechanism of photoprotective energy dissipation in
197   higher plants. *Nature* **450**, 575-U522, doi:10.1038/nature06262 (2007).
198   4   Staleva, H. *et al.* Mechanism of photoprotection in the cyanobacterial ancestor of plant
199   antenna proteins. *Nature Chemical Biology* **11**, 287-U296, doi:10.1038/Nchembio.1755
200   (2015).
201   5   Berera, R. *et al.* A simple artificial light-harvesting dyad as a model for excess energy
202   dissipation in oxygenic photosynthesis. *Proceedings of the National Academy of Sciences*
203   *of the United States of America* **103**, 5343-5348, doi:10.1073/pnas.0508530103 (2006).
204   6   Holt, N. E. *et al.* Carotenoid cation formation and the regulation of photosynthetic light
205   harvesting. *Science* **307**, 433-436, doi:10.1126/science.1105833 (2005).
206   7   Ahn, T. K. *et al.* Architecture of a charge-transfer state regulating light harvesting in a
207   plant antenna protein. *Science* **320**, 794-797, doi:10.1126/science.1154800 (2008).
208   8   Bode, S. *et al.* On the regulation of photosynthesis by excitonic interactions between
209   carotenoids and chlorophylls. *Proceedings of the National Academy of Sciences of the*
210   *United States of America* **106**, 12311-12316, doi:10.1073/pnas.0903536106 (2009).
211   9   Kloz, M. *et al.* Carotenoid Photoprotection in Artificial Photosynthetic Antennas. *Journal*
212   *of the American Chemical Society* **133**, 7007-7015, doi:10.1021/ja1103553 (2011).
213   10 Muller, M. G. *et al.* Singlet Energy Dissipation in the Photosystem II Light-Harvesting
214   Complex Does Not Involve Energy Transfer to Carotenoids. *Chemphyschem* **11**, 1289-
215   1296, doi:10.1002/cphc.200900852 (2010).
216   11 Komenda, J. & Sobotka, R. Cyanobacterial high-light-inducible proteins - Protectors of
217   chlorophyll-protein synthesis and assembly. *Biochim. Biophys. Acta-Bioenerg.* **1857**, 288-
218   295, doi:10.1016/j.bbabio.2015.08.011 (2016).
219   12 Shukla, M. K. *et al.* Binding of pigments to the cyanobacterial High-light-inducible protein
220   HliC. *Photosynthesis Research*, doi:10.1007/s11120-017-0475-7 (2017).
221   13 Llansola-Portoles, M. J. *et al.* Twisting a beta-Carotene, an Adaptive Trick from Nature for
222   Dissipating Energy during Photoprotection. *Journal of Biological Chemistry* **292**, 1396-
223   1403, doi:10.1074/jbc.M116.753723 (2017).
224   14 Balevicius, V. *et al.* Fine control of chlorophyll-carotenoid interactions defines the
225   functionality of light-harvesting proteins in plants. *Scientific reports* **7** (2017).
226   15 Polivka, T. & Sundstrom, V. Ultrafast dynamics of carotenoid excited states - From
227   solution to natural and artificial systems. *Chemical Reviews* **104**, 2021-2071,
228   doi:10.1021/cr020674n (2004).
229   16 Kukura, P., McCamant, D. W. & Mathies, R. A. in *Annual Review of Physical Chemistry* Vol.
230   58 *Annual Review of Physical Chemistry*   461-488 (2007).
231   17 Kloz, M., Weissenborn, J., Polivka, T., Frank, H. A. & Kennis, J. T. M. Spectral watermarking
232   in femtosecond stimulated Raman spectroscopy: resolving the nature of the carotenoid S-
233   star state. *Physical Chemistry Chemical Physics* **18**, 14619-14628, doi:10.1039/c6cp01464j
234   (2016).
235   18 Kloz, M., van Grondelle, R. & Kennis, J. T. M. Wavelength-modulated femtosecond
236   stimulated raman spectroscopy-approach towards automatic data processing. *Physical*
237   *Chemistry Chemical Physics* **13**, 18123-18133, doi:10.1039/c1cp21650c (2011).

238 19   Hontani, Y. *et al.* The photochemistry of sodium ion pump rhodopsin observed by
239   watermarked femto- to submillisecond stimulated Raman spectroscopy. *Physical*
240   *Chemistry Chemical Physics* **18**, 24729-24736, doi:10.1039/c6cp05240a (2016).
241 20   Nuijs, A. M., Shuvalov, V. A., Vangorkom, H. J., Plijter, J. J. & Duysens, L. N. M.
242   PICOSECOND ABSORBENCY DIFFERENCE SPECTROSCOPY ON THE PRIMARY REACTIONS
243   AND THE ANTENNA-EXCITED STATES IN PHOTOSYSTEM-I PARTICLES. *Biochimica Et*
244   *Biophysica Acta* **850**, 310-318, doi:10.1016/0005-2728(86)90186-6 (1986).
245 21   Zigmantas, D., Hiller, R. G., Sundstrom, V. & Polivka, T. Carotenoid to chlorophyll energy
246   transfer in the peridinin-chlorophyll-a-protein complex involves an intramolecular charge
247   transfer state. *Proceedings of the National Academy of Sciences of the United States of*
248   *America* **99**, 16760-16765, doi:10.1073/pnas.262537599 (2002).
249 22   Kloz, M., van Grondelle, R. & Kennis, J. T. M. Correction for the time dependent inner
250   filter effect caused by transient absorption in femtosecond stimulated Raman
251   experiment. *Chemical Physics Letters* **544**, 94-101, doi:10.1016/j.cplett.2012.07.005
252   (2012).
253 23   Nagae, H. *et al.* Vibronic coupling through the in-phase, C=C stretching mode plays a
254   major role in the 2A(g)(-) to 1A(g)(-) internal conversion of all-trans-beta-carotene.
255   *Journal of Physical Chemistry A* **104**, 4155-4166, doi:10.1021/jp9924833 (2000).
256 24   McCamant, D. W., Kukura, P. & Mathies, R. A. Femtosecond time-resolved stimulated
257   Raman spectroscopy: Application to the ultrafast internal conversion in beta-carotene.
258   *Journal of Physical Chemistry A* **107**, 8208-8214, doi:10.1021/jp030147n (2003).
259 25   Mendes-Pinto, M. M. *et al.* Electronic Absorption and Ground State Structure of
260   Carotenoid Molecules. *J. Phys. Chem. B* **117**, 11015-11021, doi:10.1021/jp309908r (2013).
261 26   Kuki, M., Hashimoto, H. & Koyama, Y. THE 2 1AG- STATE OF A CAROTENOID BOUND TO
262   THE CHROMATOPHORE MEMBRANE OF RHODOBACTER-SPHAEROIDES 2.4.1 AS REVEALED
263   BY TRANSIENT RESONANCE RAMAN-SPECTROSCOPY. *Chemical Physics Letters* **165**, 417-
264   422, doi:10.1016/0009-2614(90)85452-i (1990).
265 27   Pandit, A. *et al.* An NMR comparison of the light-harvesting complex II (LHCII) in active
266   and photoprotective states reveals subtle changes in the chlorophyll a ground-state
267   electronic structures. *Biochim. Biophys. Acta-Bioenerg.* **1827**, 738-744,
268   doi:10.1016/j.bbabio.2013.02.015 (2013).

269

270

271

Supporting Information:

Molecular Origin of Photoprotection in Oxygenic Photosynthesis Probed by Femtosecond Raman Spectroscopy

Yusaku Hontani, Miroslav Kloz, Tomáš Polívka, Mahendra K. Shukla, Roman Sobotka and John T.M. Kennis

Methods

Sample preparation: The HliC protein was purified and prepared as reported previously[1]. The HliC sample at pH 6.5 in 20 mM MES buffer solution including 10 mM $CaCl_2$, 0.1% β-DM and 25% glycerol was filled in a 2-mm quartz cuvette (100-QS, Hellma Analytics) for time-resolved experiments. The sample absorbance was ~2 and ~0.4 per 2 mm at 480 nm on time-resolved Raman and transient absorption experiments, respectively. A home-built vibrating sample holder was used to avoid irradiation damage during experiments.

Baseline-free femtosecond stimulated Raman spectroscopy (FSRS): Femtosecond stimulated Raman experiments were performed with the watermarking baseline-free stimulated Raman setup reported previously. Raman pump (800 nm, ~7 μJ) and Raman probe (~840–960 nm) were spatiotemporally overlapped at the sample position with the diameter of ~100 μm. Actinic pump (675 nm, 532 or 488 nm, ~280 nJ) was focused on the sample to the diameter of ~150 μm with a time delay from -10 ps to 200 ps. A narrow-band (Δ~10 nm) interference filter was used for each excitation wavelength. In 675-nm excitation experiments, 17 time points were measured. In 532- and 488-nm excitation experiments, 25 time points were measured. The sample exposure time to the

beams was ~2400 s for 675 nm excitation and ~3000 s for 532- and 488-nm excitation in total for each FSRS experiment.

Transient absorption spectroscopy: Femtosecond transient absorption measurements were performed with a pump-probe setup as reported previously[2,3]. A sapphire plate was used for supercontinuum white light generation, and selected wavelength regions; 470–800 nm were detected by the photodiode array. The time delay was varied up to 2 ns at 95 data points with the minimum temporal step of 20 fs. The diameters of the pump and the probe beams at the sample position were ~240 µm and ~90 µm, respectively. The wavelength of the pump beam was centered at 675, 532 or 488 nm with a narrow-band (Δ~10 nm) interference filter, and the power was attenuated to ~300 nJ. The instrumental response function was ~70 fs, estimated from global analysis.

Global analysis methodology: Global analysis was performed for the transient absorption spectra using the Glotaran program[3,4]. With global analysis, all wavelengths were analyzed simultaneously with a set of common time constants[5]. A kinetic model was applied consisting of sequentially interconverting, evolution-associated difference spectra (EADS), *i.e.* $1 \rightarrow 2 \rightarrow 3 \rightarrow \dots$ in which the arrows indicate successive mono-exponential decays of a time constant, which can be regarded as the lifetime of each EADS[5]. The first EADS corresponds to the difference spectrum at time zero. The first EADS evolves into the second EADS with time constant τ_1, which in turn evolves into the third EADS with time constant τ_2, etc. The procedure clearly visualizes the evolution of the intermediate states of the protein[6]. Decay-associated difference spectra (DADS) indicate the spectral changes with parallel decay channels and independent decay time constants. It is important to note that parallel and sequential analysis are mathematically equivalent and yield identical time constants[7]. The standard errors in time constants were less than 5%[4-6].

References

1   Shukla, M. K. *et al.* Binding of pigments to the cyanobacterial High-light-inducible protein HliC. *Photosynthesis Research*, doi: 10.1007/s11120-017-0475-7 (2017).

2   Hontani, Y. *et al.* Bright blue-shifted fluorescent proteins with Cys in the GAF domain engineered from bacterial phytochromes: fluorescence mechanisms and excited-state dynamics. *Scientific reports* **6**, 37362, doi:10.1038/srep37362 (2016).

3   Ravensbergen, J. *et al.* Unraveling the Carrier Dynamics of BiVO4: A Femtosecond to Microsecond Transient Absorption Study. *The Journal of Physical Chemistry C* **118**, 27793-27800, doi:10.1021/jp509930s (2014).

4   Snellenburg, J. J., Laptenok, S. P., Seger, R., Mullen, K. M. & van Stokkum, I. H. M. Glotaran: A Java-Based Graphical User Interface for the R Package TIMP. *J Stat Softw* **49**, 1-22 (2012).

5   van Stokkum, I. H., Larsen, D. S. & van Grondelle, R. Global and target analysis of time-resolved spectra. *Biochim et Biophysica acta* **1657**, 82-104, doi:10.1016/j.bbabio.2004.04.011 (2004)

6   Kennis, J. T. M. & Groot, M. L. Ultrafast spectroscopy of biological photoreceptors. *Curr Opin Struc Biol* **17**, 623-630, doi:DOI 10.1016/j.sbi.2007.09.006 (2007).

7   Toh, K. C., Stojkovic, E. A., van Stokkum, I. H., Moffat, K. & Kennis, J. T. Fluorescence quantum yield and photochemistry of bacteriophytochrome constructs. *Physical chemistry chemical physics : PCCP* **13**, 11985-11997, doi:10.1039/c1cp00050k (2011).
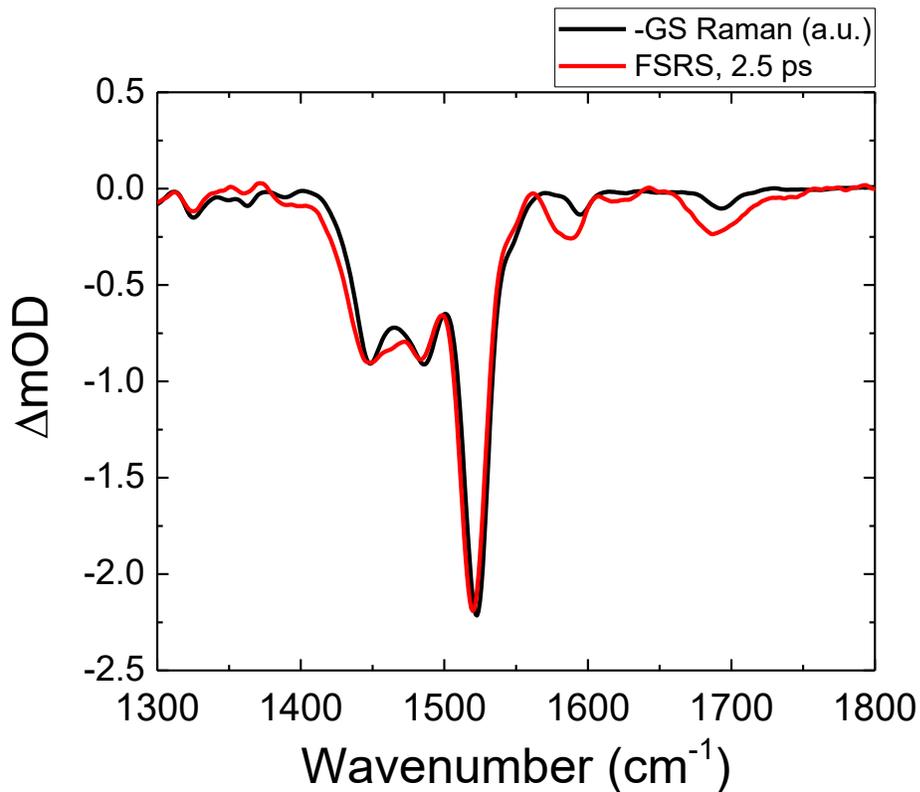
Figure S1. FSRS of a Chl *a* – β-carotene mixture in tetrahydrofuran (THF). Red line: FSRS spectrum at 2.5 ps upon excitation at 675 nm. Black line: ground state stimulated Raman spectrum, inverted and scaled to the red line on the 1520 cm^{-1} β-carotene C=C stretch. The bands at 1580 and 1690 cm^{-1} arise from Chl *a*, whereas the bands at 1430 and 1480 cm^{-1} arise from the THF solvent.
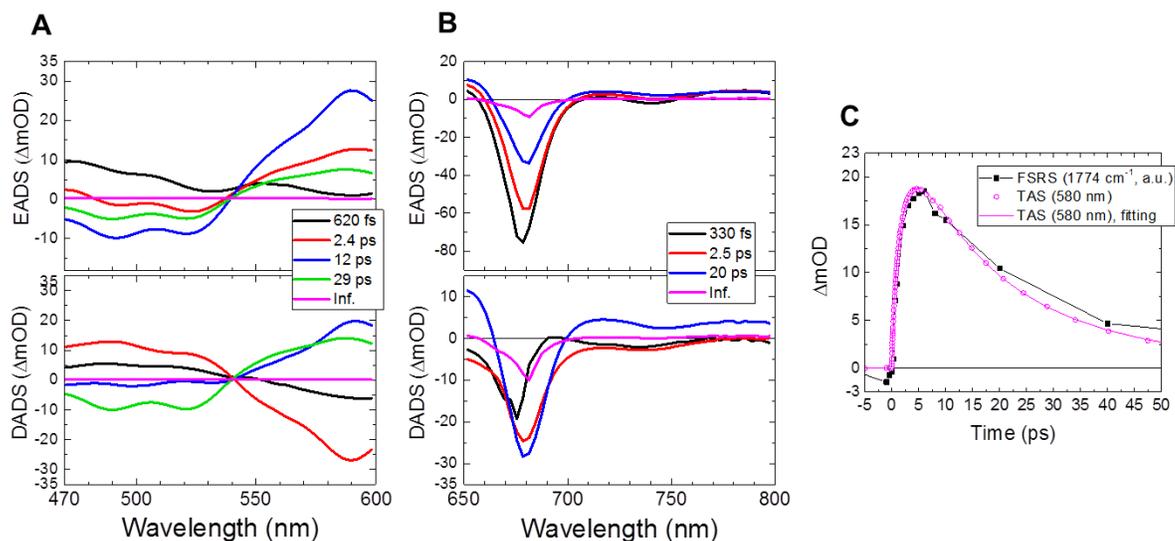
Figure S2. Transient absorption spectrum of HliC upon 675-nm excitation. EADS and DADS of (**A**) 470–600 nm and (**B**) 650–800 nm spectral regions. (**C**) Time trace at 580 nm (magenta open dots) with a fitting curve (magenta line) overlapped with FSRS data at 1774 cm^{-1} (black closed squares).
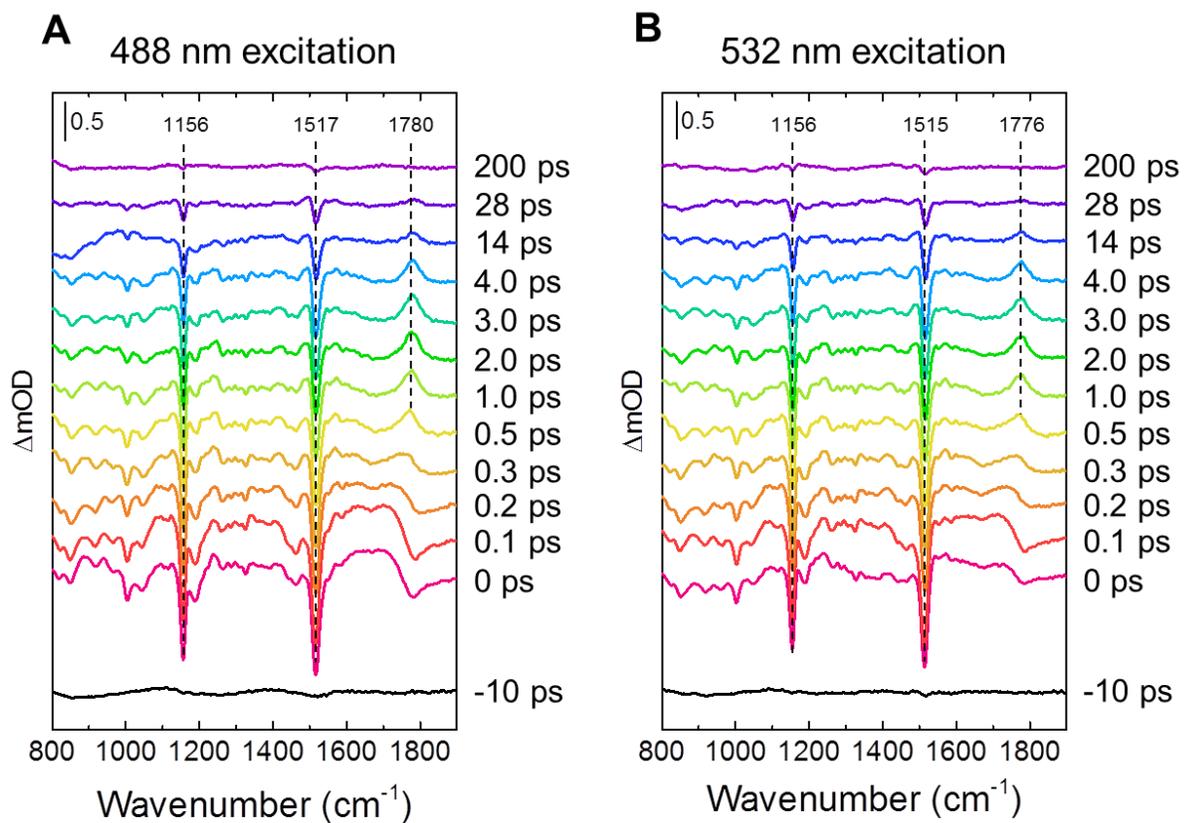
Figure S3. FSRS of HliC with β-car excitation. Upon excitation at (**A**) 488 nm and (**B**) 532 nm.
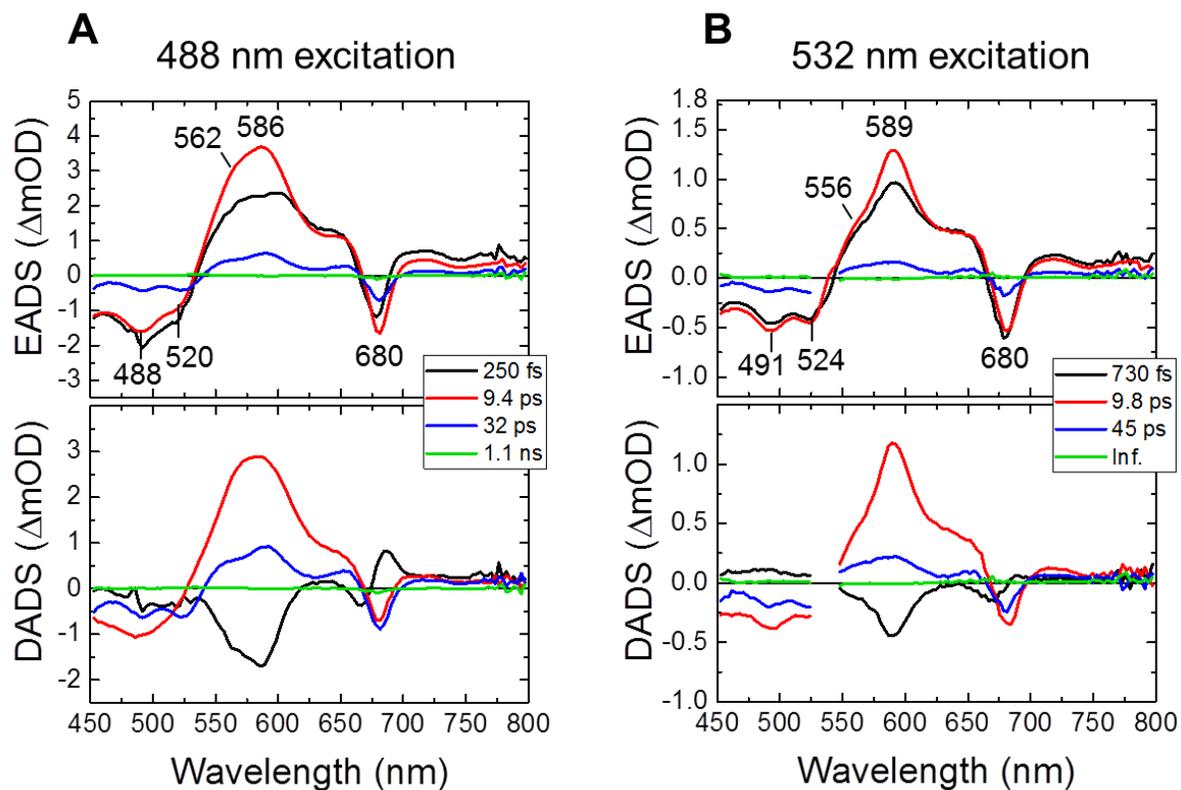
Figure S4. Transient absorption spectra of HliC with β-car excitation.
Upon excitation at (**A**) 488 nm and (**B**) 532 nm. Spectral region of 524–544 nm was omitted in (**B**) because of the strong pump light scattering.

4 CONCLUSIONS

This PhD thesis demonstrates the role of high light protein (Hlips) in regulation/photoprotection of the biogenesis of photosynthetic machinery. It elucidates pigments binding of HliC and HliD, members of the Hlips family from the cyanobacterium *Synechocystis* PCC 6803. This thesis also describes the regulatory role of HliC protein under stress conditions. It consists of one first author publication, two co-author publications, one first author manuscript and one co-author manuscript. The main conclusions of the thesis are as follows:

- The HliD protein binds Chls and β-carotene, in 3:1 ratio, in energy dissipative conformation where the excess energy is quenched via direct energy transfer from Chl to β-carotene. The minimal possible configuration for pigments binding to HliD is a dimer where it binds two different populations of β-carotene.

- The HliC protein binds Chls and β-carotene in 2:1 ratio in a energy dissipative conformation. The isolated HliC forms a stable dimer and the population of β-carotene with the lowered energy of S_1 state is responsible for the energy dissipation.

- The stress-induced HliC protein plays a regulatory role via a re-organization of the Chl-synthase-HliD complexes. Under stress condition, the HliC dissociates oligomeric forms of Chl-synthase and also releases the Ycf39 protein otherwise bound to Chl-synthase-HliD complex. The stress-induced Ycf39-HliC-HliD complex facilitates the repair of PSII.

- Chl-synthase is docked to monomeric and trimeric PSI complexes as well as to a low abundant form of PSI, which is designed PSI [1]*. The last interaction however requires the HliC protein.

5   REFERENCES

Aro EM, Virgin I, Andersson B (1993) Photoinhibition of photosystem II inactivation, protein damage and turnover. Biochim. Biophys. Acta **1143:** 113-134

Bhaya D, Dufresne A, Vaulot D, Grossman A (2002) Analysis of the hli gene family in marine and freshwater cyanobacteria. FEMS Microbiol. Lett. **215:** 209-219

Blankenship RE (2013) Molecular mechanisms of photosynthesis. John Wiley & Sons

Bode S, Quentmeier CC, Liao PN, Hafi N, Barros T, Wilk L, Bittner F, Walla PJ (2009) On the regulation of photosynthesis by excitonic interactions between carotenoids and chlorophylls. Proc. Natl. Acad. Sci. U.S.A. **106:** 12311-12316

Boehm M, Romero E, Reisinger V, Yu JF, Komenda J, Eichacker LA, Dekker JP, Nixon PJ (2011) Investigating the early stages of Photosystem II assembly in *Synechocystis* sp PCC 6803. Isolation of CP47 and CP43 complexes. J. Biol. Chem. **286:** 14812-14819

Boehm M, Yu JF, Krynicka V, Barker M, Tichy M, Komenda J, Nixon PJ, Nield J (2012) Subunit organization of a *Synechocystis* hetero-oligomeric thylakoid FtsH complex involved in photosystem II Repair. Plant Cell **24:** 3669-3683

Bučinská L, Kiss E, Konik P, Knoppova J, Komenda J, Sobotka R (2018) The ribosome-bound protein Pam68 promotes insertion of chlorophyll into the CP47 subunit of Photosystem II. Plant Physiology, DOI: 10.1104/pp.18.00061

Chidgey JW, Linhartová M, Komenda J, Jackson PJ, Dickman MJ, Canniffe DP, Koník P, Pilný J, Hunter CN, Sobotka R (2014) A cyanobacterial chlorophyll synthase-HliD complex associates with the Ycf39 protein and the YidC/Alb3 insertase. Plant Cell **26:** 1267-1279

Chua NH, Blobel G, Siekevitz P, Palade GE (1976) Periodic variations in the ratio of free to thylakoid-bound chloroplast ribosomes during the cell cycle of *Chlamydomonas reinhardtii*. J. Cell Biol. **71:** 497-514

Czarnecki O, Grimm B (2012) Post-translational control of tetrapyrrole biosynthesis in plants, algae, and cyanobacteria. J. Exp. Bot. **63:** 1675-1687

Dalbey RE, Wang P, Kuhn A (2011) Assembly of bacterial inner membrane proteins. Annu. Rev Biochem. **80:** 161-187

De Las Rivas J, Balsera M, Barber J (2004) Evolution of oxygenic photosynthesis: genome-wide analysis of the OEC extrinsic proteins. Trends Plant Sci. **9:** 18-25

Deusch O, Landan G, Roettger M, Gruenheit N, Kowallik KV, Allen JF, Martin W, Dagan T (2008) Genes of cyanobacterial origin in plant nuclear genomes point to a heterocyst-forming plastid ancestor. Mol. Biol. Evol. **25:** 748-761

Dobáková M, Sobotka R, Tichý M, Komenda J (2009) Psb28 protein is involved in the biogenesis of the photosystem II inner antenna CP47 (PsbB) in the cyanobacterium *Synechocystis* sp PCC 6803. Plant Physiol. **149:** 1076-1086

Dolganov NA, Bhaya D, Grossman AR (1995) Cyanobacterial protein with similarity to the chlorophyll a/b binding proteins of higher plants: evolution and regulation. Proc Natl Acad Sci U S A **92:** 636-640

Dolganov NAM, Bhaya D, Grossman AR (1995) Cyanobacterial protein with similarity to the chlorophyll a/b binding proteins of higher plants: Evolution and regulation. Proc. Natl. Acad. Sci. U.S.A. **92:** 636-640

Eggink LL, Hoober JK (2000) Chlorophyll binding to peptide maquettes containing a retention motif. J. Biol. Chem. **275:** 9087-9090

Eichacker LA, Helfrich M, Rudiger W, Muller B (1996) Stabilization of chlorophyll a-binding apoproteins P700, CP47, CP43, D2, and D1 by chlorophyll a or Zn-pheophytin a. J. Biol. Chem. **271:** 32174-32179

Falcón LI, Magallón S, Castillo A (2010) Dating the cyanobacterial ancestor of the chloroplast. The Isme Journal **4:** 777

Ferreira KN, Iverson TM, Maghlaoui K, Barber J, Iwata S (2004) Architecture of the photosynthetic oxygen-evolving center. Science **303:** 1831-1838

Guskov A, Kern J, Gabdulkhakov A, Broser M, Zouni A, Saenger W (2009) Cyanobacterial photosystem II at 2.9-angstrom resolution and the role of quinones, lipids, channels and chloride. Nat. Struct. Mol. Biol. **16:** 334-342

Havaux M, Kloppstech K (2001) The protective functions of carotenoid and flavonoid pigments against excess visible radiation at chilling temperature investigated in Arabidopsis npq and tt mutants. Planta **213:** 953-966

He Q, Dolganov N, Bjorkman O, Grossman AR (2001) The high light-inducible polypeptides in *Synechocystis* PCC 6803. Expression and function in high light. J. Biol. Chem. **276:** 306-314

He QF, Brune D, Nieman R, Vermaas W (1998) Chlorophyll a synthesis upon interruption and deletion of por coding for the light-dependent NADPH : protochlorophyllide oxidoreductase in a photosystem-I-less/chlL(-) strain of *Synechocystis* sp. PCC 6803. Eur. J. Biochem. **253:** 161-172

Heddad M, Engelken J, Adamska I (2012) Light stress proteins in viruses, cyanobacteria and photosynthetic eukaryota. *In* JJ EatonRye, BC Tripathy, TD Sharkey, eds, Photosynthesis: Plastid Biology, Energy Conversion and Carbon Assimilation. **34:** 299-317

Hohmann-Marriott MF, Blankenship RE (2011) Evolution of Photosynthesis. Annu. Rev. Plant Biol. **62:** 515-548

Holland HD (2006) The oxygenation of the atmosphere and oceans. Philos Trans R Soc Lond B Biol Sci **361:** 903-915

Hollingshead S, Kopečná J, Armstrong DR, Bučinská L, Jackson PJ, Chen GE, Dickman MJ, Williamson MP, Sobotka R, Hunter CN (2016) Synthesis of chlorophyll-binding proteins in a fully segregated D*ycf54* strain of the cyanobacterium *Synechocystis* PCC 6803. Front. Plant Sci. **7:** 292

Holt NE, Zigmantas D, Valkunas L, Li XP, Niyogi KK, Fleming GR (2005) Carotenoid cation formation and the regulation of photosynthetic light harvesting. Science **307:** 433-436

Hoober JK, Eggink LL, Chen M (2007) Chlorophylls, ligands and assembly of light-harvesting complexes in chloroplasts. Photosynth. Res. **94:** 387-400

Jansson S (1999) A guide to the Lhc genes and their relatives in Arabidopsis. Trends Plant Sci. **4:** 236-240

Jarvi S, Suorsa M, Aro EM (2015) Photosystem II repair in plant chloroplasts - Regulation, assisting proteins and shared components with photosystem II biogenesis. Biochim. Biophys. Acta **1847:** 900-909

Jordan P, Fromme P, Witt HT, Klukas O, Saenger W, Ktrauss N (2001) Three-dimensional structure of cyanobacterial photosystem I at 2.5 A resolution. Nature **411:** 909-917

Kim J, Eichacker LA, Rudiger W, Mullet JE (1994) Chlorophyll regulates accumulation of the plastid-encoded chlorophyll proteins P700 and D1 by increasing apoprotein stability. Plant Physiol. **104:** 907-916

Knoppová J, Sobotka R, Tichý M, Yu J, Koník P, Halada P, Nixon PJ, Komenda J (2014) Discovery of a chlorophyll binding protein complex involved in the early steps of photosystem II assembly in *Synechocystis*. Plant Cell **26:** 1200-1212

Komenda J, Knoppová J, Kopečná J, Sobotka R, Halada P, Yu JF, Nickelsen J, Boehm M, Nixon PJ (2012) The Psb27 assembly factor binds to the CP43 complex of photosystem II in the cyanobacterium *Synechocystis* sp PCC 6803. Plant Physiol. **158:** 476-486

Komenda J, Nickelsen J, Tichý M, Prášil O, Eichacker LA, Nixon PJ (2008) The cyanobacterial homologue of HCF136/YCF48 is a component of an early photosystem II assembly complex and is important for both the efficient assembly and repair of photosystem II in *Synechocystis* sp PCC 6803. J. Biol. Chem. **283:** 22390-22399

Komenda J, Reisinger V, Muller BC, Dobáková M, Granvogl B, Eichacker LA (2004) Accumulation of the D2 protein is a key regulatory step for assembly of the photosystem II reaction center complex in *Synechocystis* PCC 6803. J. Biol. Chem. **279:** 48620-48629

Komenda J, Sobotka R (2016) Cyanobacterial high-light-inducible proteins - Protectors of chlorophyll-protein synthesis and assembly. Biochim. Biophys. Acta **1857:** 288-295

Komenda J, Sobotka R, Nixon PJ (2012) Assembling and maintaining the Photosystem II complex in chloroplasts and cyanobacteria. Curr. Opin. Plant Biol. **15:** 245-251

Kopečná J, Komenda J, Bučinská L, Sobotka R (2012) Long-term acclimation of the cyanobacterium *Synechocystis* sp PCC 6803 to high light is accompanied by an enhanced production of chlorophyll that is preferentially channeled to trimeric Photosystem I. Plant Physiol. **160:** 2239-2250

Kopečná J, Sobotka R, Komenda J (2013) Inhibition of chlorophyll biosynthesis at the protochlorophyllide reduction step results in the parallel depletion of Photosystem I and Photosystem II in the cyanobacterium *Synechocystis* PCC 6803. Planta **237:** 497-508

Kopf M, Klahn S, Scholz I, Matthiessen JK, Hess WR, Voss B (2014) Comparative analysis of the primary transcriptome of *Synechocystis* sp. PCC 6803. DNA Res **21:** 527-539

Krüger TPJ, Ilioaia C, Johnson MP, Ruban AV, van Grondelle R (2014) Disentangling the low-energy states of the major light-harvesting complex of plants and their role in photoprotection. Biochim. Biophys. Acta **1837:** 1027-1038

Krynická V, Shao S, Nixon PJ, Komenda J (2015) Accessibility controls selective degradation of photosystem II subunits by FtsH protease. Nature Plants **1:** 15168

Kuhlbrandt W, Wang DN, Fujiyoshi Y (1994) Atomic model of plant light-harvesting complex by electron crystallography. Nature **367:** 614-621

Li M, Semchonok DA, Boekema EJ, Bruce BD (2014) Characterization and evolution of tetrameric photosystem I from the thermophilic cyanobacterium Chroococcidiopsis sp TS-821. The Plant Cell **26:** 1230-1245

Liu LN (2016) Distribution and dynamics of electron transport complexes in cyanobacterial thylakoid membranes. Biochim. Biophys. Acta **1857:** 256-265

Llansola-Portoles MJ, Sobotka R, Kish E, Shukla MK, Pascal AA, Polívka T, Robert B (2017) Twisting a β-carotene, an adaptive trick from nature for dissipating energy during photoprotection. J. Biol. Chem. **292:** 1396-1403

Masuda T, Fujita Y (2008) Regulation and evolution of chlorophyll metabolism. Photochem. Photobiol. Sci. **7:** 1131-1149

Minagawa J (2011) State transitions--the molecular remodeling of photosynthetic supercomplexes that controls energy flow in the chloroplast. Biochim. Biophys. Acta **1807:** 897-905

Muller B, Eichacker LA (1999) Assembly of the D1 precursor in monomeric photosystem II reaction center precomplexes precedes chlorophyll a-triggered accumulation of reaction center II in barley etioplasts. Plant Cell **11:** 2365-2377

Nagamori S, Smirnova IN, Kaback HR (2004) Role of YidC in folding of polytopic membrane proteins. J. Cell Biol. **165:** 53-62

Nelson N, Ben-Shem A (2004) The complex architecture of oxygenic photosynthesis. Nature reviews. Molecular cell biology **5:** 971

Nickelsen J, Rengstl B (2013) Photosystem II assembly: from cyanobacteria to plants. Annu. Rev. Plant Biol. **64:** 609-635

Niedzwiedzki DM, Tronina T, Liu H, Staleva H, Komenda J, Sobotka R, Blankenship RE, Polívka T (2016) Carotenoid-induced non-photochemical quenching in the cyanobacterial chlorophyll synthase-HliC/D complex. Biochim. Biophys. Acta **1857:** 1430-1439

Nishiyama Y, Allakhverdiev SI, Murata N (2011) Protein synthesis is the primary target of reactive oxygen species in the photoinhibition of photosystem II. Physiol. Plant **142:** 35-46

Nixon PJ, Barker M, Boehm M, de Vries R, Komenda J (2004) FtsH-mediated repair of the photosystem II complex in response to light stress. J. Exp. Bot. **56:** 357-363

Nixon PJ, Michoux F, Yu JF, Boehm M, Komenda J (2010) Recent advances in understanding the assembly and repair of photosystem II. Annals of Botany **106:** 1-16

Nomata J, Swem LR, Bauer CE, Fujita Y (2005) Overexpression and characterization of dark-operative protochlorophyllide reductase from *Rhodobacter capsulatus*. Biochim. Biophys. Acta **1708:** 229-237

Papenbrock J, Mock H, Kruse E, Grimm B (1999) Diurnal and circadian rhythms in tetrapyrrole biosynthesis: antagonistic maxima of magnesium chelatase and ferro chelatase. Planta **208:** 264-273

Promnares K, Komenda J, Bumba L, Nebesářová J, Vácha F, Tichý M (2006) Cyanobacterial small chlorophyll-binding protein ScpD (HliB) is located on the periphery of photosystem II in the vicinity of PsbH and CP47 subunits. J. Biol. Chem. **281:** 32705-32713

Rees DC, Tezcan FA, Haynes CA, Walton MY, Andrade S, Einsle O, Howard JB (2005) Structural basis of biological nitrogen fixation. Philosophical Transactions of the Royal Society a-Mathematical Physical and Engineering Sciences **363:** 971-984

Ruban AV, Berera R, Ilioaia C, van Stokkum IH, Kennis JT, Pascal AA, van Amerongen H, Robert B, Horton P, van Grondelle R (2007) Identification of a mechanism of photoprotective energy dissipation in higher plants. Nature **450:** 575-578

Schottkowski M, Ratke J, Oster U, Nowaczyk M, Nickelsen J (2009) Pitt, a novel tetratricopeptide repeat protein involved in light-dependent chlorophyll biosynthesis and thylakoid membrane biogenesis in *Synechocystis* sp PCC 6803. Mol. Plant **2:** 1289-1297

Sharma P, Jha AB, Dubey RS, Pessarakli M (2012) Reactive oxygen species, oxidative damage, and antioxidative defense mechanism in plants under stressful conditions. Journal of botany **2012**

Shukla MK, Llansola-Portoles MJ, Tichý M, Pascal AA, Robert B, Sobotka R (2017) Binding of pigments to the cyanobacterial high-light-inducible protein HliC. Photosynth Res, DOI: 10.1007/s11120-017-0475-7

Sobotka R (2014) Making proteins green; biosynthesis of chlorophyll-binding proteins in cyanobacteria. Photosynth. Res. **119:** 223-232

Sobotka R, Tichý M, Wilde A, Hunter CN (2011) Functional assignments for the carboxyl-terminal domains of the ferrochelatase from *Synechocystis* PCC 6803: The CAB domain plays a regulatory role, and region II is essential for catalysis. Plant Physiol. **155:** 1735-1747

Staleva H, Komenda J, Shukla MK, Šlouf V, Kaňa R, Polívka T, Sobotka R (2015) Mechanism of photoprotection in the cyanobacterial ancestor of plant antenna proteins. Nat. Chem. Biol. **11:** 287-291

Standfuss J, Terwisscha van Scheltinga AC, Lamborghini M, Kuhlbrandt W (2005) Mechanisms of photoprotection and nonphotochemical quenching in pea light-harvesting complex at 2.5 A resolution. EMBO J. **24:** 919-928

Storm P, Hernandez-Prieto MA, Eggink LL, Hoober JK, Funk C (2008) The small CAB-like proteins of Synechocystis sp PCC 6803 bind chlorophyll. Photosynth. Res. **98:** 479-488

Suga M, Akita F, Hirata K, Ueno G, Murakami H, Nakajima Y, Shimizu T, Yamashita K, Yamamoto M, Ago H (2015) Native structure of photosystem II at 1.95 Å resolution viewed by femtosecond X-ray pulses. Nature **517:** 99

Suzuki T, Minagawa J, Tomo T, Sonoike K, Ohta H, Enami I (2003) Binding and functional properties of the extrinsic proteins in oxygen-evolving photosystem II particle from a green alga, Chlamydomonas reinhardtii having His-tagged CP47. Plant Cell Physiol. **44:** 76-84

Tyystjarvi T, Herranen M, Aro EM (2001) Regulation of translation elongation in cyanobacteria: membrane targeting of the ribosome nascent-chain complexes controls the synthesis of D1 protein. Mol. Microbiol. **40:** 476-484

Umena Y, Kawakami K, Shen JR, Kamiya N (2011) Crystal structure of oxygen-evolving Photosystem II at a resolution of 1.9 Å. Nature **473:** 55-60

Vavilin D, Vermaas W (2007) Continuous chlorophyll degradation accompanied by chlorophyllide and phytol reutilization for chlorophyll synthesis in *Synechocystis* sp PCC 6803. Biochim. Biophys. Acta **1767:** 920-929

Vavilin D, Yao D, Vermaas WFJ (2007) Small cab-like proteins retard degradation of photosystem II-associated chlorophyll in *Synechocystis* sp PCC 6803 - Kinetic analysis of pigment labeling with N-15 and C-13. J. Biol. Chem. **282:** 37660-37668

Wang P, Grimm B (2015) Organization of chlorophyll biosynthesis and insertion of chlorophyll into the chlorophyll-binding proteins in chloroplasts. Photosynth. Res. **126:** 189-202

Xu H, Vavilin D, Funk C, Vermaas W (2002) Small Cab-like proteins regulating tetrapyrrole biosynthesis in the cyanobacterium Synechocystis sp PCC 6803. Plant Mol. Biol. **49:** 149-160

Xu H, Vavilin D, Funk C, Vermaas WFJ (2004) Multiple deletions of small Cab-like proteins in the cyanobacterium *Synechocystis* sp. PCC 6803: consequences for pigment biosynthesis and accumulation. J. Biol. Chem. **279:** 27971-27979

Yamashita A, Nijo N, Pospíšil P, Morita N, Takenaka D, Aminaka R, Yamamoto Y, Yamamoto Y (2008) Quality control of photosystem II reactive oxygen species are responsible for the damage to photosystem II under moderate heat stress. J. Biol. Chem. **283:** 28380-28391

Yamazaki S, Nomata J, Fujita Y (2006) Differential operation of dual protochlorophyllide reductases for chlorophyll biosynthesis in response to environmental oxygen levels in the cyanobacterium *Leptolyngbya boryana*. Plant Physiol. **142:** 911-922

Yao D, Kieselbach T, Komenda J, Promnares K, Prieto MAH, Tichy M, Vermaas W, Funk C (2007) Localization of the small CAB-like proteins in photosystem II. J. Biol. Chem. **282:** 267-276

Yao DCI, Brune DC, Vermaas WFJ (2012) Lifetimes of photosystem I and II proteins in the cyanobacterium *Synechocystis* sp PCC 6803. FEBS Lett. **586:** 169-173

CURRICULUM VITAE

Personal details

Name: Mahendra Kumar Shukla

Date of birth: January 1, 1983

Place of birth: Basti, U.P., India

Nationality: Indian

Present address: Centre Algatech, Institute of Microbiology, Academy of Sciences of the Czech Republic, Novohradska 237. Opatovický mlýn, 37981 Třeboň, Czech Republic

E-mail: shukla@alga.cz

Education and experience

2006-2008:   School of Biochemistry, Devi Ahilya University, Indore, India, Masters degree in biochemistry.

2009-2013:   Research Fellow in Marine Biotechnology and Ecology, CSIR-Central Salt and Marine Chemicals Research Institute, Bhavnagar, Gujarat, India

20013-present: University of South Bohemia, Czech Republic, Faculty of Science, Molecular and Cell Biology and Genetics study programme, PhD studies.

International research visit

May-June 2016: A short research visit in the laboratory of Prof. Neil Hunter, University of Sheffield, UK.

Publications

Shukla, M.K., Llansola-Portoles, M.J., Tichý, M., Pascal, A.A., Robert, B., Sobotka, R. Binding of pigments to the cyanobacterial high-light-inducible protein HliC. Photosynthesis Research, 2017, doi.org/10.1007/s11120-017-0475-7.

LIansola-Portoles, M.J., Sobotka, R. Kish, E., **Shukla, M.K.,** Pascal, A.A., Polívka, T., Robert, B. Twisting a β-carotene, an adaptive trick from nature for dissipating energy during photoprotection. Journal of Biological Chemistry, 2016, 292:1396-1403.

Staleva, H., Komenda, J., **Shukla, M.K.**, Šlouf, V., Kana, R., Polívka, T., Sobotka, R. Mechanism of photoprotection in the cyanobacterial ancestor of plant antenna proteins. Nature Chemical Biology, 2015, 11:287-291.

Singh, R.P., **Shukla, M.K.,** Mishra, A., Reddy, C.R.K., Jha, B. Bacterial extracellular polymeric substances and their effect on settlement of zoospore of *Ulva fasciata*. Colloids and Surfaces B: Biointerfaces, 2013, 103:223-230.

Shukla, M.K., Singh, R.P., Reddy, C.R.K., Jha, B. Synthesis and characterization of agar-based silver nanoparticles and nanocomposite film with antibacterial applications. Bioresource Technology 2012, 107:295–300.

Singh, R.P., **Shukla, M.K.**, Mishra, A., Kumari, P., Reddy, C.R.K., Jha, B. Isolation and characterization of exopolysaccharides from seaweed associated bacteria *Bacillus licheniformis*. Carbohydrate Polymers, 2011, 84:1019-1026.

Shukla, M.K., Kumar, M., Prasad, K., Reddy, C.R.K. Jha, B. Partial characterization of sulfohydrolase from *Gracilaria dura* and evaluation of its potential application in improvement of the agar quality. Carbohydrate Polymers, 2011, 85: 157-163.

Kumar, M., Kumari, P., Trivedi, N., **Shukla, M.K.,** Gupta, V., Reddy, C.R.K., Jha, B. Minerals, PUFAs and antioxidant properties of some tropical seaweeds from Saurashtra coast of India. Journal of Applied Phycology, 2011, 23:797-810.

Manuscripts

Shukla, M.K., Jackson, P.J., Brindley A.A., Hunter, C.N., and Sobotka R. Cyanobacterial LHC-like proteins control formation of the chlorophyll-synthase-Ycf39 complex. (*Unsubmitted manuscript*).

Jianfeng Yu., Knoppová J., Michoux F., Bialek W., Cota E., **Shukla M.K.**, *et al,*. Ycf48 involve in the biogenesis of the oxygen evolving photosystem II complex is a 7 bladed beta-propeller protein. (*Under review in PNAS*).

Hontani, Y., Kloz, M., Polívka, T., **Shukla, M.K.**, Sobotka, R. *et al*. Molecular origin of photoprotection in oxygenic photosynthesis probed by femtosecond Raman spectroscopy (Submitted manuscript – *J. Phys. Chem. Lett*).

Conferences

- 10th European Workshop on the Molecular Biology of Cyanobacteria, Cluj Napoca, Romania 20-24 August 2017 (Selected **talk**)

- Conference on Chlorophyll Biogenesis, Humboldt University, Berlin, 9-12 October 2016 (**Talk**)

- Conference of Doctoral Students of the Institute of Microbiology, ASCR, December 2014 (**Talk**)

- 9th European Workshop on the Molecular Biology of Cyanobacteria, NIOZ, Texel, The Nederlands, 7-11 September 2014 (**Poster**)

Research Grant

- Isolation of the cyanobacterial ribosome-translocon machinery stalled during synthesis of the photosystem core proetin. Individual research grant, Grant agency of University of South Bohemia (031/2015/P).